Geological Survey of Japan Cruise Report No. 23, p. 87-163, 1994

VIII. MANGANESE NODULE FACIES IN THE WESTERN PART OF THE PENRHYN BASIN, SOUTH PACIFIC (GH83-3 AREA)

Akira Usui

Introduction

The GH83-3 is the fifth and last cruise of GSJ's 5-year program "Manganese Nodule Investigation in the Central Pacific Ocean (1979-1983)" on the Wake-Tahiti Transect (Fig.VIII-1; Usui, 1983). The variations of manganese nodule deposits were studied on regional and small scales in the western part of the Penrhyn Basin of the South Pacific by the Geological Survey of Japan (GSJ) during the two-month Cruise GH83-3 with R/V Hakurei-maru. Reconnaissance surveys of nodule deposits of the Penrhyn Basin areas had been carried out by France, New Zealand, and Cook Islands in 1970's (Bäker *et al.*, 1976; Landmesser *et al.*, 1976; Monzier and Missegue, 1977; Glasby, 1981). After our cruise, two exploration cruises of R/V Hakurei-maru II were carried out in the Exclusive Economic Zone of the Cook Islands government in 1985 and 1986 for the purpose of economic evaluation of metal resources over this area (Metal Mining Agency of Japan, 1986; 1987). These surveys revealed abundant distribution of manganese nodule deposits in the western Penrhyn Basin (Fig. VIII-2). The objective of this investigation of the GH83-3 area is to characterize the regional and local variation patterns of manganese nodule facies and to understand their relationships to sedimentary processes in the deep sea.

This work was funded by Agency of Industrial Science and Technology, MITI, Japan. I acknowledge captain and crew of Hakurei-Maru for their assistance and help during the cruise. Dr. A. Mizuno, Ehime University, Dr. S. Nakao, Dr. A. Nishimura GSJ are appreciated for fruitful discussion and suggestion. The SOPAC Technical Secretariat, Fiji kindly provided me an opportunity of referencing unpublished official reports on marine mineral resources exploration in the Cook Islands sea area.

Method

Reconnaissance geological survey and sampling were done mainly during the first leg of the cruise using corers and free-fall grabs at 98 stations. The station intervals are about 30 and 10 nautical miles. During the second leg, nodule and sediment sampling was carried out in the detailed survey area within the survey area by using free-fall grabs, deep-sea cameras, piston corers, box corers and dredges together with geophysical study. The shortest station interval in the detailed survey area is around

Keywords: manganese nodule, acoustic stratigraphy, hydrogenetic diagenetic, small-scale variation, bottom current, AABW, Manihiki Plateau, Hakurei-Maru, Penrhyn Basin

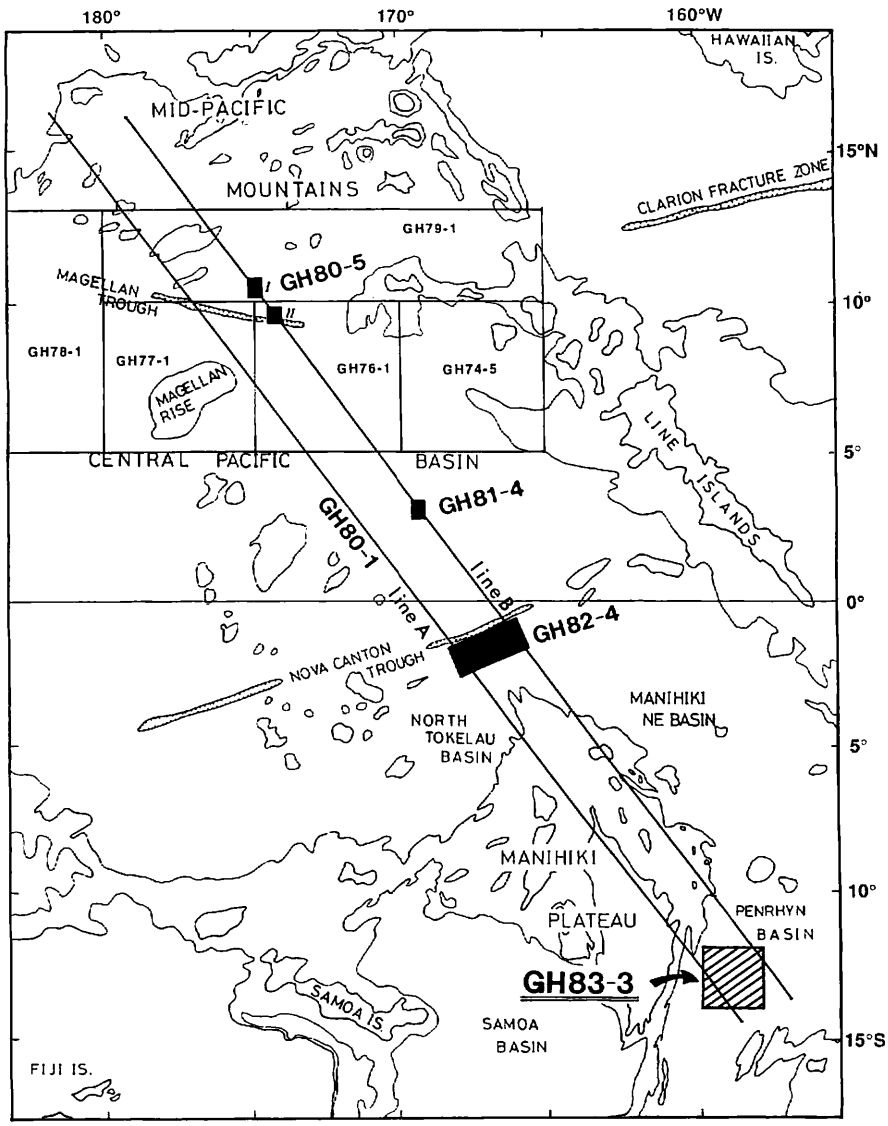

Fig. VIII-1 Location map of the GH83-3 study area and earlier study areas. Base map modified from Chase *et al.* (1977) published by Scripps Institution of Oceanography. Contours denote 2000 and 2600 fathoms.

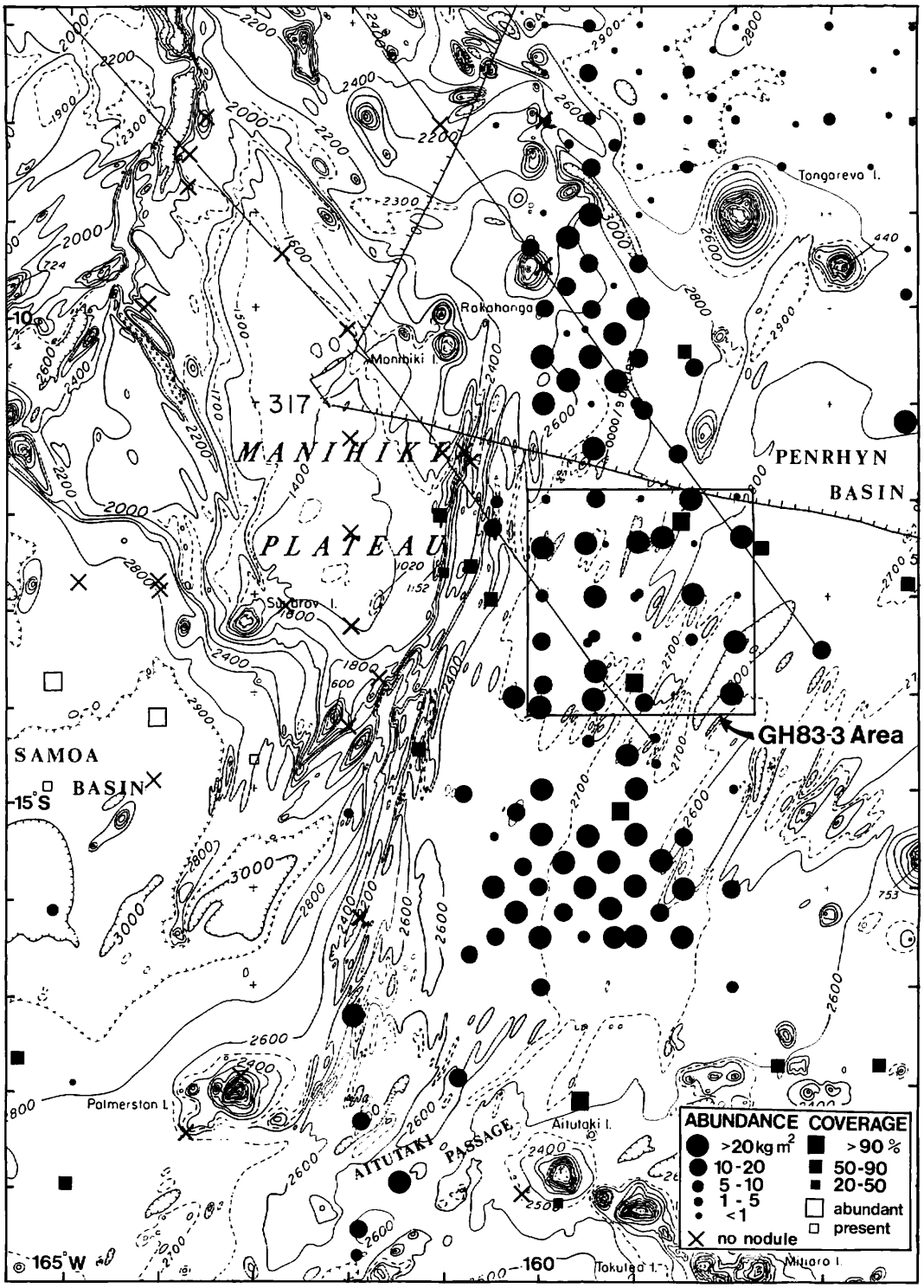

Fig. VIII-2 Compiled abundance distribution map of manganese nodules in the western part of Penrhyn Basin. Note a N-S trending high-abundance zone in the western margin of the basin. Data from Bäcker *et al.* (1976), Landmesser *et al.* (1976), Monzier and Missegue (1977), Glasby (1981) and MMAJ (1986, 1987).

one kilometer which is nearly equal to the maximum ship positioning error. Methods of sampling, sea-bed photography, and on-board description employed are the same as those during our previous Hakurei-maru cruises GH80-5, GH81-4, and GH82-4 (Usui and Nakao, 1984; Usui, 1986; Usui *et al.*, 1986; Usui, 1992).

Survey area

The GH83-3 area (12°00′S-14°00′S, 158°00′W-160°00′W) is located in the western part of the Penrhyn Basin to the east of the Manihiki Plateau. The area is characterized by flat but sometimes rolled deep-sea floors at water depths between 5100 to 5300 m. The most prominent topographic feature is the N-S trending asymmetric deep trough which divides the survey area. The greatest water depth of the bottom of the trough is 6000 m or more. The western basin to the trough is generally flat with some scattered deep-sea hills and depressions with relative height of ±hundred meters to the floor. The eastern basin, by contrast, are more dominated by deep-sea hills and depressions which form rugged topography. The highest elevation of 1100 m is encountered at a hill (12°17′S, 159°00′W) in the eastern basin. A detailed survey area (12°30′S-12°55′S, 159°00′W-159°35′W) was selected in the center of the survey area just to the west of the trough, where seismic reflection and bathymetric surveys were done along line of 2-nautical mile intervals (Okuda, Chapter II of this volume).

The surface sediment is zeolitic and pelagic deep-sea clays over the survey area, but no calcareous or siliceous biogenic sediments were found. The sedimentological study on surface and core sediments by Nishimura and Saito (Chapter IIV, this volume) reveals frequent outcrop of the Paleogene or possibly Cretaceous zeolitic claystone suggesting a dominant long-term sedimentary hiatus in this area.

Occurrence and morphology

Among 175 locations of bottom sampling, the 157 samplers (133 free-fall grabs, 11 box cores, 12 piston cores, and one dredge) recovered manganese nodules and/or crusts from the sea floor. Among 134 successful sea-bed photographs operated with box or piston corers, the 115 sea-bed photographs show nodules or crusts on the sea floor. Shipboard description data (Appendix VIII-1) and sea-bed and onboard photographs (Appendix VIII-2) are listed after the text.

The criteria for morphological description of nodules established during previous GSJ cruises in the northern Central Pacific Basin (Moritani *et al.*, 1977) was again adopted and proved available in describing nodules in the GH83-3 area. All of the surface and sub-surface nodules in the area principally belong to the smooth-surface type of hydrogenetic origin (type s). The surface color is generally black but rather brownish. Their surface is sometimes granular consisting of 0.5 to 1 mm growth cusps, but their mineralogy and texture are identical to hydrogenetic vernadite (Usui and Mita, Chapter IX of this volume). A rough-surface type nodule (type r) which is typical of high-Ni and Cu diagenetic deposits is not found in this area. The surface feature and morphology of the nodules of this area are considerably constant in comparison with Central Pacific nodules (cf. Usui *et al.*, 1986). However the rare occurrence of flattened large tabular shape accompany a little buserite and moderate

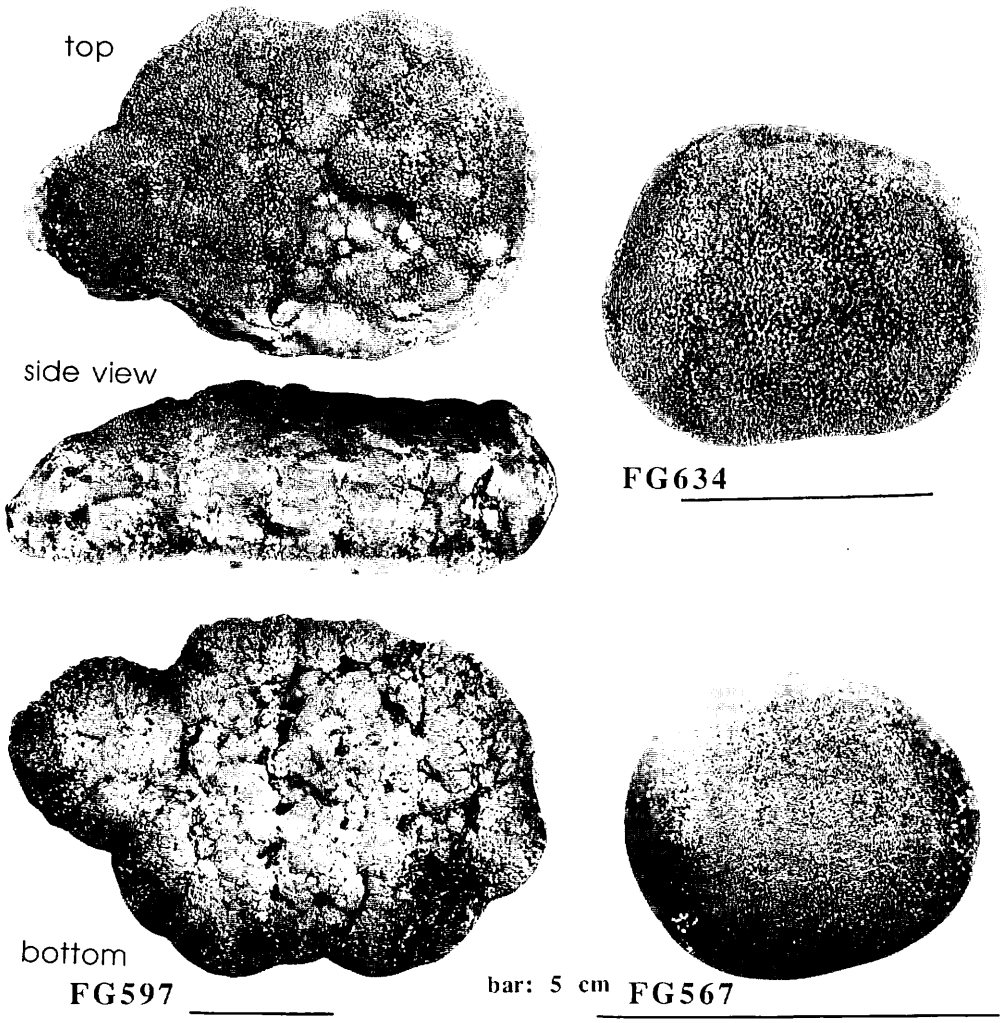

Fig. VIII-3 Typical shapes of GH83-3 nodules. Spherical nodules with groth cusps (right side) and difference of top and bottom surface of a tabular nodule.

Ni and Cu at the bottom side nevertheless it shows no rough growth structure (Fig. VIII- 3).

The shape is generally spheroidal (Fig. VIII-3) but sometimes show broken feature along internal radial cracks, whereas the size is variable ranging from less than 1 cm to 8 cm in long diameter (Fig. VIII-4). Summary of frequency diagram of median diameters for each station (Fig. VIII-5) demonstrates a bi-modal distribution pattern: small nodules (1.2-2.2 cm) and large nodules (2.4-4.0 cm). This clear separation in nodule diameter reflects thickness of ferromanganese layers, and probably two growth generations of nodules if assumed constant growth rates.

Most of the nodules of this area is highly exposed to overlying sea water. The exposed nature is quite different from that of the Central Pacific diagenetic nodule

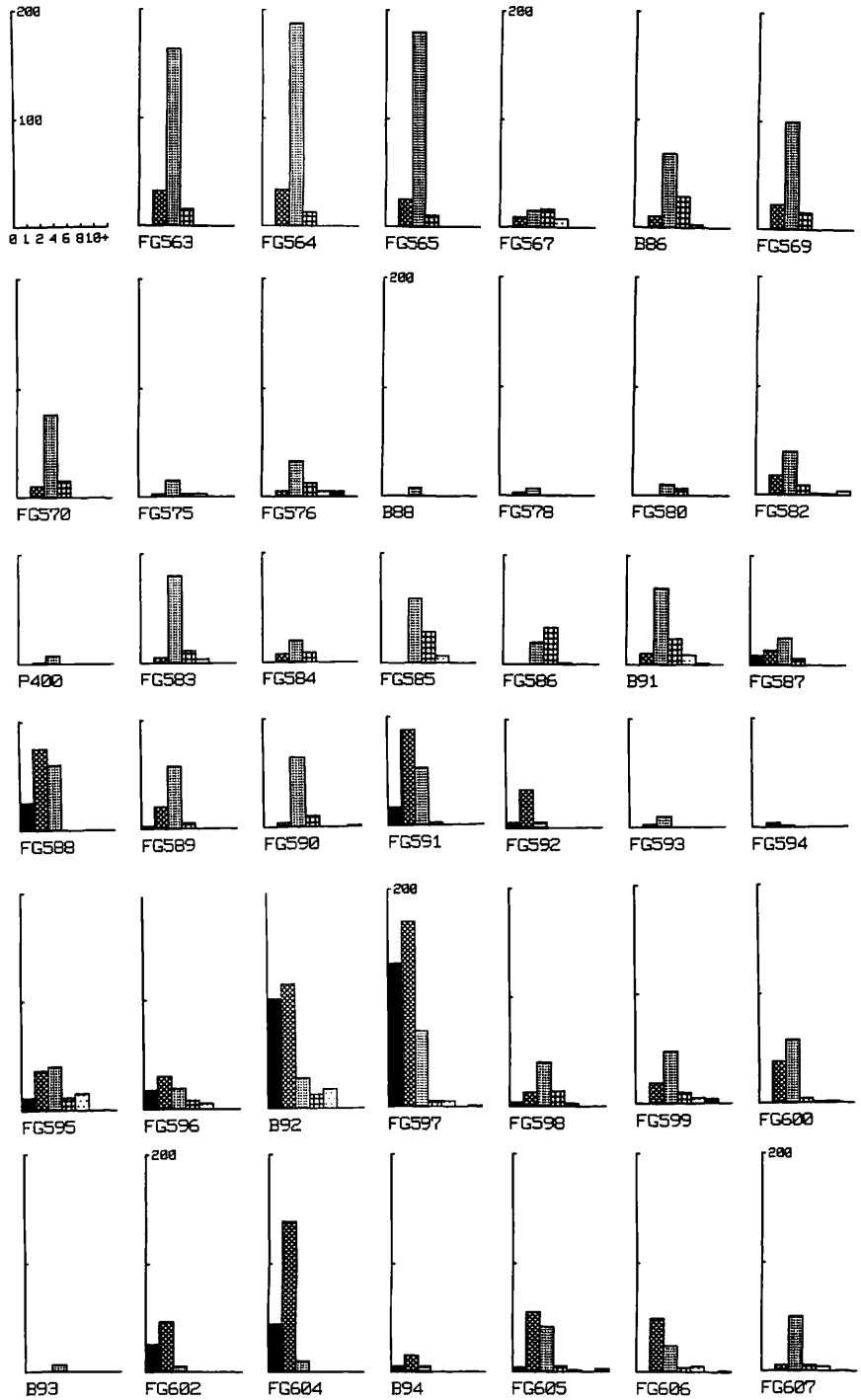

Fig. VIII-4 Frequency distribution of nodule long axis. Unit of Y axis is population of nodules in each sampler.

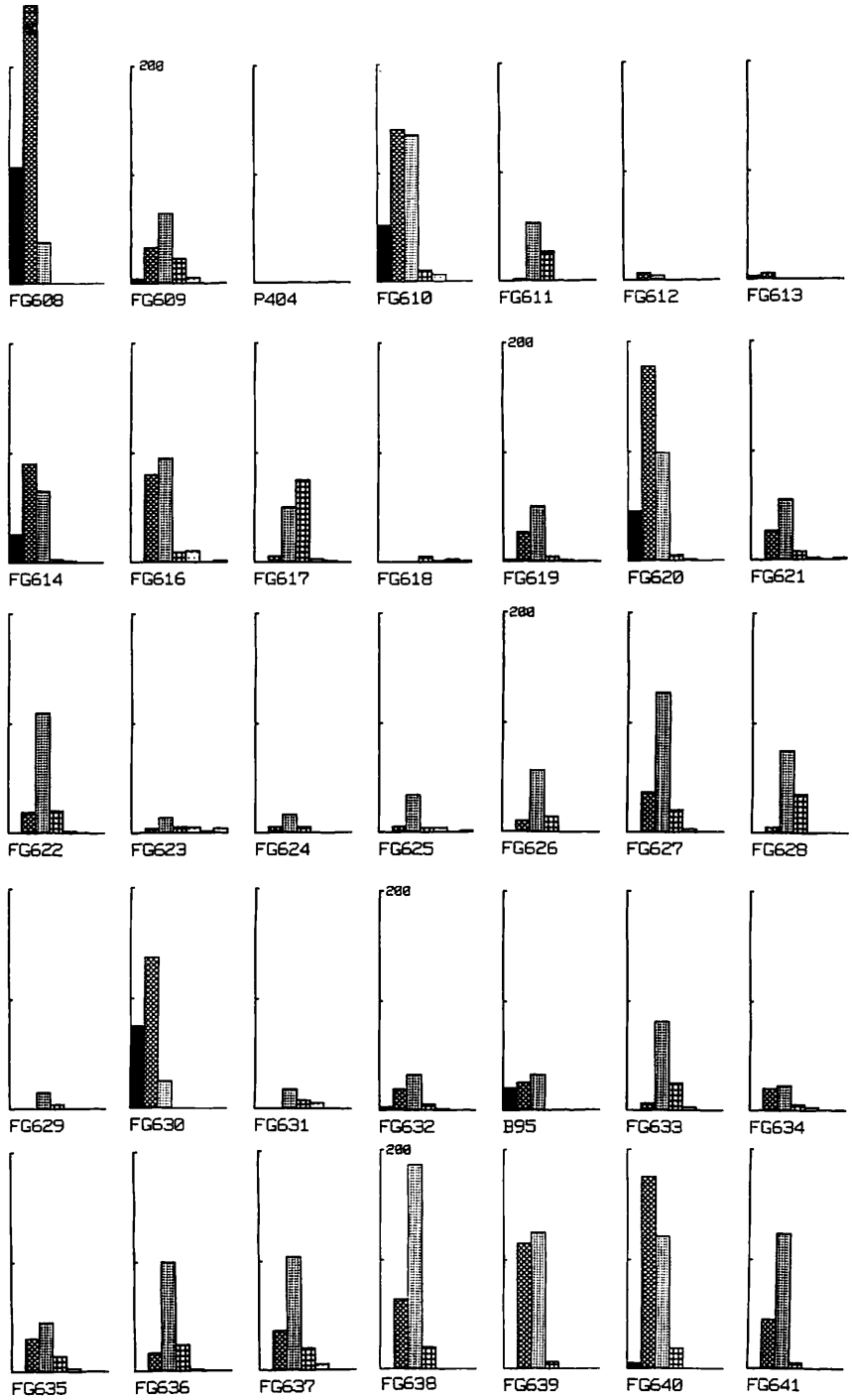

Fig. VIII-4 (continued)

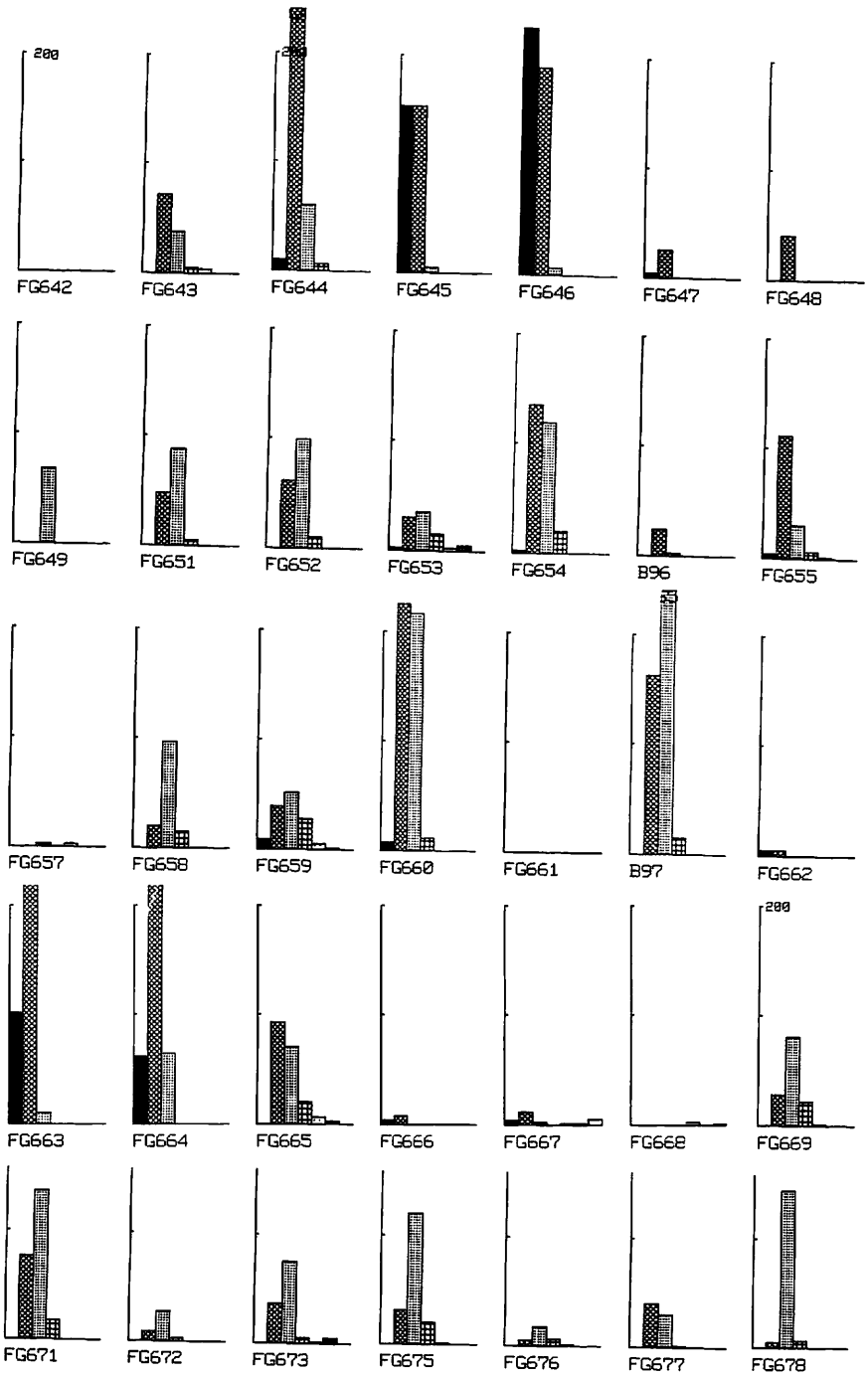

Fig. VIII-4 (continued)

deposits which are often associated with thin coverage by siliceous surface sediments. In the plots of nodule coverage and abundance (Fig. VIII-6) we find a significant correlation between them but no plots are on the abundance axis, which is consistent with exposed nature of sea-bed nodules. Our experience of on-board operation of box cores together with free-fall grabs reveals that the total weight of recovered nodules by free-fall grabs occasionally underestimate the abundance due to incomplete grab operation in case of high-abundance nodule pavement on the sea bed.

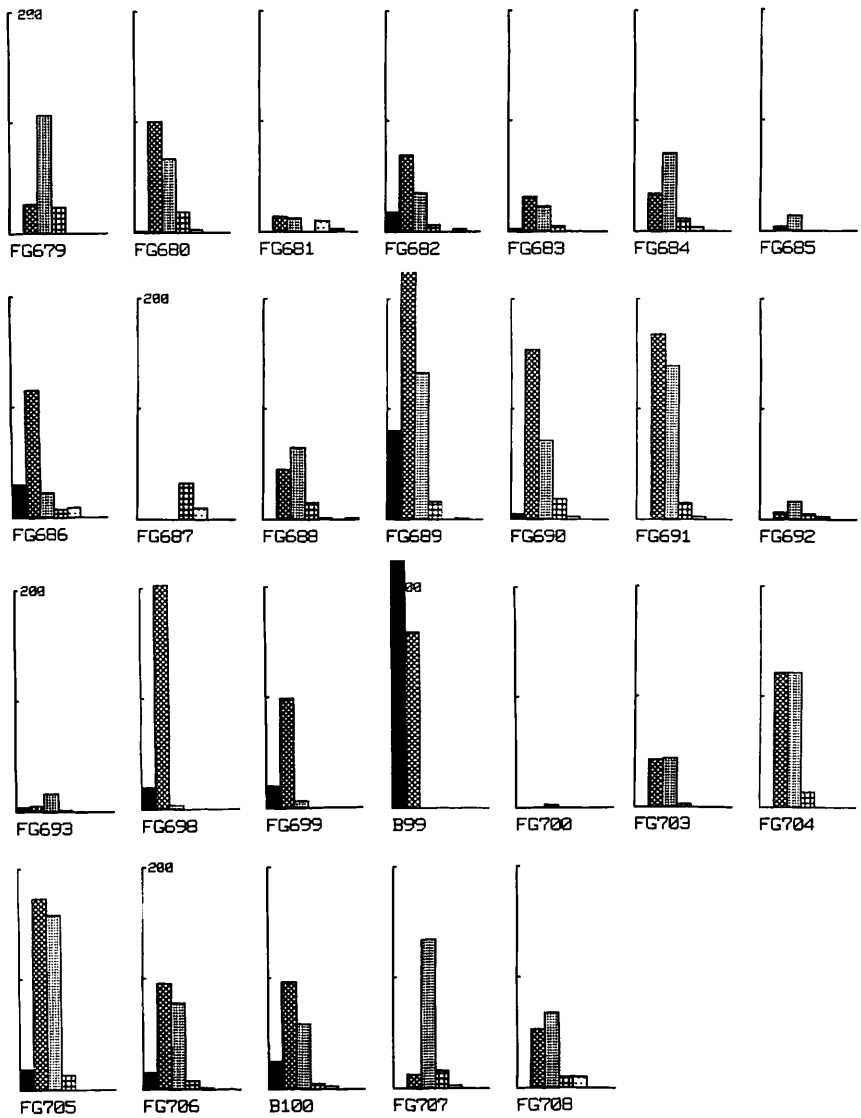

Fig. VIII-4 (continued)

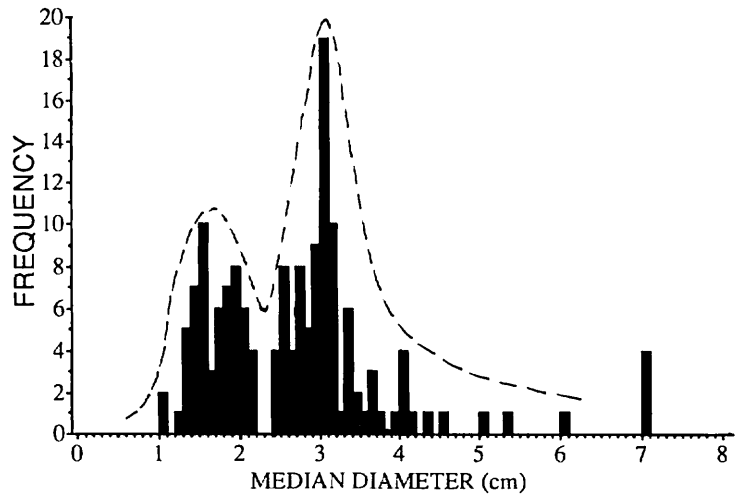

Fig. VIII-5 Frequency diagram of median diameter for nodules from each sampler.

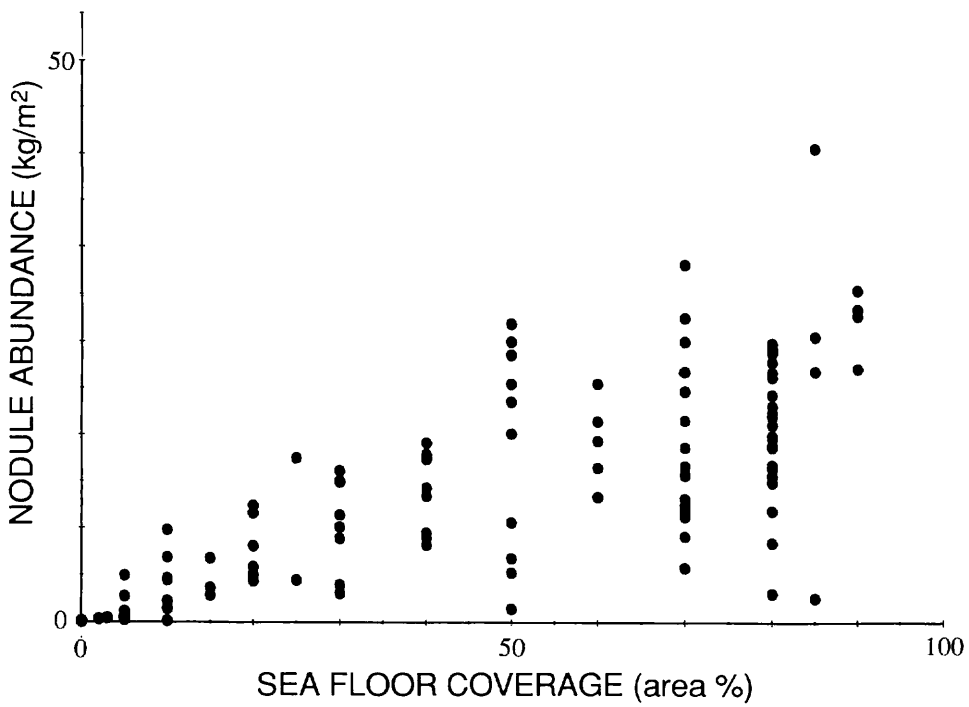

Fig. VIII-6 Plots of nodule abundance and seafloor coverage. Note a positive correlation.

Together with sea-bed photography, the observed nodule abundances are rather greater than the nodules in the Central Pacific Basin (Usui and Moritani, 1991) and Northeast Manganese Nodule Belt (Halbach *et al.*, 1988). The abundance ranges from 0 to 40 kg/m^2, and is greater than 20 kg/m^2 in a third of total sampling sites in this area. The abnormally high abundance of sea floor nodules and closely packed nature of large nodules have been observed only in areas of strong bottom current such as the Samoan Passage floors in the South Pacific (Bäcker *et al.*, 1976).

Another typical feature of manganese deposits of this area is frequent occurrence of manganese crusts which cover the outcrop of consolidated old clayey rocks. Similar occurrence of manganese crusts are known on some volcanic pinnacles on the Manihiki Plateau to the west of the survey area (Grau and Kudrass, 1991).

Large and flattened nodules usually contain highly altered volcanic rocks, fossil shark teeth, and/or old claystones. Components of the nuclei are markedly different from associated surface sediments but rather similar to pre-Neogene claystone from the depth of cores. This evidence strongly suggests that those material have been lifted upward during sedimentation and served as nodule nuclei without burial.

Characterization of manganese nodule facies

Based on the general description of nodules and crusts in the above section, manganese nodule/crust facies is classified to the following three types.

Facies A (small-size and low-abundance nodules): Many small nodules (up to about 2 cm in diameter, Fig. VIII-7: see in Appendix VIII-2) are dispersed on the sea bed. Thickness of oxide is up to several millimeters. Its abundance ranges from traceable to about 5 kg/m^2. The shape is generally discoidal with frequent polynucleated feature.

Facies B (large-size and high-abundance nodules): Large nodules (2 to 12 cm in diameter, Fig. VIII-7: see in Appendix VIII-2) are nearly closely packed on the sea bed. Abundance ranges from 10 to 40 kg/m^2. The shape is generally spherical in case of a small nucleus, but sometimes elongated or flattened with large block of nuclei. Thickness of oxide layer ranges from 10 to 40 mm. The outermost thin brownish oxide layer is common, which covers the inside older nodules. The outer layer is megascopically similar to the encrusting layers of small nodules of Facies A. Small nodules similar to Facies A are occasionally associated with this facies at a single site.

Facies C (manganese crust): Encrustation on outcrops of hard rocks and large boulders, or flattened plates like hardpans. The occurrence is mainly observed by sea-bed photographs, but few samples can be recovered.

The typical facies of nodules are shown in Figure VIII-7. The areal distribution of these three facies are variable throughout the GH83-3 survey area and even within the detailed survey area (50×60 km^2).

Regional and local variation of manganese nodule facies

During the 30-nautical mile grid survey, there found no significant difference in regional variation pattern between the eastern and western basins within the survey area (Figs. 8 and 9), except that nodules are rare on the bottom of the trough. Nodule facies is variable rather on the scale of several kilometers than regional scale, as

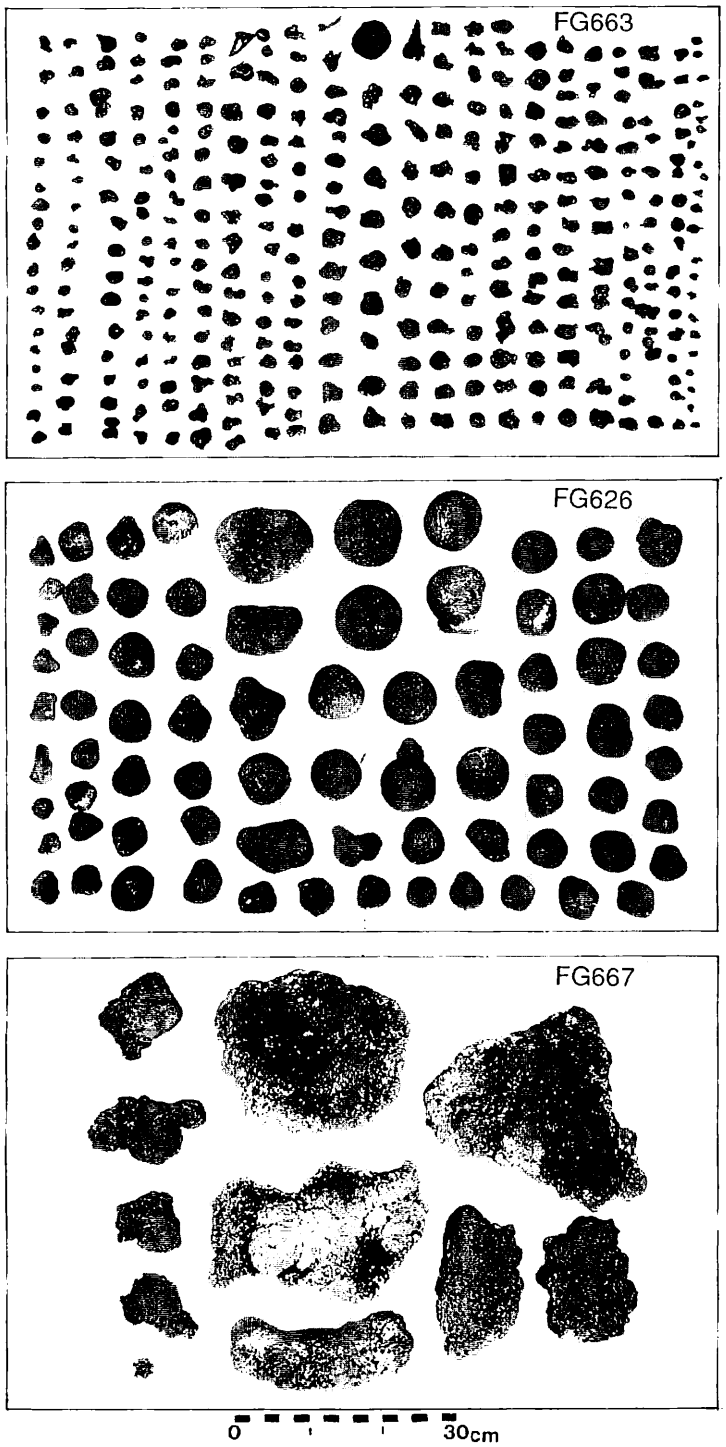

Fig. VIII-7 Typical facies of manganese nodules collected by freefall grabs (photo taken by Dr. K. Harada).

revealed based on the small-scale sampling in the detailed survey area.

In the detailed survey area, facies A, B, and C are irregularly distributed despite monotonically flat topography at depths between 5100–5250 m, although Facies B is dominant. Within a small box (12°54′S–13°10′S, 159°07′W–159°22′W) of the detailed survey area, the three facies occupy specific area over the flat floors. We find no clear relationship between nodule facies and topography. However the lithology of substrate is quite variable on the scale of kilometers in the box. A comparative study of 13 sediment cores and 3.5 kHz subbottom profiles (SBP) revealed three characteristic lithological units I, II, and III (Nishimura *et al.*, Chapter III of this volume; Nishimura and Saito, Chapter IV of this volume). Unit I (highly transparent) is unconsolidated reddish pelagic-zeolitic brown clay sediment, Unit II (semi-opaque) is semiconsolidated dark brown pelagic clay sediment, and Unit III (opaque, acoustic basement on SBP records) is alternation of semiconsolidated pelagic clay and yellow-

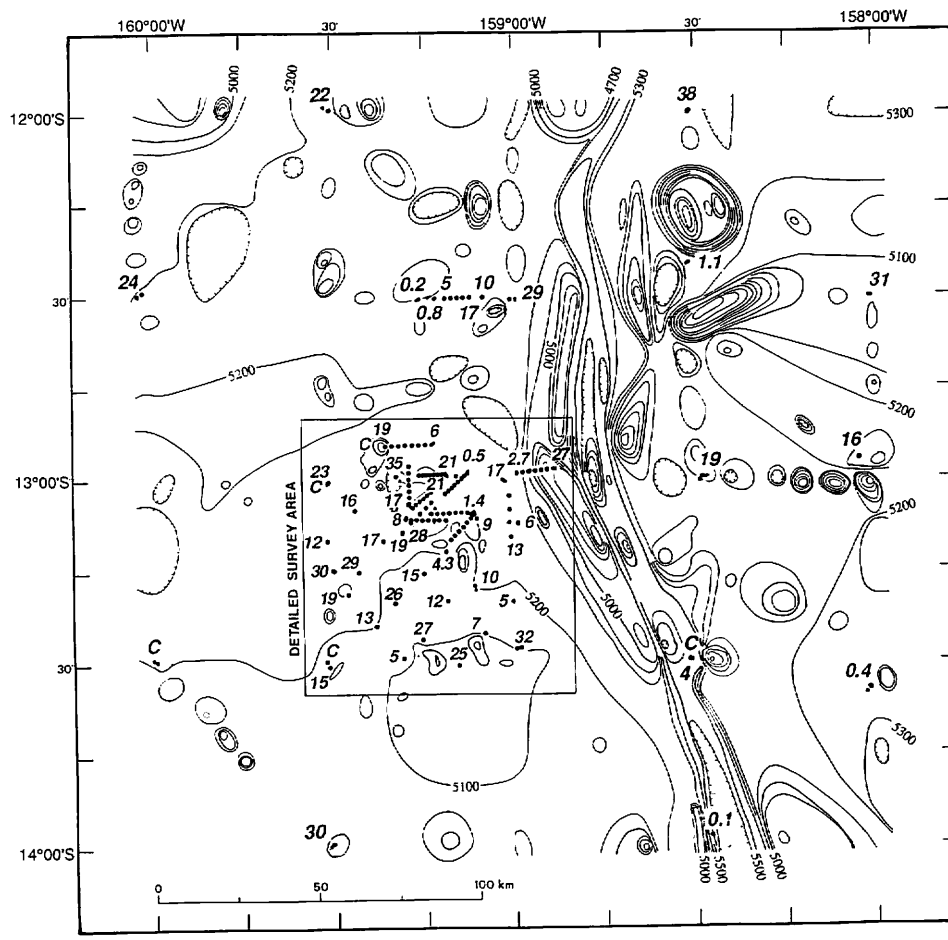

Fig. VIII-8 Distribution of abundance of manganese nodules in the GH83-3 area (only grid survey). Data in kg/m². C means occurrence of manganese crusts.

ish brown stiff claystone. Nishimura and Saito found pre-Miocene (probably Oligocene to Cretaceous) microfossils from Unit II and Unit III, and suggest a long-term sedimentary hiatus between Units I and II.

A plot of nodule abundance over the distribution map of lithological units of the sea floor demonstrates a nice agreement of nodule facies to subbottom sediments. In Figure VIII-10, Unit I with variable thickness of several meters to 30 meters yields low abundance of small manganese nodules (=Facies A), whereas Unit II does abundant large-nodule deposits (=Facies B). Outcrop of Unit III distributed like windows in the box is covered with manganese crusts (=Facies C), suggesting no sedimentation or erosion during a long period. This relationship between nodule facies and lithology is well demonstrated along line profiles in Figure VIII-11 together with topography and 3.5 KHz SBP. The relationship is again observed outside the detailed area.

The plots of nodule abundance and thickness of Unit I (Fig. VIII-12) also support

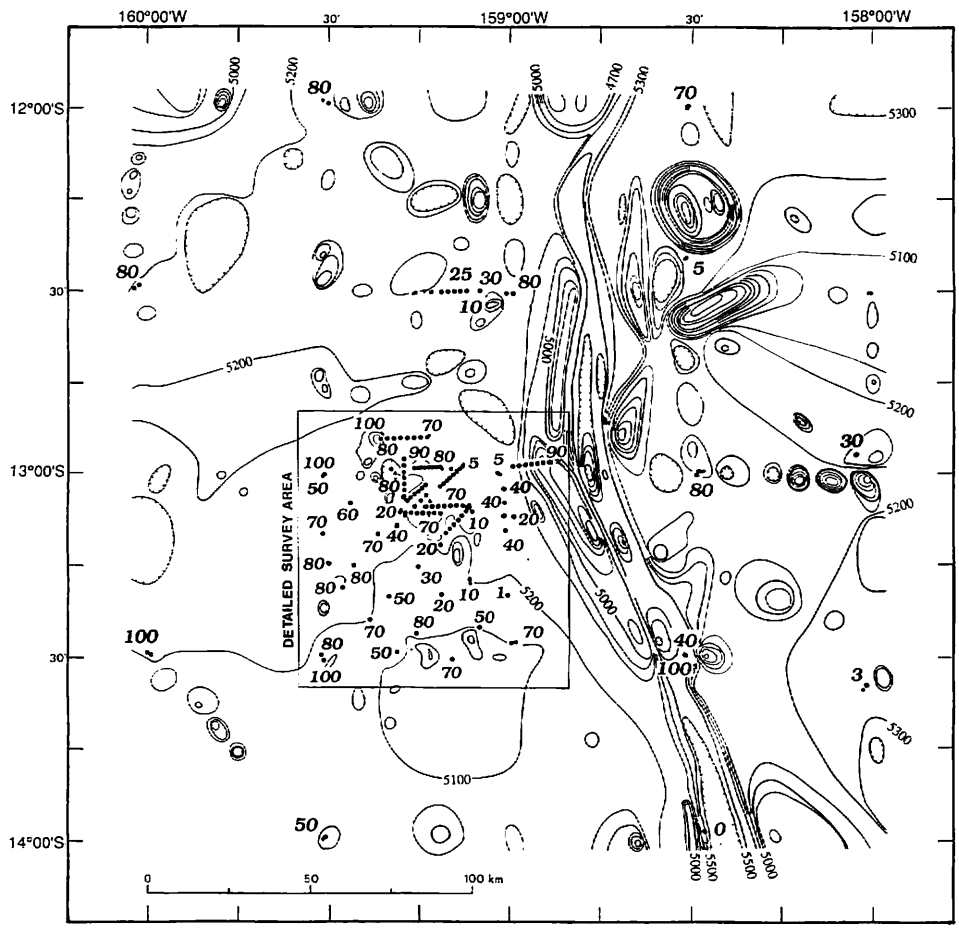

Fig. VIII-9 Distribution of sea floor coverage of manganese nodules in the GH83-3 area (only grid survey). Data in area percent.

that thick young (Neogene - Quaternary) sediments is not preferable to abundant nodule growth. It is interpreted that a continuous pelagic sedimentation of Unit I has prevented nodules from growing. The age of bottom of Unit I is unknown, but a rather high sedimentation rate can be assumed.

This relationship is most probably related to strong bottom currents of the Antarctic Bottom Water (AABW). Our data of nodule facies and sediment distribution strongly support the idea that a long-term continuous flow of oxygenated water promoted abundant manganese nodule fields over the survey area. Pautot and Melguen (1976) assumed a branch of AABW flow to the northeast passing through Aitutaki Passage into the Penrhyn Basin on the basin of previous bottom water temperature data. Yamazaki (Chapter XII of this volume), by contrast, suggested a clockwise flow of AABW around the Manihiki Plateau and a southward or eastward branch to the Penrhyn Basin. An abundant nodule field around the Aitutaki Passage and western margin of the Penrhyn Basin (Fig. VIII-2) prefers the former assumption.

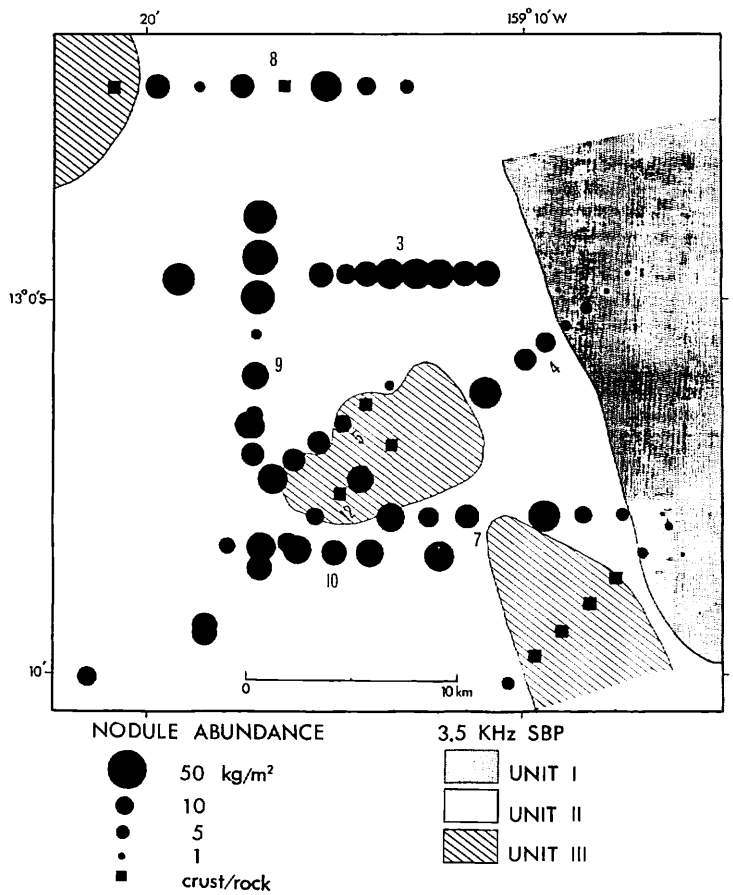

Fig. VIII-10 Relationship between distributions of nodule abundance and acoustic units. Note a agreement of nodule facies and lithological units. Numbers on the map denote line numbers.

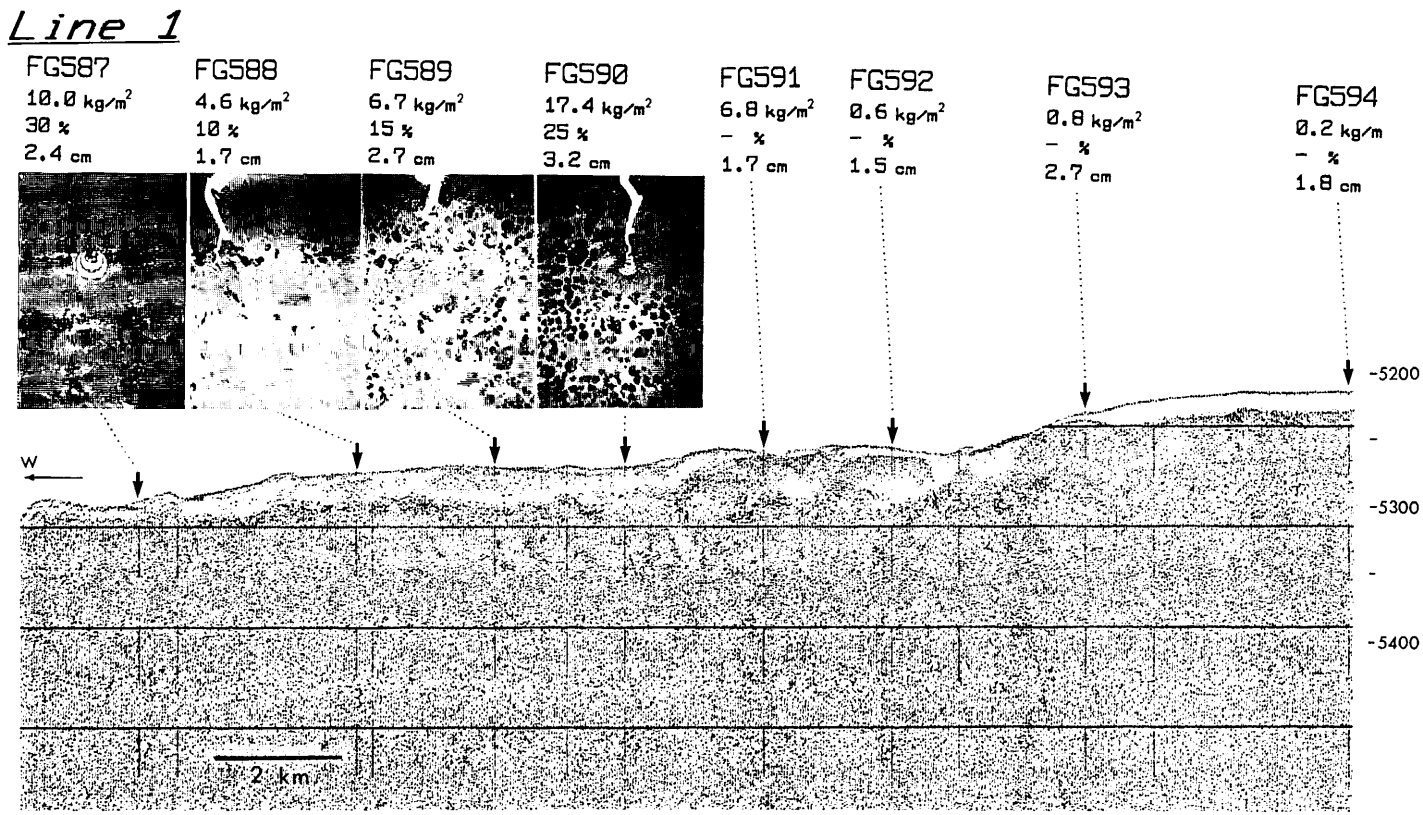

Fig. VIII-11 Local variation of manganese nodule facies along SBP line profiles. For line numbers see in Figure VIII-10.

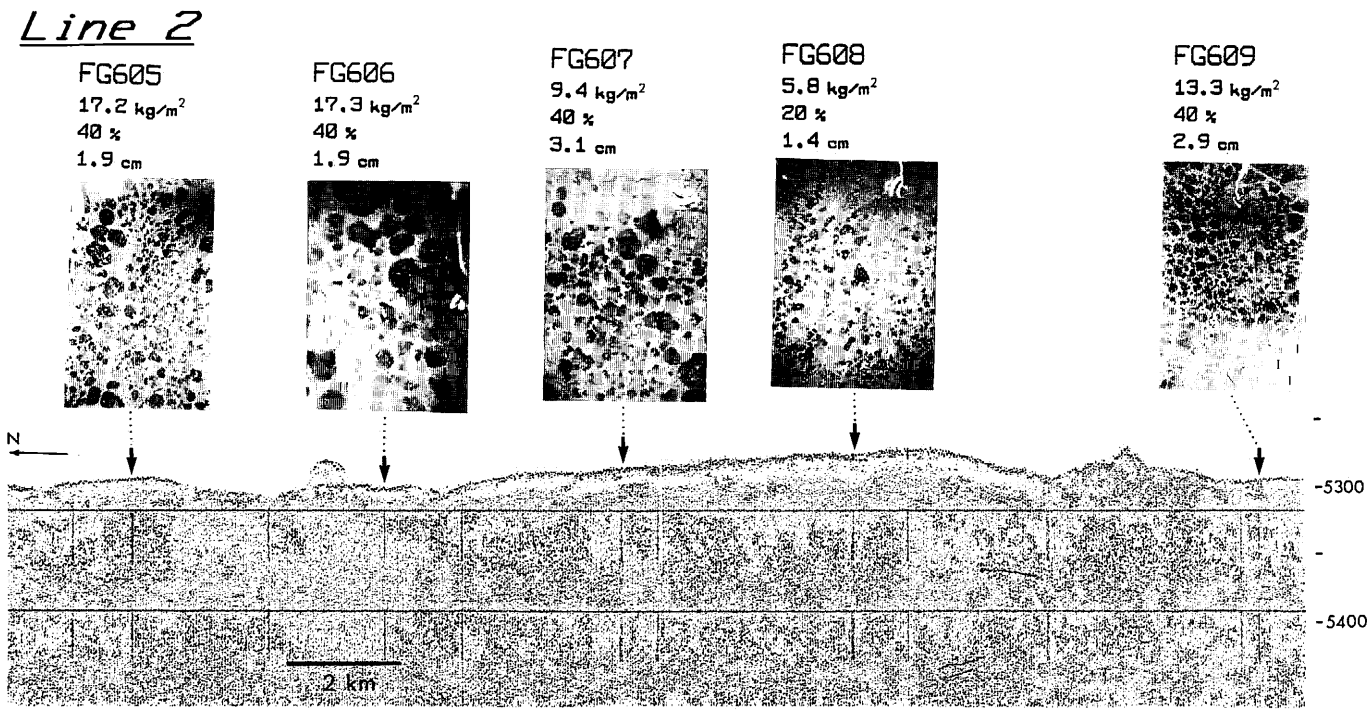

Fig. VIII-11 (continued)

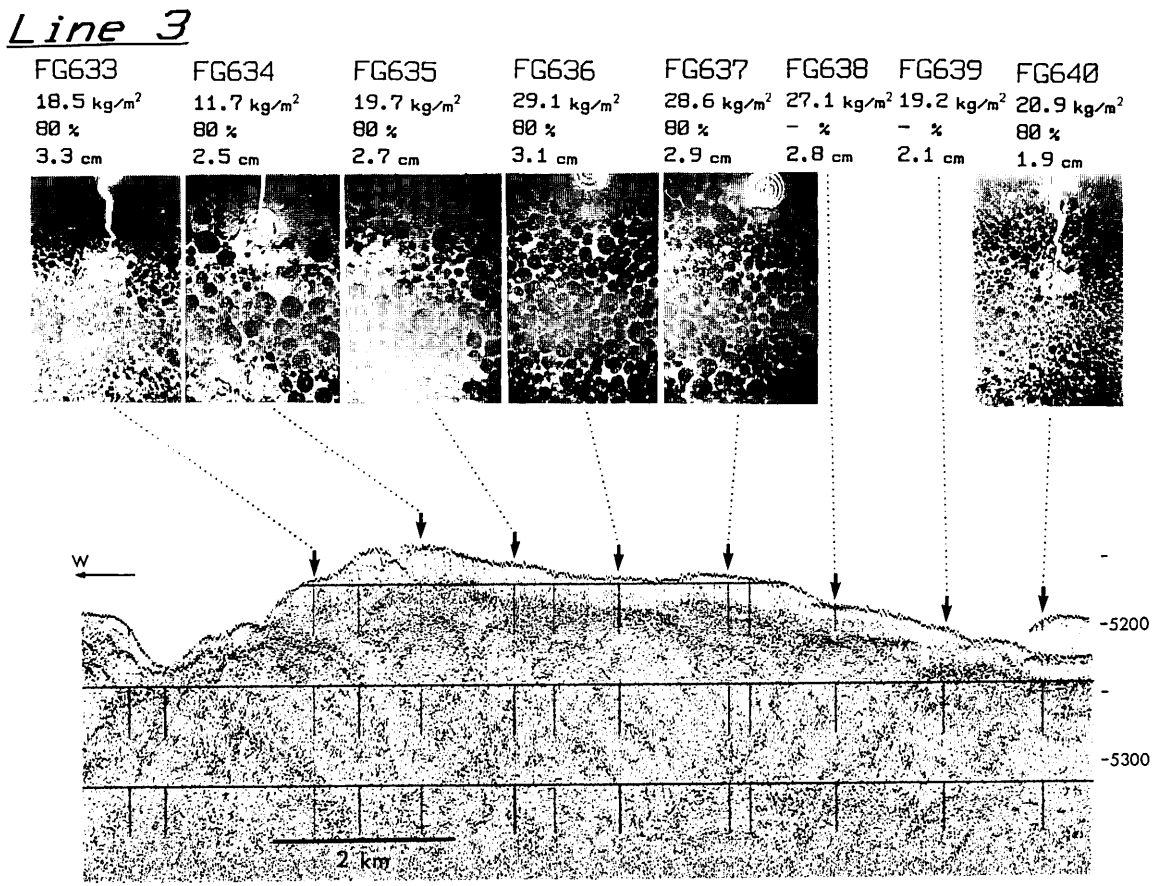

Fig. VIII-11 (continued)

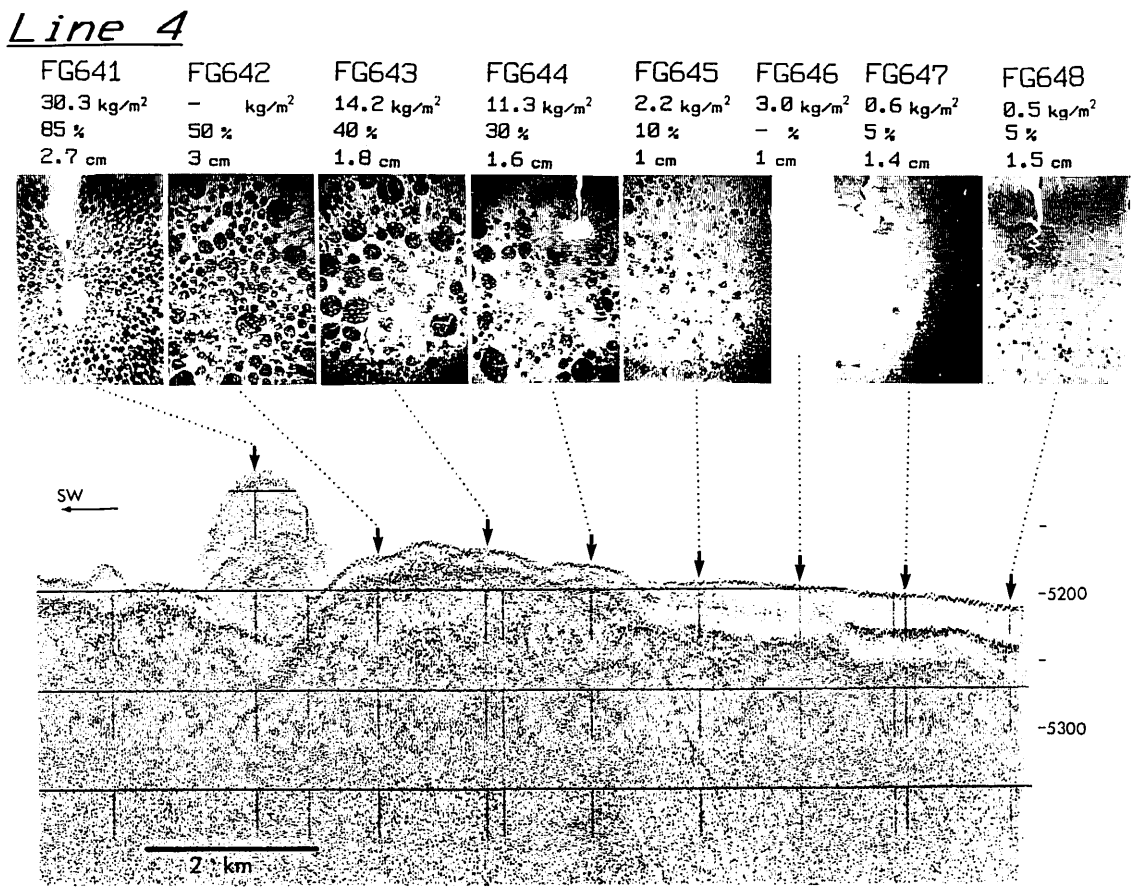

Fig. VIII-11 (continued)

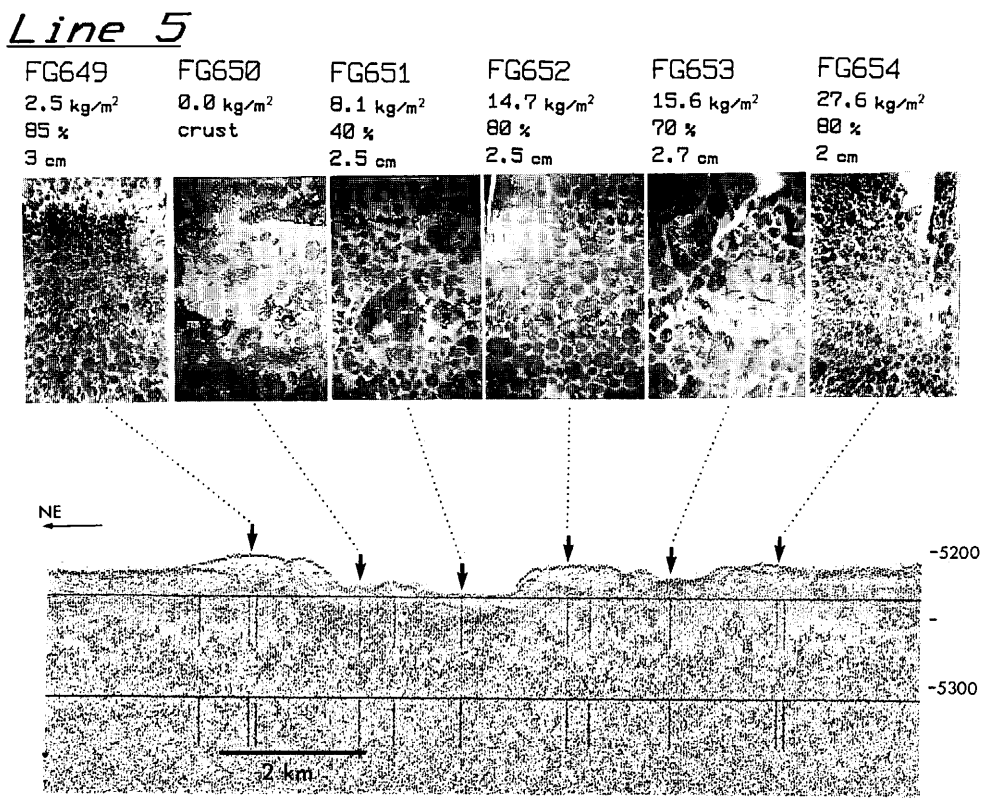

Fig. VIII-11 (continued)

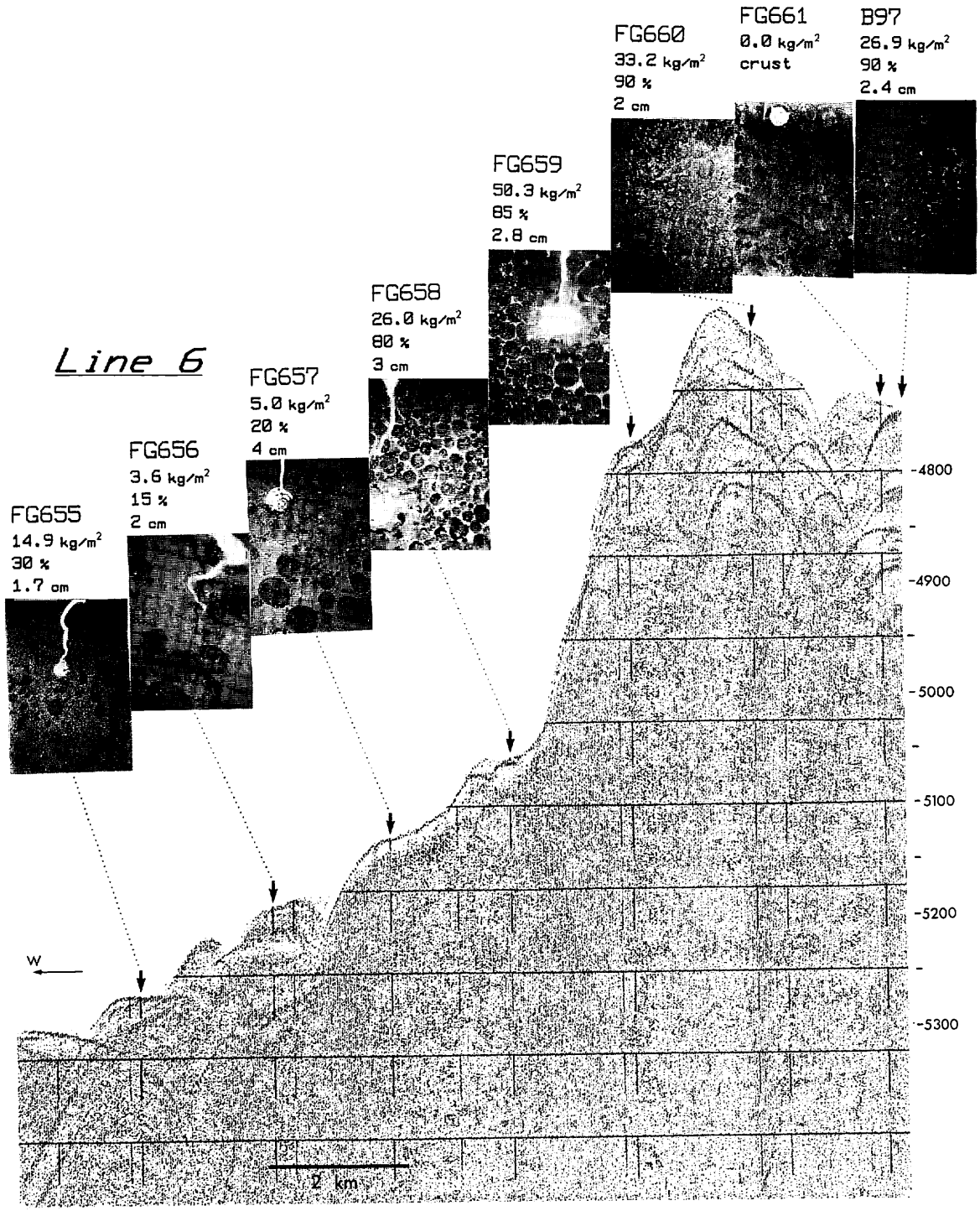

Fig. VIII-11 (continued)

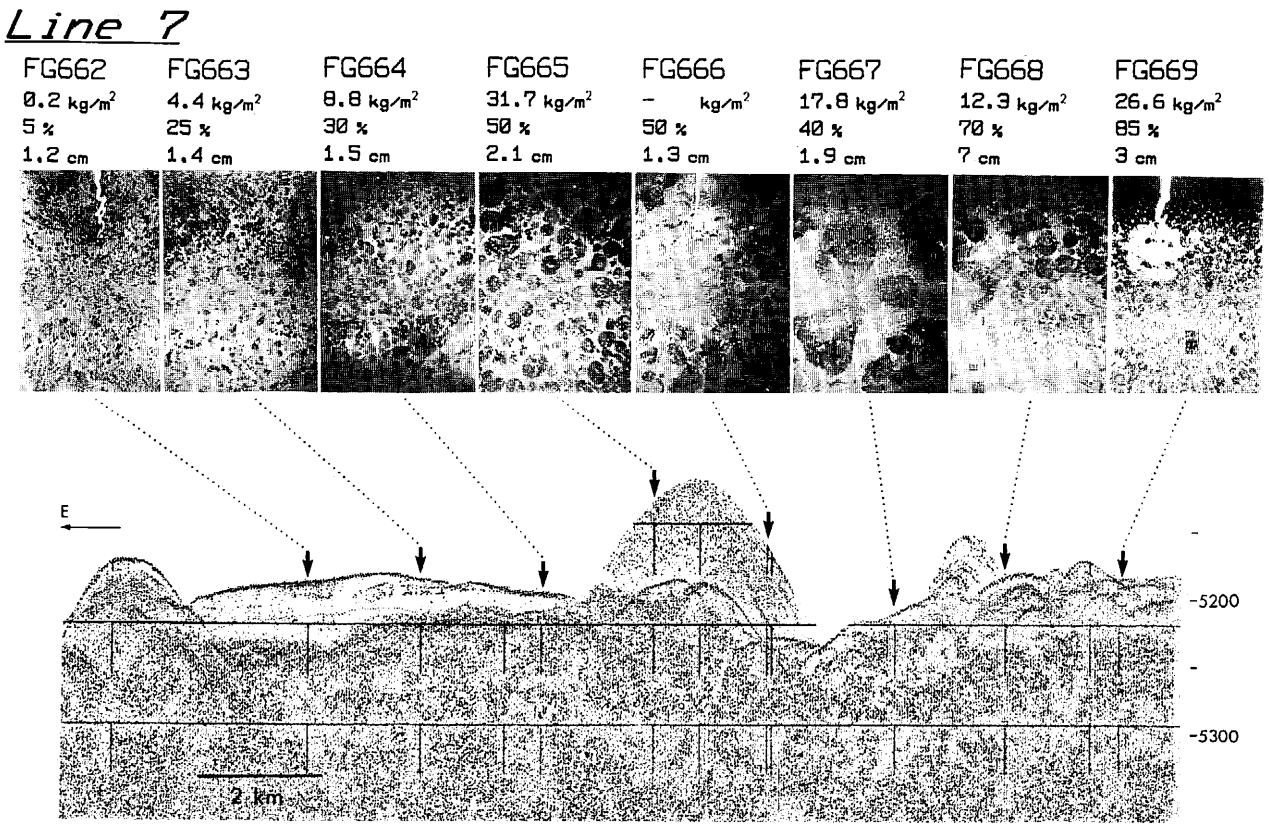

Fig. VIII-11 (continued)

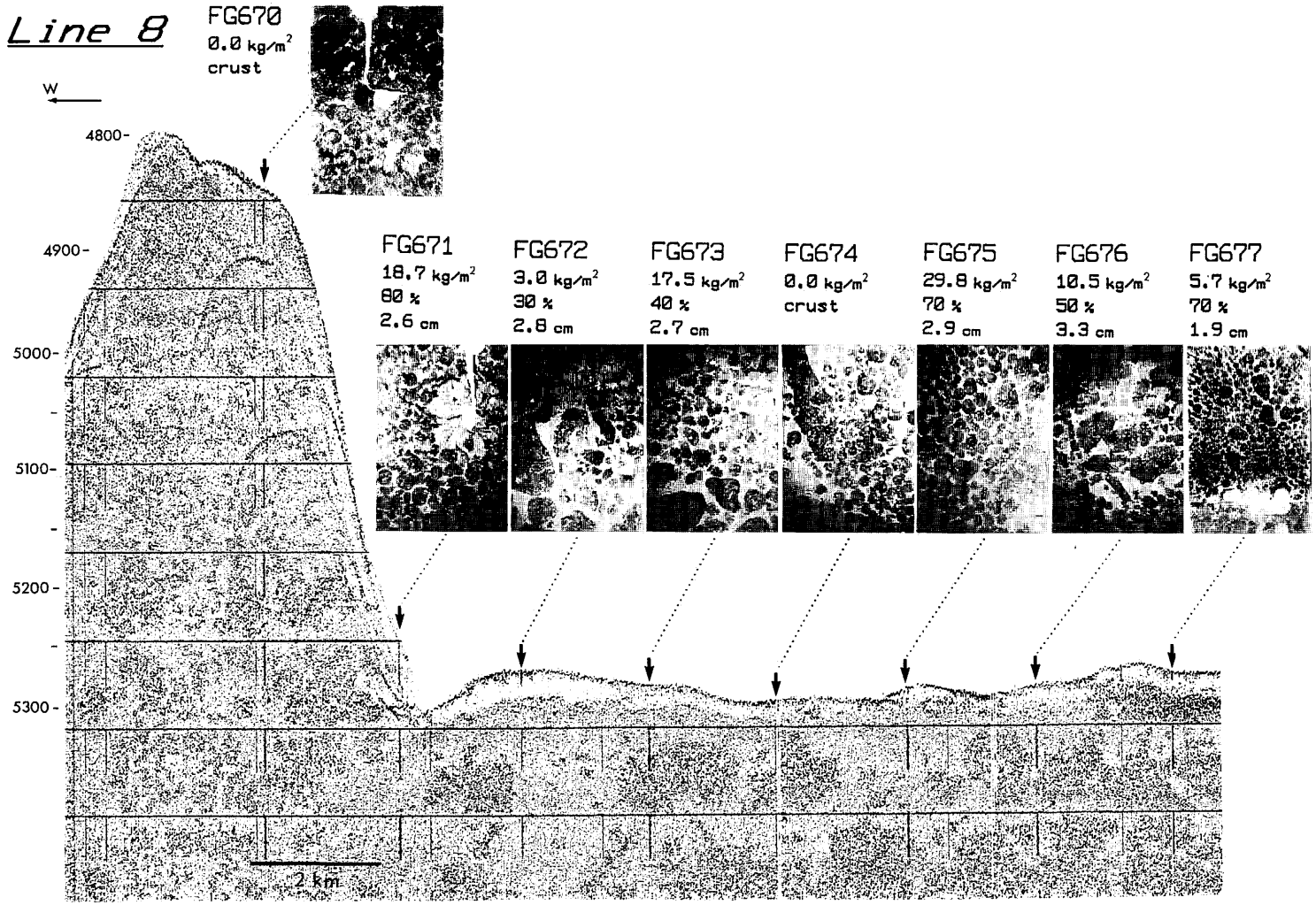

Fig. VIII-11 (continued)

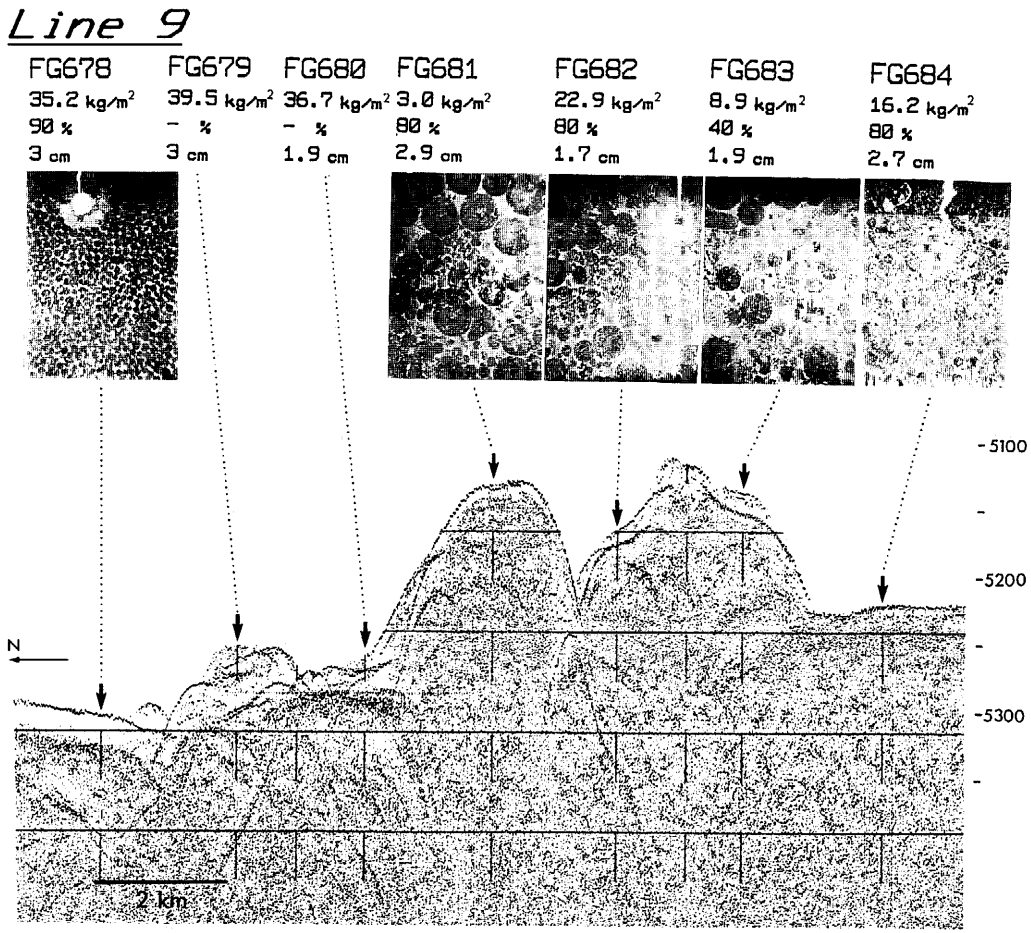

Fig. VIII-11 (continued)

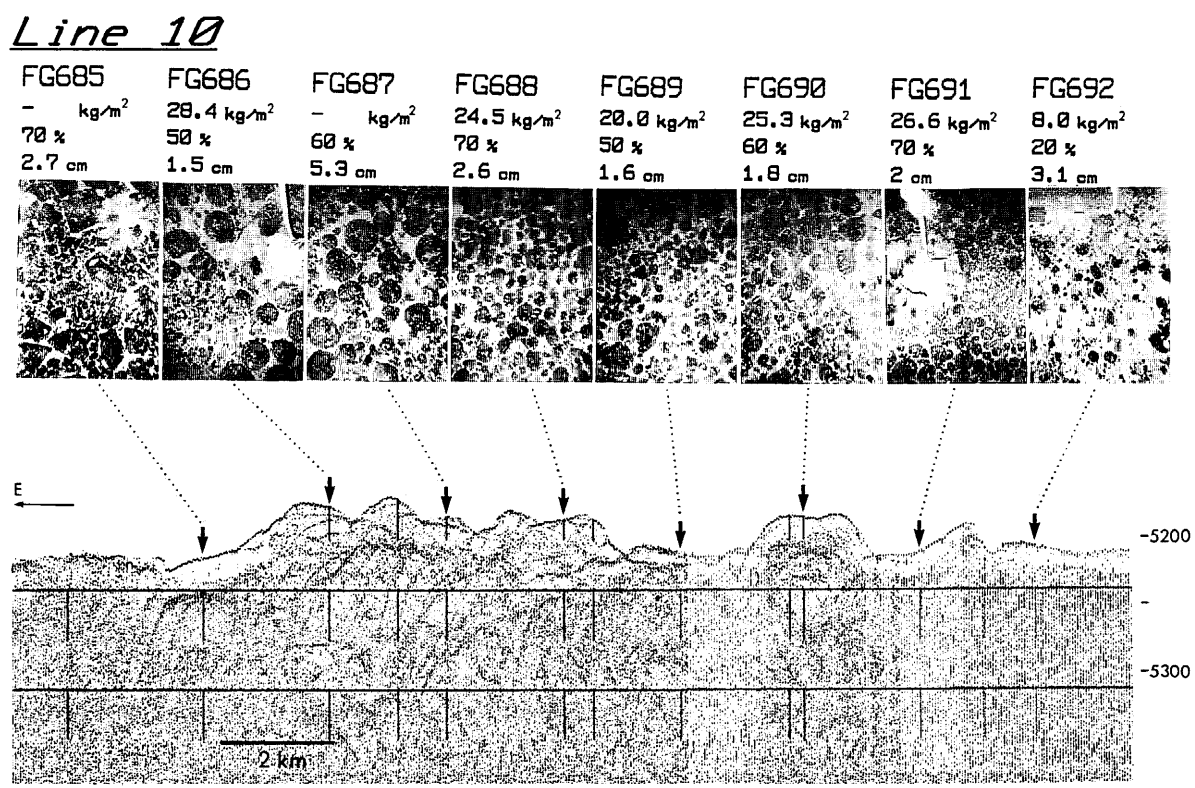

Fig. VIII-11 (continued)

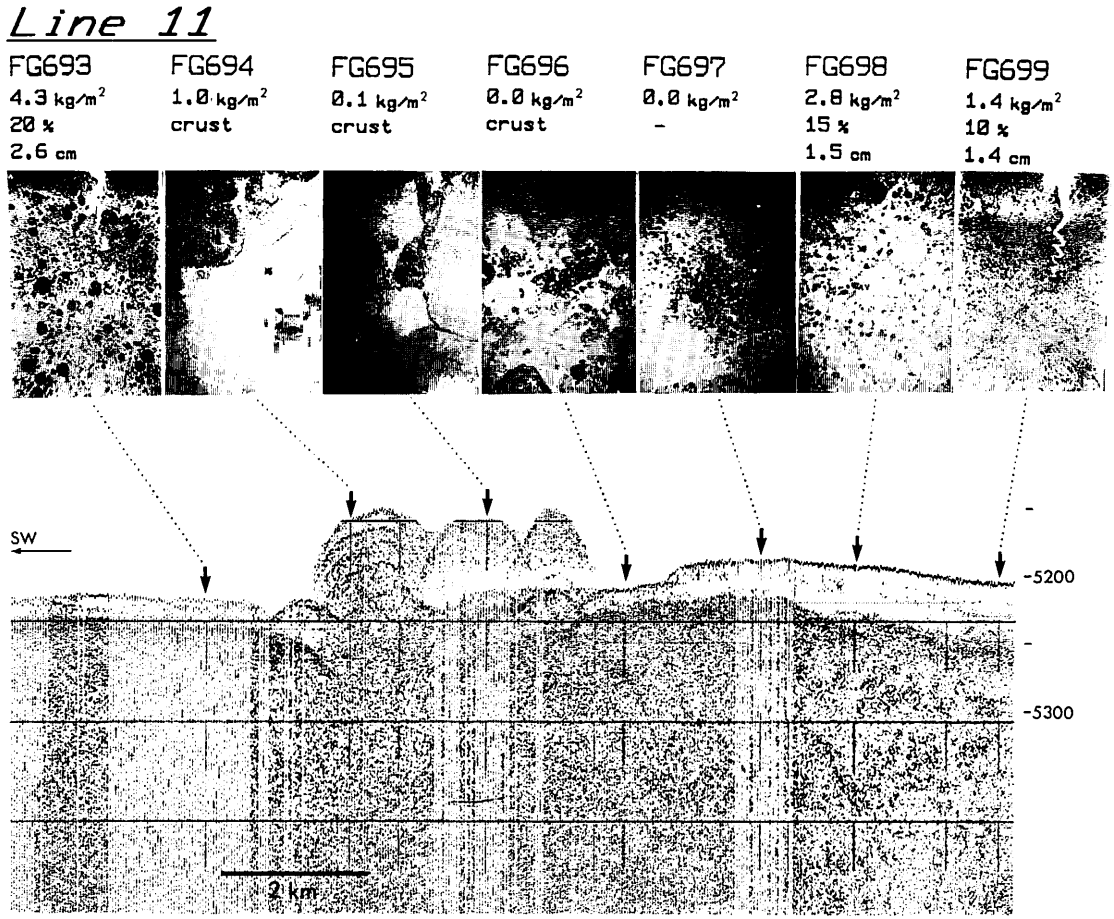

Fig. VIII-11 (continued)

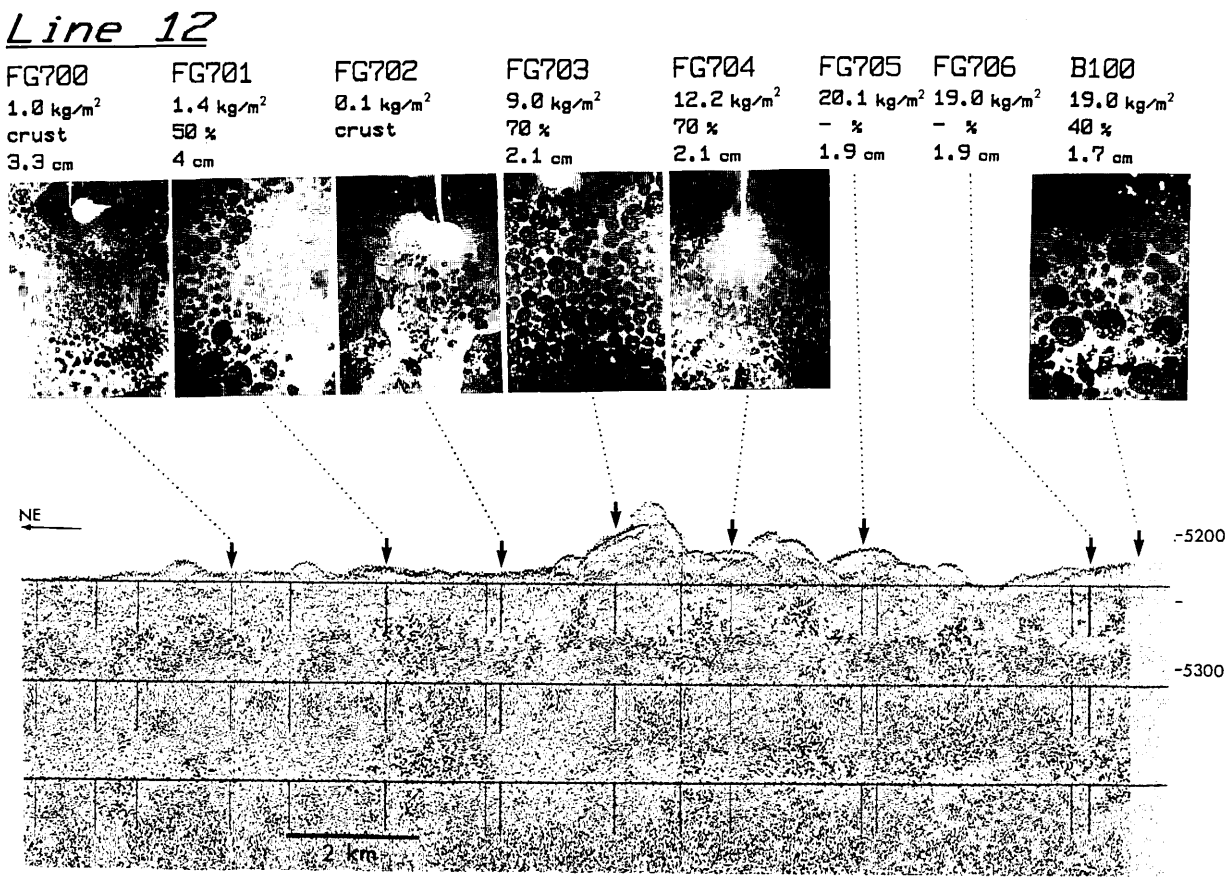

Fig. VIII-11 (continued)

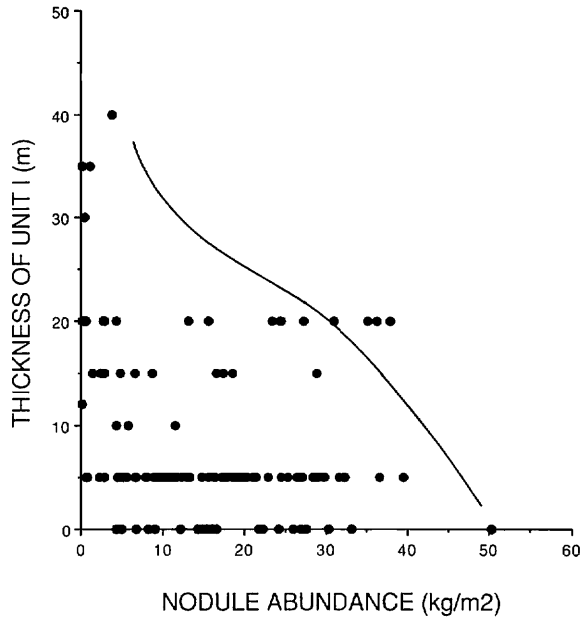

Fig. VIII-12 Plots of thickness of Unit I on 3.5 kHz SBP versus nodule abundance.

It is considered that AABW flows into the Penrhyn Basin through the Aitutaki Passage during a long geologic time and possibly at present, and runs northward as western boundary currents. This currents may have been optimal for growth of manganese nodules and crusts under the condition of substantially no sedimentation or partly erosion.

Age of nodules

The following radiochemical and paleontological data constrain the ages of growth of nodules. Only one ^{10}Be measurement of a spherical nodule of 6.5 cm diameter collected within the survey area during the previous cruise GH80-1 (13°47.15'S, 159° 28.26'W: 5147 m water depth) shows a very slow growth rate, 1.07 mm/m.y. (pers. comm., Dr. Teruo Inoue, Daiich Isotope Laboratory, 1986). If assumed a zero age at the nodule surface, the age of nucleus is extrapolated as 30 Ma (Oligocene).

Fossil shark teeth often serve as nuclei of nodules (Fig. VIII-13). Many of large shark teeth may be identified *Megalodon Carcharodon* which assigns Oligocene to Miocene. Another paleontological evidence of old age of the nodules is the Dictyomitra-type radiolarian (probably Cretaceous: A. Nishimura, pers. comm.) found as a nucleus cemented by hydrothermal manganese oxide (Usui and Mita, Chapter IX of this volume).

Another evidence is a nice coincidence in physical and chemical characteristic between the nodules buried within Unit II sediments (Cretaceous to Oligocene; Nishimura and Saito, this volume) in piston cores and the innermost old nodules within the large nodules on sea bed. This shows that some of the old nodules formed during Cretaceous through Neogene have been uplifted and accumulated thick

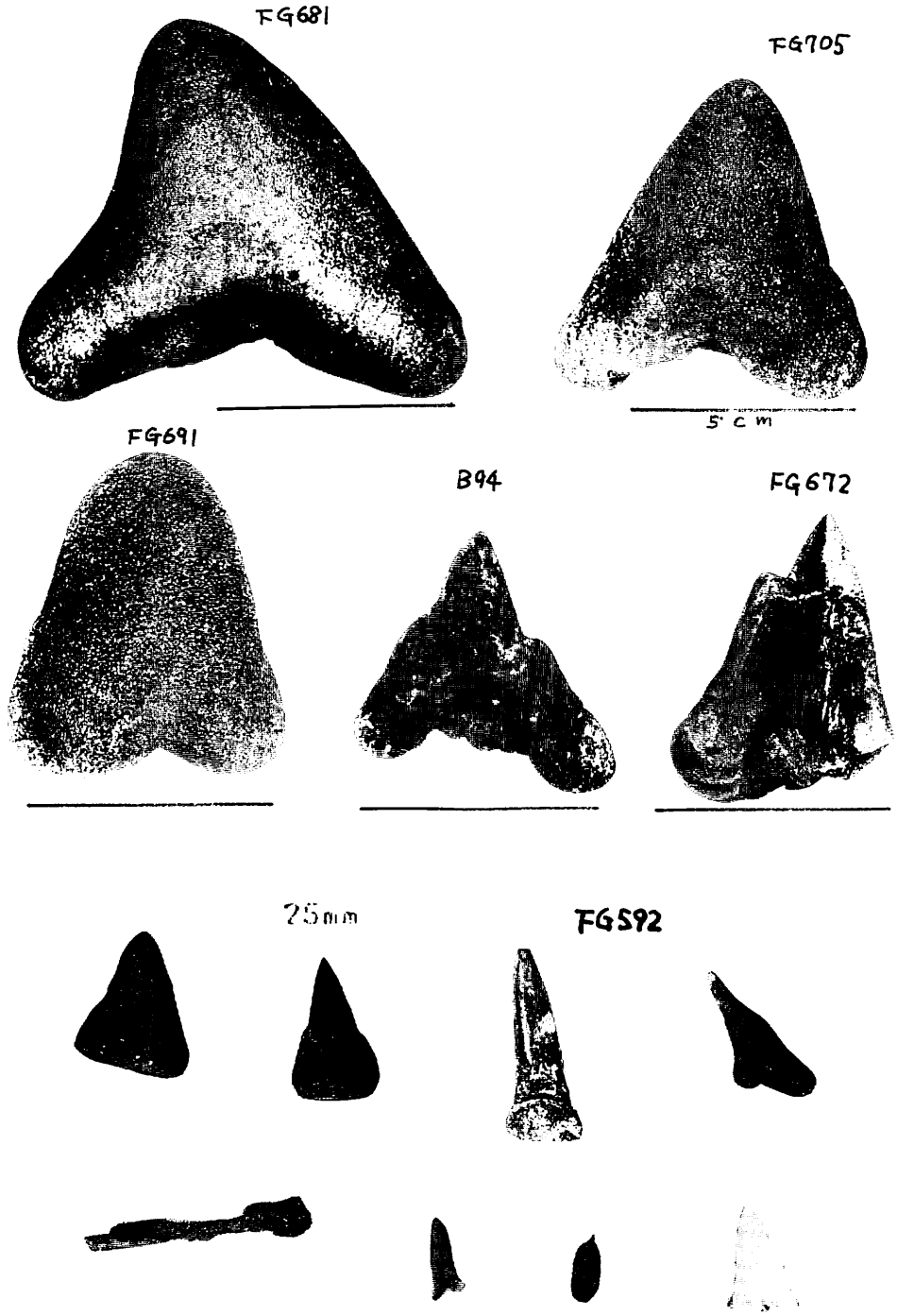

Fig. VIII-13 Some of collected shark teeth often covered with several-centimiter thick manganese oxide layers.

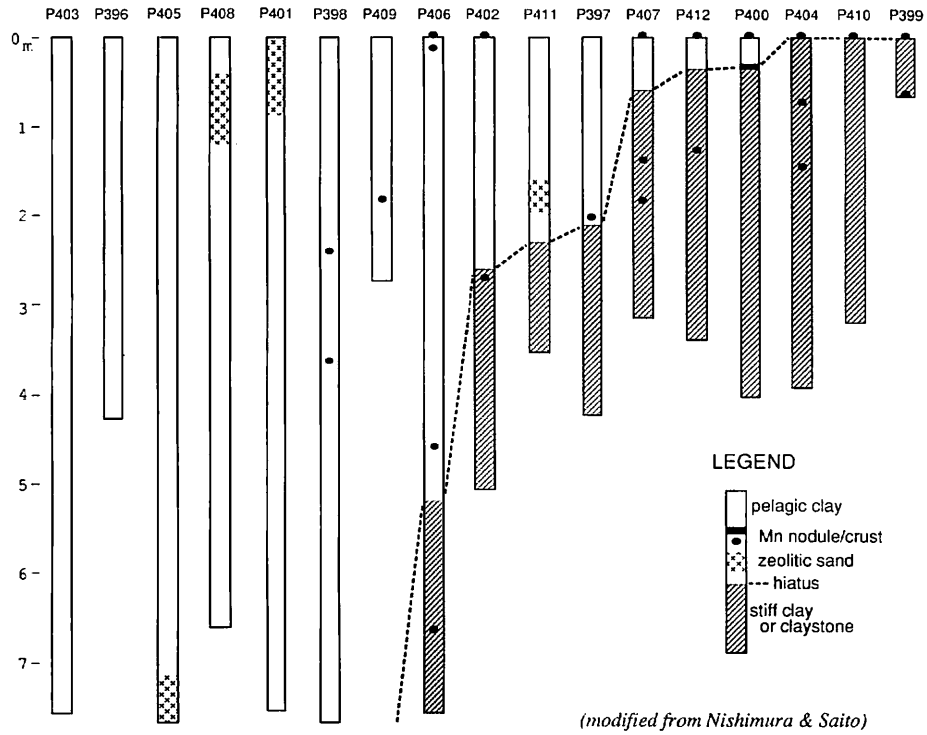

Fig. VIII-14 Occurrence of manganese nodules on sediment surface and buried within piston cores. The thick dashed line (hiatus) is the boundary between Unit I and Unit II. Note more frequency occurrence of nodules below it.

younger layers but some were left behind and buried within ambient sediments. Figure VIII-14 shows the relationship of occurrence of buried nodules and lithological units in piston cores.

All of these age data most probably indicate a slow and probably continuous growth of thick (up to about 4 cm) manganese oxide layers since Cretaceous or later.

Summary

High-abundance (up to 40 kg/m^2) manganese nodule field extend over the southwestern part of the Penrhyn Basin. Collected nodules in the GH83-3 area are hydrogenetic nodules of type s (smooth surface). The nodule facies are classified into three types: 1) Large nodule deposits which have grown since the Cretaceous or Paleogene in the areas of traceable younger sedimentary unit (Unit I). 2) Small nodule deposits which have grown during the sedimentation of Unit I since Neogene time, 3) Manganese crusts which cover outcrops of Unit II in the areas of long-term erosion or no sedimentation. The relationship of nodule facies to sedimentary units are most probably affected by active inflow of Antarctic Bottom Water which probably runs northward as a western boundary current along the eastern margin of Manihiki

Plateau and promoted nodule growth.

References

Bäcker, H., Glasby, G.P. and Meylan, M.A. (1976) Manganese nodules from the Southwestern Pacific Basin. *New Zealand Ocenogr. Field Rept.*, No. 6, pp. 88.

Grau, R. and Kudrass, H.R. (1991) Pre-Eocene and younger manganese crusts from the Manihiki Plateau, South Pacific Ocean. *Marine Mining*, vol. 10, p. 231-246.

Landmesser, C.W., Kroenke, L.W., Glasby, G.P., Sawtell, G.H., Kingan, S., Utanga, E., Utanga, A. and Cowan, G. (1976) Manganese nodules from the South Penrhyn Basin, Southwest Pacific. *South Pacific Marine Geological Notes*, vol. 1, no. 3, p.17-40.

Glasby, G.P. (1981) Manganese nodule studies in the Southwest Pacific 1975-1980: A Review. *South Pacific Marine Geological Notes*, vol. 2, no. 3, p.37-46.

Halbach, P., Friedrich, G. and von Stackelberg, U. (1988) *The Manganese Nodule Belt of the Pacific Ocean.* F. Enke Verlag, Stuttgart, pp. 254.

Monzier, M. and Missegue, F. (1977) Polymetallic nodules sampling in the Cook Islands archipelago: "Danaïdes 2" and "Geotransit 2" Surveys. *Preliminary Report of ORSTOM,* Unpublished manuscript.

Pautot, G. and Melguen, M. (1979) Influence od deep water circulation and sea floor morphology on the abundance and grade of Central South Pacific Manganese Nodules. In: Bischoff, J.L. and Piper, D.Z. (eds.), *Marine Geology and Oceanography of the Pacific Manganese Nodule Province,* Plenum Press, Marine Science ser., vol. 9, p. 621-649.

Metal Mining Agency of Japan (1986) Ocean Resources Investigation in the Sea Area of CCOP/SOPAC: *Report on the Joint Basic Study for the Development of Resources.* vol. 1, Sea Area of Cook Islands, JICA-MMAJ, Tokyo.

———— (1987) Ocean Resources Investigation in the Sea Aea of CCOP/SOPAC: *Report on the Joint Basic Study for the Development of Resources.* vol. 2, Sea Area of Cook Islands, JICA-MMAJ, Tokyo.

Moritani, T., Maruyama, S., Matsumoto, K., Ogitsu, T. and Moriwaki, H. (1977) Description, classification, and distribution of manganese nodules. *Geol. Surv. Japan Cruise Rept.*, no. 8, p. 136-158.

Usui, A. (1983) Regional variation of manganese nodule facies on the Wake-Tahiti Transect: morphological, chemical and mineralogical study. *Mar. Geol.*, 54, p. 27-51.

———— (1984) Mineralogy and internal structure of manganese nodules of the GH80-5 area. *Geol. Surv. Japan Cruise Rept.*, no. 20, p. 215-226.

———— (1986) Local variability of manganese nodule deposits in the GH81-4 area. *Geol. Surv. Japan Cruise Rept.*, no. 21, p. 98-159.

———— (1992) Regional and local variations of manganese nodule deposits in the southern part of the Central Pacific Basin (GH82-4 area). *Geol. Surv. Japan Cruise Rept.*, no. 22, p. 145-217.

Usui, A. and Moritani, T. (1992) Manganese nodule deposits in the Central Pacific Basin: Distribution, geochemistry, mineralogy, and genesis. In: B.H. Keeting and B.R. Bolton (eds.), *Geology and Offshore Mineral Resources of the Central Pacific Basin,* Springer-Verlag, N.Y., vol. 14, p. 205-223.

——— and Nakao, S. (1984) Local variability of manganese nodule deposits in the GH80-5 area. *Geol. Surv. Japan Cruise Rept.*, no. 20, p. 106-164.

———, Nishimura, A., Tanahashi, M. and Terashima, S. (1986) Local variability of manganese nodule facies on small abyssal hills of the Central Pacific Basin. *Mar. Geol.*, vol. 74, p. 237-275.

Appendix VIII-1 Sample list and results of shipboard observations of manganese nodules.

St#	Sam#	Cov	Sed.	Manganese nodule deposits												Buried nodules //other samples
				type	abd.	size distribution (in number)						median	total thick.	internal structure [nuclei]	poly.	<RESULT OF OPERATION>
		(%)			kg/m2	>10	10-8	8-6	6-4	4-2	2-1<1 cm	(cm)	(g) (mm)		no%	
3901	B85	-	cO		0.0	-	-	-	-	-	-		0		-	
3902	FG563	80	pC	ISs, ISPs	21.8	0	0	0	15	164	33	0 2.9	2515	8 monotonous dense layer [shark teeth]	40	
	FG564	70	pC	IDPs, DPs	15.5	0	0	0	13	188	34	0 2.9	1794	8 monotonous dense layer	70	//shark tooth
	FG565	60	zrC	IDPs, IDs	13.2	0	0	0	11	181	26	0 2.9	1524	8 monotonous dense layer [shark teeth]	90	
	FG566	100	-	Vs	5.9	1	0	0	0	0	0	0 <10>	680	8 monotonous dense layer [claystone]	-	
	P396	-	zC	ISPs	-	0	0	0	0	0	1	0 <1.5>	2	-	-	
3903	FG567	80	pC	Ss, ISs	24.1	0	1	8	17	15	9	0 4.1	2781	20 monotonous dense layer [claystone]	50	
	FG568	100	-	Fs	0.1	0	0	0	0	0	1	0 <1.5>	1	-	100	
	B86	-	pC	Ss, ISs	21.8	0	0	3	29	69	10	0 3.3	3313	20 laminated layer with radial pattern [claystone]	10	
3904	FG569	50	zC	Ss, ISs	29.8	1	1	0	15	101	23	0 2.9	3445	15 laminated layer with radial pattern (soft nodule inside) [claystone]	10	
	FG570	60	zrC	Ss, ISs	21.3	0	1	1	15	77	11	0 3.1	2465	20 laminated layer with radial pattern [claystone, shark teeth]	20	crust and nodule (85g) at 200 cm depth
	P397	-	zC	ISPs	-	0	0	0	0	2	0	0 <3>	20	10 monotonous dense layer	100	
3905	FG571	100	-	IDs, IDPs	1.3	0	0	1	0	1	0	0 <4>	155	20 monotonous dense layer [claystone]	50	
	FG572	100	-	Cs	-	-	-	-	-	-	-	- -	0		-	
	B87	-	-		-	-	-	-	-	-	-	- -	-		-	<UNSUCESSFUL>
3906	FG573	0	zC		0.0	-	-	-	-	-	-	- -	0		-	
	FG574	0	zrC	Vs	0.1	0	0	0	0	1	0	0 <3>	7		-	
	P398	-	zrC		-	-	-	-	-	-	-	- -	0		-	nodule (5 g) at 231 cm depth
	P398											-			0	nodule (3 g) at 368 cm depth
3907	FG575	60	-	ISs, IDs	19.2	1	1	3	3	16	3	0 3.3	2221	20 laminated layer with radial pattern [claystone]	10	//shark tooth
	FG576	70	zrC	Ts, ISs	32.3	0	6	5	13	33	5	0 3.6	3732	15 laminated layer with radial pattern (soft nodule inside) [mudstone]	20	
	B88	-	zrC	ISs	-	0	0	0	0	8	0	0 3	-	20 laminated layer with radial pattern [mudstone]	0	
3908	FG577	2	zC	IDPs	0.3	0	0	0	1	1	0	0 <4>	29	-	100	
	FG578	3	zC	IDs, IDPs	0.4	0	0	0	0	7	3	1 2.4	52	7 monotonous dense layer [mudstone]	50	
	P399	-	-	Cs	-	0	0	0	0	1	0	0 <3>	11	22 laminated layer with radial pattern [mudstone]	-	nodule(22 g) at 58 cm depth
3909	FG579	100	-	Cs	0.0	-	-	-	-	-	-	- -	0		-	
	FG580	30	zC	IDs, IDPs	3.9	0	0	0	7	10	1	0 3.6	455	5 monotonous dense layer [mudstone]	30	
	B89	-	-		-	-	-	-	-	-	-	- -	-		-	<UNSUCESSFUL>
3910	FG581	100	-	Cs	-	-	-	-	-	-	-	- -	0		-	
	FG582	50	zrC	IDs, IDPs	23.4	4	2	2	9	41	18	0 3	2705	20 monotonous dense layer [mudstone, shark teeth]	50	
	P400	-	zrC	IDs	-	0	0	0	0	8	2	0 2.8	40	7 monotonous dense layer	30	crust at 43 cm depth//zeolitic claystone
3911	FG583	80	-	Ts, IDs	15.4	0	0	4	12	81	6	0 3.1	1776	4 monotonous dense layer [claystone]	20	
	FG584	80	-	Ts, IDs	8.3	0	1	0	9	20	8	0 3.1	956	4 monotonous dense layer [claystone]	20	
	B90	100	-	Cs	-	-	-	-	-	-	-	-	-		-	<UNSUCESSFUL>

Appendix VIII-1 (continued)

St#	Sam#	Cov	Sed.	Manganese nodule deposits												Buried nodules //other samples
				type	abd.	size distribution (in number)						median	total thick.	internal structure [nuclei]	poly.	<RESULT OF OPERATION>
		(%)			kg/m2	>10	10-8	8-6	6-4	4-2	2-1<1 cm	(cm)	(g)	(mm)	no%	
3912	FG585	80	pC	Ts, IDs	28.8	0	1	7	29	59	0	3.6	3335	20 monotonous dense layer [shark teeth]	10	
	FG586	80	zrC	IDs, Ds	16.6	0	0	2	34	20	0	4.5	1920	15 monotonous dense layer [claystone, shark teeth]	10	
	B91	70	pC	Ts, IDs	18.5	0	2	9	24	70	10	3.4	2816	15 monotonous dense layer [chert?]	10	
3913	FG587	30	zrC	IDPs, IDs	10.0	1	0	0	7	26	14	2.4	1156	15 monotonous dense layer [claystone]	10	
3914	FG588	10	zrC	IDs, IDPs	4.6	0	0	0	1	60	75	1.7	529	10 monotonous dense layer [claystone]	30	//shark tooth
3915	FG589	15	pC	IDPs, IDs	6.7	0	0	1	5	58	21	2.7	771	10 monotonous dense layer [claystone]	40	
3916	FG590	25	zrC	IDs, IDPs	17.4	2	1	1	11	64	4	3.2	2014	15 monotonous dense layer [claystone]	10	//shark tooth
3917	FG591	-	zrC	IDs, IDPs	6.8	0	0	0	3	53	88	1.7	782	20 monotonous dense layer	30	//shark tooth
3918	FG592	-	pC	IDs, IDPs	0.6	0	0	0	0	6	35	1.5	70	5 monotonous dense layer	30	
3919	FG593	-	zrC	IDs, IDPs	0.8	0	0	0	0	11	3	2.7	593	5 monotonous dense layer	50	
3920	FG594	-	zrC	IDs, IDPs	0.2	0	0	0	0	2	4	1.8	18	10 monotonous dense layer [claystone]	30	
	P401	-	zC		-	-	-	-	-	-	-	-	0		0	
3921	FG595	-	pC	Ss, ISs	36.4	0	0	15	12	41	37	12	2.5	4205	40 monotonous dense layer (soft nodule inside)	20	
	FG596	-	-	Ss, ISs	24.4	0	1	6	8	19	31	18	1.8	2823	35 monotonous dense layer [claystone, mudstone]	30	
	B92	70	zrC	Ss, ISs	37.9	0	1	18	13	28	114	100	1.3	5785	20 monotonous dense layer, laminated layer with radial pattern [claystone]	40	
3922	FG597	-	zC	Ss, Ts	30.9	2	0	6	5	69	171	132	1.4	3567	30 laminated layer with radial pattern [claystone]	30	//shark tooth
	FG598	-	zC	Ss, ISs	27.2	0	0	3	14	40	13	4	3	3140	35 laminated layer with radial pattern [claystone]	10	
	P402	-	zC		-	0	0	0	0	7	0	0	3	101	15 monotonous dense layer	-	2 nodules (3 g) at 270 cm depth
	P402												-			0	nodule (1 g) at 393 cm depth
3923	FG599	-	zrC	Ts, IDPs	20.2	0	4	6	10	48	19	0	3	2331	15 monotonous dense layer [claystone]	30	
	FG600	80	-	Ts, IDs	18.6	1	2	2	4	58	38	0	2.5	2153	20 monotonous dense layer [claystone, shark teeth]	40	
	B93	-	zrC	Ss	-	0	0	0	1	7	0	0	3.1	140	20 monotonous dense layer [volcanic rock]	-	
3924	FG601	-	-		-	-	-	-	-	-	-	-	-	-		-	<UNSUCESSFUL>
	FG602	5	zrC	Ds, DPs	1.1	0	0	0	0	5	47	25	1.3	124	5 monotonous dense layer	20	
	P403	-	zC		-	-	-	-	-	-	-	-	-	0		-	
3925	FG603	5	zrC	IDPs, IDs	0.4	0	0	0	1	1	0	1	<3>	46	10 monotonous dense layer [claystone]	70	
	FG604	5	zC	Ds, IDs	2.7	0	0	0	1	10	139	44	1.4	315	5 monotonous dense layer [shark teeth]	30	//zeolitic claystone
	B94	-	-	IDPs	0.5	0	0	1	0	6	16	6	1.5	78	4 monotonous dense layer [shark teeth]	20	
3926	FG605	40	zC	Ts, IDPs	17.2	3	1	2	5	42	56	4	2	1988	10 monotonous dense layer [claystone]	20	
3927	FG606	40	zC	Ts, IDPs	17.3	2	1	6	4	24	49	0	1.9	2003	20 monotonous dense layer, laminated layer (soft nodule inside) [claystone	40	
3928	FG607	40	zC	Ts, IDPs	9.4	0	1	4	5	51	6	0	3.1	1090	8 monotonous dense layer [mudstone, shark teeth]	50	//shark tooth
3929	FG608	20	zrC	Ds, IDs	5.8	0	0	0	1	38	257	108	1.4	670	8 monotonous dense layer [shark teeth?]	30	//shark tooth
3930	FG609	40	zrC	Ts, Fs	13.3	0	0	5	23	64	33	4	2.9	1535	5 monotonous dense layer [claystone, mudstone]	20	
	P404	-	-	IDs	-	0	0	1	0	0	0	0	<7>	85		-	nodule (3 g) at 79 cm depth

Appendix VIII-1 (continued)

St#	Sam#	Cov	Sed.	Manganese nodule deposits												Buried nodules //other samples
			type	abd.	size distribution (in number)							median	total thick.	internal structure [nuclei]	poly.	<RESULT OF OPERATION>
		(%)		kg/m2	>10	10-8	8-6	6-4	4-2	2-1	<1 cm	(cm)	(g)	(mm)	no%	
	P404											-			0	nodule (<1 g) at 155 cm depth
	P404											-			0	nodule (12 g) at 180 cm depth
3931	FG610	70	pC	IDs, IDPs	21.4	0	0	7	11	135	140	52	1.9	2475	30 laminated layer with radial pattern [claystone]	30	
3932	FG611	90	pC	Ss, ISs	32.5	0	0	0	27	53	2	0	3.5	3761	20 laminated layer with radial pattern [claystone]	0	
3933	FG612	-	zrC	IDPs	0.3	0	0	0	0	4	7	0	1.8	29	5 monotonous dense layer [mudstone]	40	
3934	FG613	10	zrC	IDs, IDPs	0.1	0	0	0	0	0	6	3	1.3	13	5 monotonous dense layer [mudstone]	10	
3935	FG614	20	zrC	Ts, IDs	11.5	1	0	2	3	65	90	26	1.8	1325	25 laminated layer (soft nodule inside) [shark teeth, claystone]	30	//shark tooth
3936	FG615	10	-	IDs, Ts	9.7	1	2	1	1	1	1	0	7	1126	30 laminated layer with radial pattern [claystone]	0	
	P405	-	zrC		0.0	-	-	-	-	-	-	-	-	0		-	
3937	FG616	80	pC	ISs, IDs	28.9	2	1	11	9	95	80	0	2.4	3341	25 monotonous dense layer, laminated layer with radial pattern [claystone]	20	//shark tooth
3938	FG617	70	pC	ISs, IDs	11.5	0	2	3	76	51	5	0	4.3	1335	25 monotonous dense layer, laminated layer with radial pattern [claystone]	40	
3939	FG618	60	zrC	IDs, Ts	16.3	2	3	2	5	0	0	0	7	1882	8 monotonous dense layer [claystone]	10	
3940	FG619	70	pC	ISs, IDs	11.1	0	0	2	4	50	27	2	2.5	1279	20 laminated layer with radial pattern [claystone]	20	
3941	FG620	30	pC	ISs, IDs	14.8	0	0	2	6	99	178	45	1.7	1712	30 laminated layer with radial pattern (soft nodule inside) [shark teeth]	40	
3942	FG621	20	zC	Ts, IDs	12.3	2	0	2	8	56	27	1	2.7	1425	30 laminated layer with radial pattern (soft nodule inside) [volcanic rock?]	40	
3943	FG622	80	pC	ISs, Fs	26.5	0	0	2	21	110	19	0	3	3050	20 laminated layer with radial pattern [claystone]	10	
3944	FG623	50	zC	Ts, IDs	25.3	4	2	5	6	14	4	0	3.9	2927	6 monotonous dense layer [volcanic rock?]	10	
3945	FG624	50	pC	IDPs, ISs	5.2	0	0	0	6	17	6	0	3	604	20 laminated layer, monotonous dense layer [claystone, mudstone]	60	
3946	FG625	70	pC	Ts, IDPs	13.0	2	0	4	4	34	6	0	3.1	1506	20 laminated layer with radial pattern, monotonous dense layer [claystone]	40	
3947	FG626	80	pC	Ss, Ds	19.4	0	0	0	14	57	10	0	3.1	2242	30 laminated layer with radial pattern [claystone]	20	
3948	FG627	80	pC	Ss, ISs	29.6	0	1	3	20	128	37	0	2.9	3424	20 laminated layer with radial pattern	20	
	P406	-	pC	IDs	-	0	0	0	0	2	0	0	<3>	12	5 monotonous dense layer	-	nodule (365 g) at 10 cm depth
	P406												-			0	nodule (1 g) at 385 cm depth
	P406												-			0	nodule (2 g) at 460 cm depth
	P406												-			0	2 nodules (27 g) at 662 cm depth
	P406												-			0	nodule (11 g) at 757 cm depth
3949	FG628	70	zrC	Ss, ISs	24.5	0	0	0	35	75	6	0	3.4	2832	25 laminated layer with radial pattern [claystone]	40	
3950	FG629	50	zrC	Ss, ISs	6.7	0	0	1	4	15	0	0	3.3	778	10 monotonous dense layer [claystone]	20	//shark tooth
3951	FG630	5	zC	IDs, IDPs	4.9	0	0	1	0	26	138	76	1.3	562	13 monotonous dense layer [mudstone]	30	//shark tooth
3952	FG631	10	zC	Ts, Fs	4.4	0	0	5	8	18	0	0	3.7	505	3 monotonous dense layer [mudstone]	0	//zeolitic claystone
	FG632	30	zC	Ts, Fs	16.0	1	1	2	5	33	19	3	2.6	1853	10 monotonous dense layer [volcanic rock?, claystone?]	10	//zeolitic claystone
	B95	10	zC	IDs, Fs	6.8	0	0	0	1	33	26	20	1.8	1037	6 monotonous dense layer [volcanic rock]	10	
3953	FG633	80	pC	Ts, ISs	18.5	1	1	3	26	82	7	1	3.3	2143	6 monotonous dense layer [claystone]	10	
3954	FG634	80	pC	ISs, IDs	11.7	0	0	3	6	23	20	0	2.5	1348	25 laminated layer with radial pattern	15	

Appendix VIII-1 (continued)

St#	Sam#	Cov	Sed.	Manganese nodule deposits												Buried nodules //other samples	
				type	abd.	size distribution (in number)						median	total thick.	internal structure [nuclei]	poly.	<RESULT OF OPERATION>
		(%)			kg/m2	>10	10-8	8-6	6-4	4-2	2-1<1 cm	(cm)	(g)	(mm)	no%	
3955	FG635	80	pC	Ss, IDs	19.7	0	0	3	14	46	30	0	2.7	2273	20 laminated layer with radial pattern [volcanic rock?, claystone?]	30	
3956	FG636	80	pC	Ss, ISs	29.1	0	0	2	24	101	17	0	3.1	3360	15 laminated layer with radial pattern [mudstone]	10	
3957	FG637	80	pC	Ss, ISs	28.6	0	0	6	21	104	37	0	2.9	3305	25 laminated layer with radial pattern	20	
3958	FG638	-	pC	ISs, IDs	27.1	0	0	0	20	187	64	1	2.8	3131	30 monotonous dense layer	30	
3959	FG639	-	pC	Ss, ISs	19.2	0	0	1	7	125	116	0	2.1	2219	20 laminated layer with radial pattern (soft nodule inside) [claystone]	20	
3960	FG640	80	zrC	Ss, ISs	20.9	0	0	1	19	122	175	6	1.9	2412	15 laminated layer with radial pattern (soft nodule inside) [claystone]	50	
	P407	-	zrC	ISPs	-	0	0	0	1	0	0	0	<5>	10	5 monotonous dense layer	-	nodule (4 g) at 200 cm depth
3961	FG641	85	pC	ISPs, IDs	30.3	0	0	0	5	124	46	0	2.7	3500	15 monotonous dense layer [claystone]	10	
3962	FG642	50	pC	ISPs, IDs	-	0	0	0	0	1	0	0	<3>	58		0	
3963	FG643	40	zrC	ISs, IDs	14.2	0	0	4	6	38	72	0	1.8	1639	30 laminated layer with radial pattern (soft nodule inside)	60	
3964	FG644	30	zrC	ISs, IDs	11.3	0	0	0	7	61	240	10	1.6	1309	25 laminated layer with radial pattern (soft nodule inside) [chert?]	40	//shark tooth
3965	FG645	10	zrC	IDs, IDPs	2.2	0	0	0	0	5	153	153	1	258	5 monotonous dense layer [chert?]	40	//shark tooth, zeolitic claystone
3966	FG646	-	zrC	IDs, IDPs	3.0	0	0	0	1	7	190	227	1	345	5 monotonous dense layer [chert?]	30	//shark tooth, zeolitic claystone
3967	FG647	5	zrC	IDs, ISs	0.6	0	0	0	0	1	25	4	1.4	66	10 monotonous dense layer [claystone?]	20	//shark tooth
3968	FG648	5	zrC	IDs, Ds	0.5	0	0	0	0	0	40	1	1.5	60	5 monotonous dense layer [shark teeth, chert?]	30	//shark tooth, zeolitic claystone
	P408	-	zC	IDs, IDPs	-	0	0	0	0	0	1	8	1.5	7	-	30	//shark tooth
3969	FG649	85	-	ISs, Ss	2.5	0	0	1	0	68	0	0	3	289	30 laminated layer with radial pattern [claystone]	30	
3970	FG650	100	-	Cs	0.0	-	-	-	-	-	-	-	-	0		-	
3971	FG651	40	-	Ts, IDs	8.1	0	0	0	5	88	48	1	2.5	936	5 monotonous dense layer [claystone]	20	//shark tooth, zeolitic claystone
3972	FG652	80	zrC	Ss, ISs	14.7	0	0	0	10	99	62	0	2.5	1695	20 laminated layer with radial pattern	40	
3973	FG653	70	-	Ts, Fs	15.6	0	5	3	15	35	31	3	2.7	1806	15 monotonous dense layer [claystone]	20	//zeolitic claystone
3974	FG654	80	pC	Ss, IDPs	27.6	0	0	0	21	119	135	3	2	3190	30 laminated layer with radial pattern (soft nodule inside)	20	//shark tooth
3975	B96	-	zrC	IDs, IDPs	-	0	0	0	0	3	24	0	1.6	41	5 monotonous dense layer [claystone]	60	
3976	FG655	30	zC	Ss, IDs	14.9	0	0	2	7	31	112	4	1.7	1726	15 monotonous dense layer, laminated layer with radial pattern	80	
3977	FG656	15	-	IDs	3.6	1	0	0	0	1	2	0	<2>	420	15 laminated layer with radial pattern [claystone]	30	
3978	FG657	20	zC	ISs, IDs	5.0	0	0	3	0	3	0	0	4	579	20 laminated layer with radial pattern [claystone]	0	
3979	FG658	80	zrC	ISs, ISPs	26.0	0	0	1	16	97	21	0	3	3003	15 monotonous dense layer	10	//shark tooth
3980	FG659	85	zcC	Ss, Ds	50.3	1	2	5	28	52	39	9	2.8	5815	25 laminated layer with radial pattern [chert?]	5	//shark tooth
3981	FG660	90	zcC	ISs, ISPs	33.2	0	0	1	12	217	225	8	2	3855		20	
3982	FG661	100	-	Cs	0.0	-	-	-	-	-	-	-	-	0		-	
	B97	90	cC	IDs, ISs	26.9	0	0	0	15	240	163	0	2.4	4090	11 monotonous dense layer [chert?]	30	
	B97X		cC	IDPs	-	0	0	0	1	1	0	0	-	92	15 monotonous dense layer [claystone]	0	2 nodules at 15 cm depth
3983	FG662	5	zrC	IDs, IDPs	0.2	0	0	0	0	1	6	5	1.2	21	4 monotonous dense layer [mudstone]	100	
3984	FG663	25	zrC	IDs, IDPs	4.4	0	0	0	0	10	333	102	1.4	505		70	

Appendix VIII-1 (continued)

St#	Sam#	Cov	Sed.	Manganese nodule deposits												Buried nodules //other samples
			type	abd.	size distribution (in number)							median	total	thick.	internal structure [nuclei]	poly. <RESULT OF OPERATION>
		(%)		kg/m2	>10	10-8	8-6	6-4	4-2	2-1	<1 cm	(cm)	(g)	(mm)		no%
3985	FG664	30	zrC IDs, IDPs	8.8	0	0	0	1	64	286	62	1.5	1012		5 monotonous dense layer [mudstone]	60 //shark tooth
3986	FG665	50	pC IDs, ISs	31.7	0	3	7	20	71	93	0	2.1	3664		10 monotonous dense layer [volcanic rock?]	40 //shark tooth
3987	FG666	50	zrC IDs, Ds	-	0	0	0	0	0	8	4	1.3	82		4 monotonous dense layer [volcanic rock]	20
3988	FG667	40	zrC Ts, IDs	17.8	5	2	2	1	3	12	4	1.9	2050		3 monotonous dense layer [claystone, mudstone]	30 //shark tooth
3989	FG668	70	pC Ts, Ss	12.3	2	0	3	1	1	0	0	7	1419		9 laminated layer with radial pattern, monotonous dense layer [claystone]	30
3990	FG669	85	zrC Ss, ISs	26.6	0	0	2	22	81	28	0	3	3075		20 laminated layer with radial pattern [claystone]	40
	P409	-	zrC	0.0	-	-	-	-	-	-	-	-	31		2 monotonous dense layer [claystone]	10 nodule (<1g) at 190 cm depth
3991	FG670	100	- Cs	0.0	-	-	-	-	-	-	-	-	0			-
3992	FG671	80	pC Fs, ISs	18.7	0	0	0	18	137	77	0	2.6	2160		20 monotonous dense layer	-
3993	FG672	30	zrC Ss, IDs	3.0	0	1	0	3	28	9	0	2.8	352		10 monotonous dense layer [claystone]	30 //shark tooth
3994	FG673	40	pC Ts, IDs	17.5	0	5	2	6	76	37	1	2.7	2023		20 laminated layer with radial pattern [claystone]	30
3995	FG674	100	- Cs	0.0	-	-	-	-	-	-	-	-	0			-
3996	FG675	70	pC Ss, ISs	29.8	0	0	2	21	121	32	0	2.9	3441		20 laminated layer with radial pattern [claystone]	20 //shark tooth
3997	FG676	50	pC IDs, IDPs	10.5	0	1	2	7	18	5	0	3.3	1216		15 laminated layer with radial pattern [claystone]	20
3998	FG677	70	pC IDs, IDPs	5.7	0	1	0	2	30	40	1	1.9	664		35 laminated layer with radial pattern [claystone]	50
	P410	-	zrC IDPs	-	0	0	0	0	5	1	0	2.8	40		10 laminated layer, monotonous dense layer [claystone]	80 crust just beneath surface nodules
3999	FG678	90	pC ISs, Ss	35.2	0	0	0	7	144	6	0	3	4069		5 monotonous dense layer	10
4000	FG679	-	pC ISs, Ss	39.5	1	0	1	24	107	27	0	3	4570		15 monotonous dense layer [claystone]	5
4001	FG680	-	pC ISs, IDPs	36.7	0	1	3	19	67	100	2	1.9	4240		20 monotonous dense layer [claystone]	20
4002	FG681	80	- Ss, Ds	3.0	0	3	10	0	13	14	0	2.9	3471		40 monotonous dense layer	20 //shark tooth
4003	FG682	80	pC Ss, IDs	22.9	0	3	1	7	36	69	18	1.7	2643		40 laminated layer, monotonous dense layer [shark teeth, claystone]	20
4004	FG683	40	zrC Ts, IDs	8.9	1	0	1	5	23	32	3	1.9	1030		20 laminated layer with radial pattern [claystone]	60
4005	FG684	80	zrC ISs, IDs	16.2	0	0	4	12	70	34	1	3	1870		30 laminated layer with radial pattern (soft nodule inside) [claystone]	40
	B98	-	-	-	-	-	-	-	-	-	-	-	-			- <UNSUCESSFUL>
4006	FG685	70	- Ts, IDs	-	0	0	0	0	14	4	0	2.7	210		5 monotonous dense layer [claystone]	0 //zeolitic claystone
4007	FG686	50	zrC Ss, IDs	28.4	0	1	9	8	23	115	31	1.5	3280		20 monotonous dense layer, laminated layer (soft nodule inside) [claystone	50
4008	FG687	60	- Ss, IDs	-	0	0	11	33	0	0	0	5.3	331		25 laminated layer with radial pattern (soft nodule inside)	30
4009	FG688	70	- Ts, IDs	24.5	2	0	2	15	66	45	0	2.6	2834		20 laminated layer, monotonous dense layer [claystone, shark teeth]	20
4010	FG689	50	zC Ts, IDs	20.0	0	2	0	17	133	318	81	1.6	2309		20 laminated layer with radial pattern (soft nodule inside) [claystone]	40
4011	FG690	60	pC Ts, IDs	25.3	0	1	3	19	72	154	6	1.8	2920		20 monotonous dense layer	30 //shark tooth
4012	FG691	70	pC Ts, IDs	26.6	0	0	3	16	139	168	1	2	3075		25 laminated layer with radial pattern (soft nodule inside) [claystone]	30
4013	FG692	20	pC ISs, IDPs	8.0	0	0	3	6	17	7	1	3.1	928		10 laminated layer with radial pattern [claystone, hydrotheral Mn oxide]	30
	P411	-	zrC IDs, IDPs	-	0	0	0	0	0	3	0	<1.5>	4			30 Mn coating at 173 cm depth
4014	FG693	20	pC IDs, ISs	4.3	0	0	1	2	17	6	4	2.6	499		35 laminated layer with radial pattern (soft nodule inside) [claystone]	50

Appendix VIII-1 (continued)

St#	Sam#	Cov	Sed.	Manganese nodule deposits												Buried nodules //other samples
				type	abd.	size distribution (in number)						median	total thick.	internal structure [nuclei]	poly.	<RESULT OF OPERATION>
		(%)			kg/m2	>10	10-8	8-6	6-4	4-2	2-1	<1 cm	(cm)	(g)	(mm)	no%	
4015	FG694	100	-	Cs	1.0	0	1	0	1	0	0	0	<6>	111	3 monotonous dense layer [volcanic rock]	0	
4016	FG695	100	-	Cs	0.1	-	-	-	-	-	-	-	-	17	6 monotonous dense layer	-	
4017	FG696	100	-	Cs	0.0	-	-	-	-	-	-	-	-	0		-	
4018	FG697	100	zrC		0.0	-	-	-	-	-	-	-	-	0		-	
4019	FG698	15	zrC	IDs, IDPs	2.8	0	0	0	1	4	203	20	1.5	329	5 monotonous dense layer	60	
4020	FG699	10	zrC	IDs, IDPs	1.4	0	0	0	0	7	99	20	1.4	164	5 monotonous dense layer [claystone]	50	
	B99	-	zC	IDs, IDPs	-	0	0	0	0	1	159	350	1.4	185	3 monotonous dense layer [claystone]	40	
4021	FG700	100	-	IDs, Fs	1.0	0	0	0	1	3	0	0	<3.3>	119	5 monotonous dense layer [claystone, shark teeth]	30	
4022	FG701	50	pC	IDs	1.4	0	0	1	0	1	0	0	<4>	158	15 monotonous dense layer	50	
4023	FG702	100	-	Cs, Fs	0.1	-	-	-	-	-	-	-	-	6		-	
4024	FG703	70	zrC	Ss, ISs	9.0	0	0	0	3	44	43	1	2.1	1036	20 monotonous dense layer [claystone]	10	
4025	FG704	70	pC	Ts, IDs	12.2	0	1	1	14	122	122	0	2.1	1413	15 monotonous dense layer [chert]	40	
4026	FG705	-	pC	Ts, IDs	20.1	0	1	1	14	158	173	19	2	2323	15 monotonous dense layer [chert?]	40	//shark tooth
4027	FG706	-	zrC	Ts, IDs	19.0	1	0	2	8	78	96	16	1.9	2191	17 laminated layer with radial pattern (soft nodule inside) [claystone]	40	
	B100	40	pC	Ts, Ss	19.0	1	0	3	6	59	97	26	1.7	2895	35 laminated layer with radial pattern (soft nodule inside)	30	
4028	C20	-	-	IDs, IDPs	-	-	-	-	-	-	-	-	-	0		-	
4029	FG707	80	zrC	ISs, IDs	22.2	1	0	3	17	134	13	0	3.1	2564		40	
	FG708	70	pC	IDs, IDPs	16.5	0	1	10	10	68	53	0	2.5	1908	8 monotonous dense layer [claystone, shark teeth]	30	
4030	P412	-	zrC	ISs, IDPs	-	0	0	0	0	2	1	0	<2.5>	16	6 monotonous dense layer [claystone]	70	nodule (2 g) at 135 cm depth
4031	D535	-	-	Ss, Ds	-	-	-	-	-	-	-	-	-	180 kg		-	//shark tooth

NOTE/

St#=station number, Sam#=sample number, Cov=seafloor coverage of nodules by sea-bed photo.
Sed: sediment type/ c=calcareous, z=zeolitic, p=pelagic, O=ooze, C=clay
Nodule type: S=spherical, D=discoidal, F=fragmented, I=irregular, T=tabular, P=polinucleated, s=smooth surface.
abd.=abundance of seabed nodules
thick.= average thickness of Mn layers
poly.= number % of polynucleated nodules.
others= associated samples with nodules of crusts.

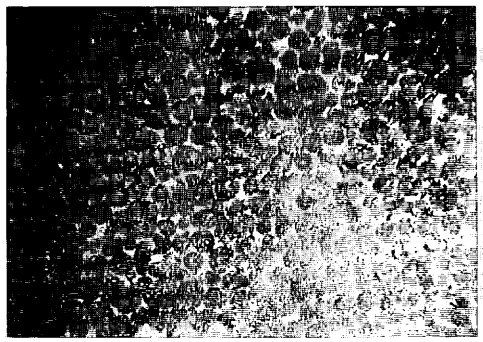

FG563 / 21.8 (80) IS, ISP

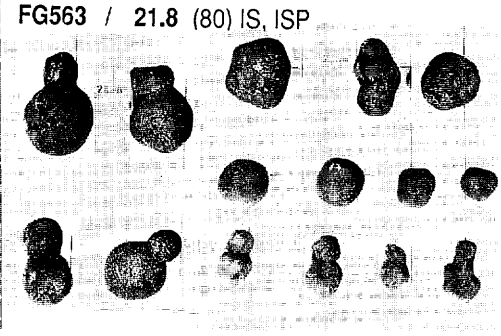

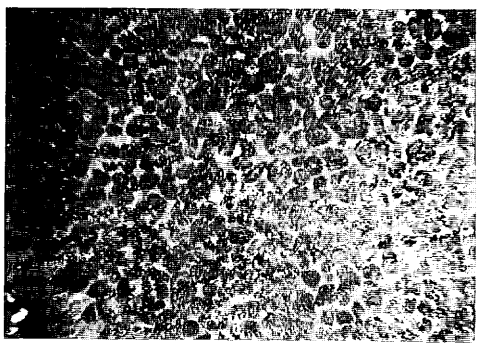

FG564 / 15.5 (70) IDP, DP

FG565 / 13.2 (60) IDP, ID

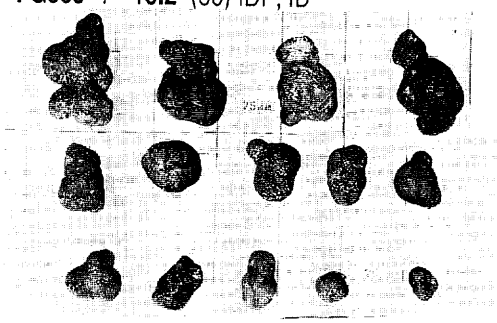

FG566 / 5.9 (100) V

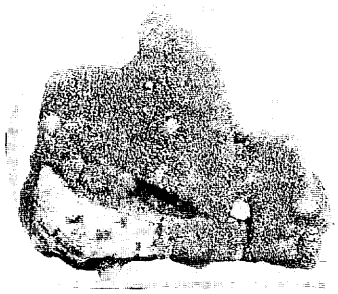

Appendix VIII-2 Sea-bed photographs and morphology of manganese nodules. Each title includes sample number, wet nodule abundance (kg/m^2), nodule coverage calculated from photos (in parenthesis), and dominant shapes (for symbols see Appendix VIII-1).

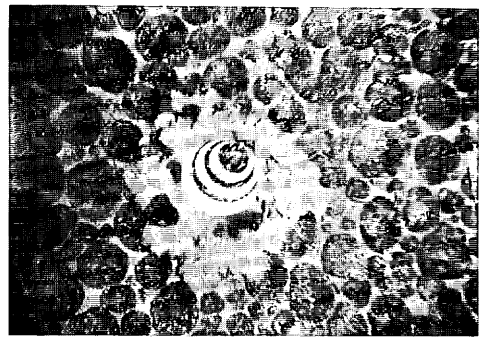

FG567 / 24.1 (80) S, IS

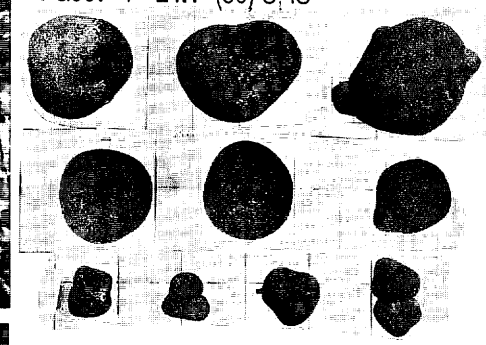

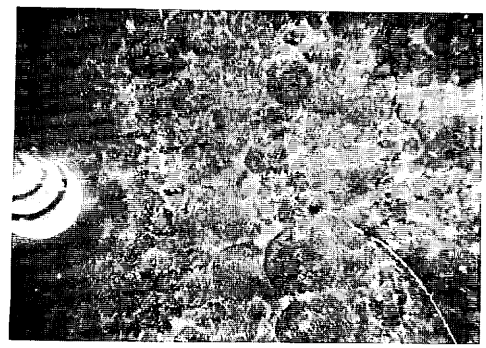

FG568 / 0.1 (100) F

B86 / 21.8 (-) S, IS

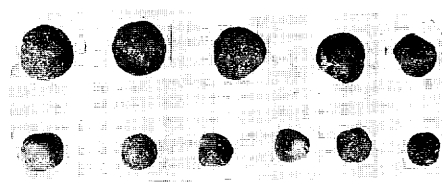

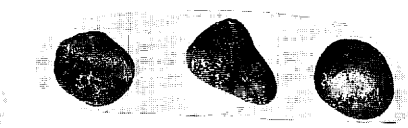

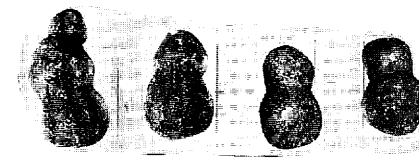

FG569 / 29.8 (50) S, IS

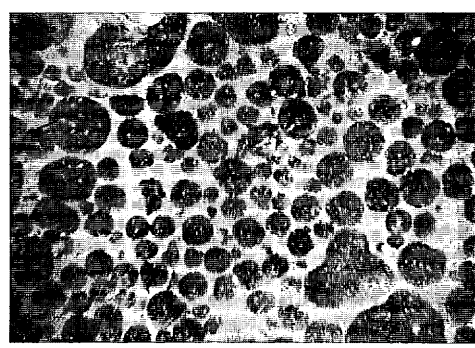

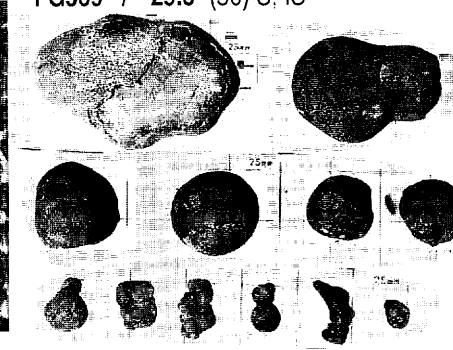

Appendix VIII-2 (continued)

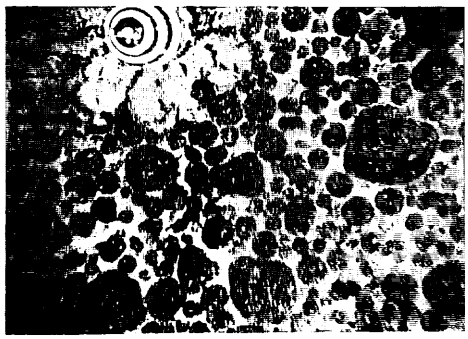

FG570 / 21.3 (60) S, IS

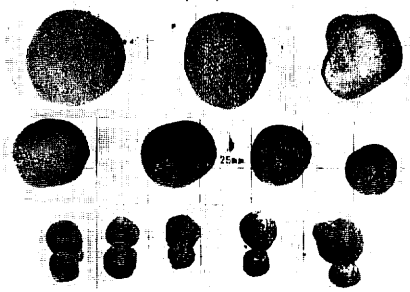

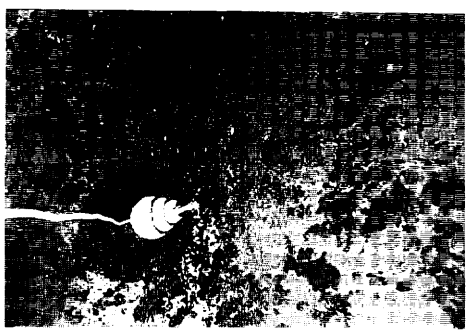

FG571 / 1.3 (100) ID, IDP

FG572 / - (100) C

FG573 / 0 (0)

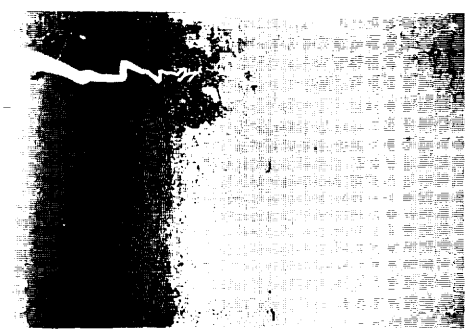

FG574 / 0.1 (0) V

Appendix VIII-2 (continued)

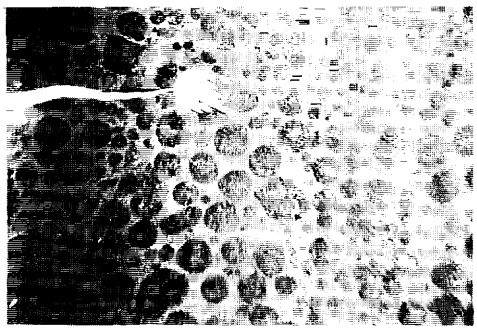

FG575 / 19.2 (60) IS, ID

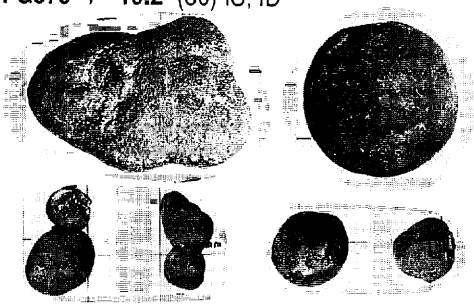

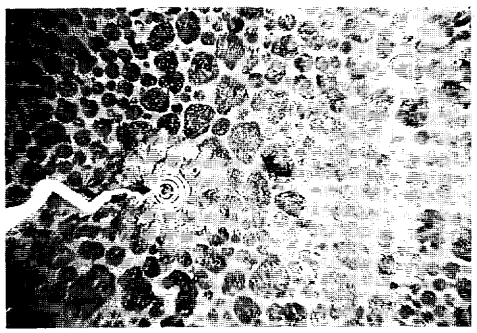

FG576 / 32.3 (70) T, IS

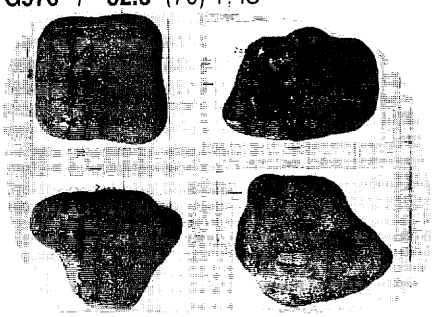

B88 / - (-) IS

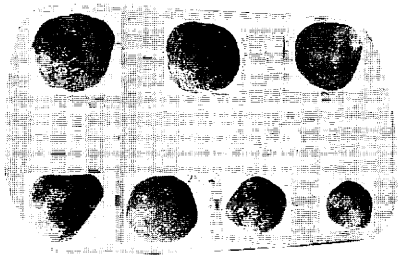

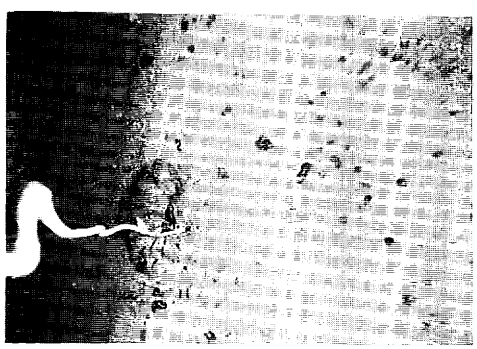

FG577 / 0.3 (2) IDP

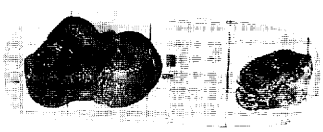

Appendix VIII-2 (continued)

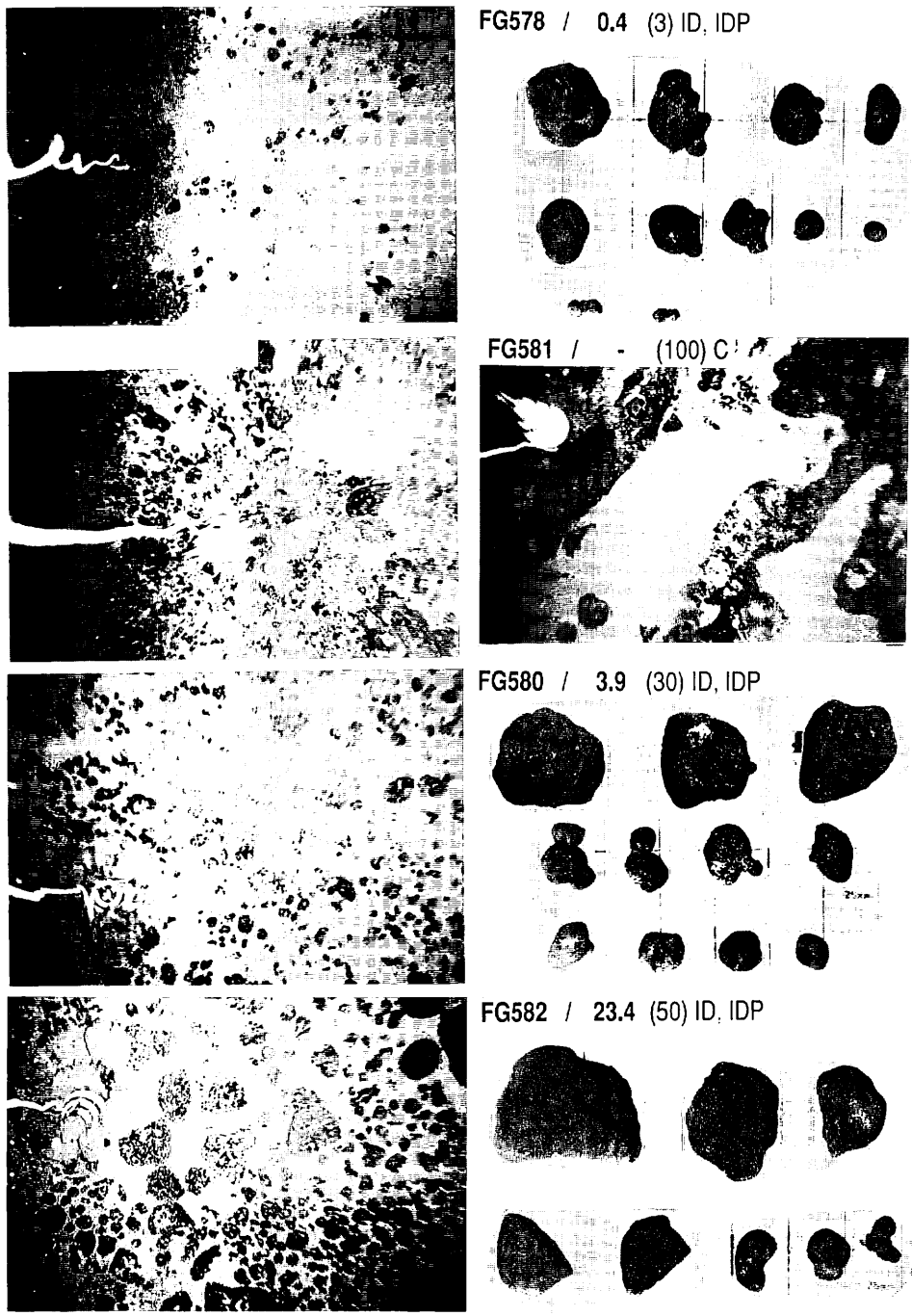

Appendix VIII-2 (continued)

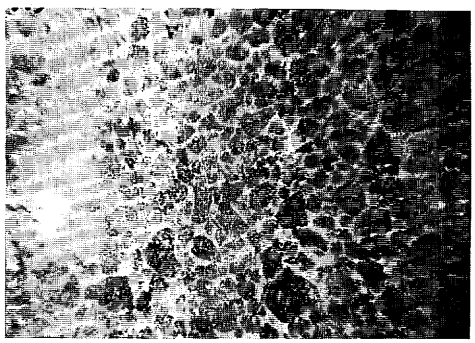

FG583 / 15.4 (80) T. ID

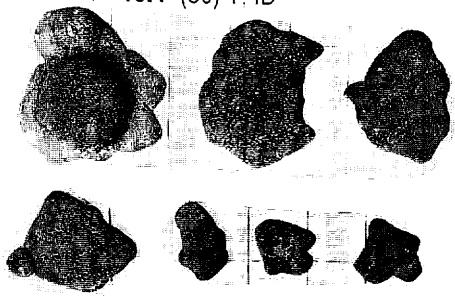

FG584 / 8.3 (80) T. ID

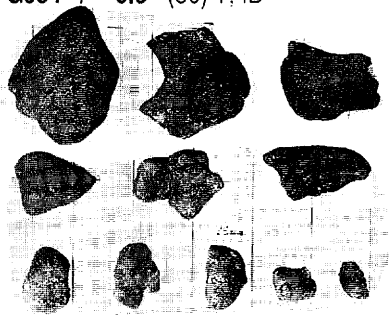

B90 / - (100) C

FG585 / 28.8 (80) T. ID

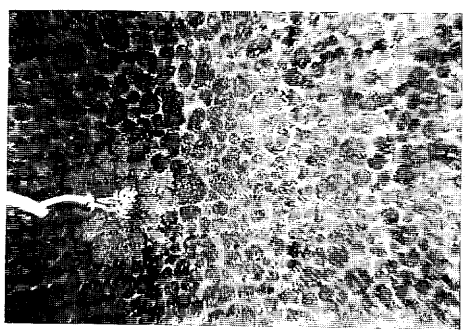

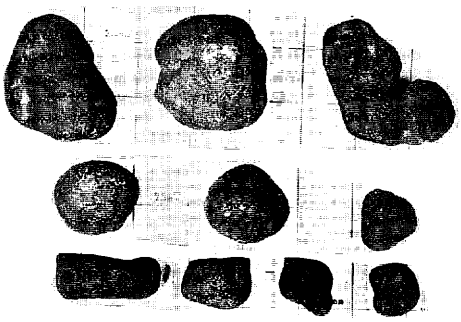

Appendix VIII-2 (continued)

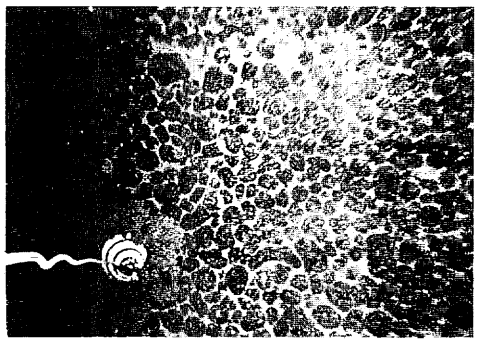

FG586 / 16.6 (80) ID, D

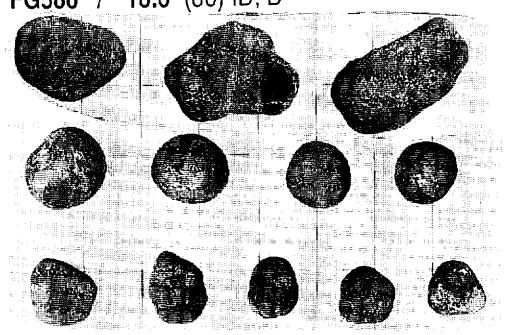

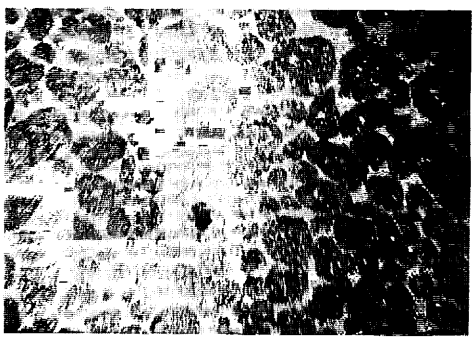

B91 / 18.5 (70) T, ID

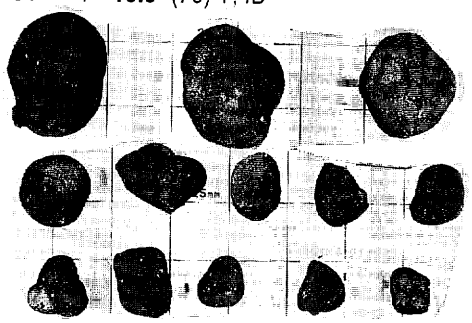

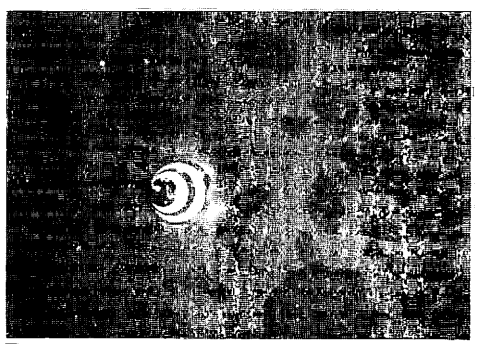

FG587 / 10 (30) IDP, ID

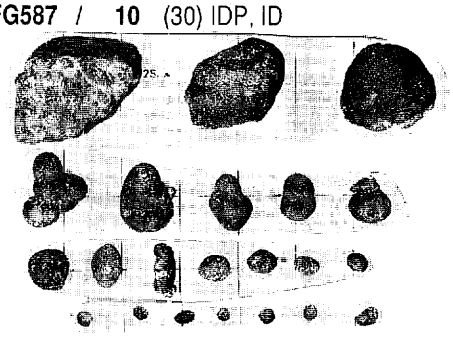

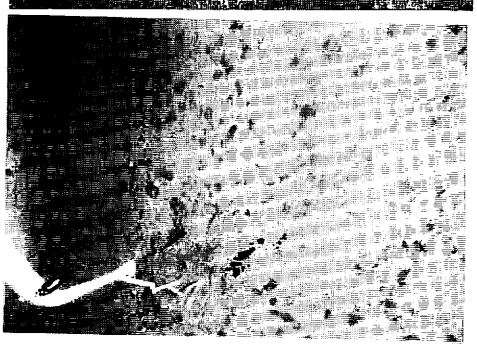

FG588 / 4.6 (10) ID, IDP

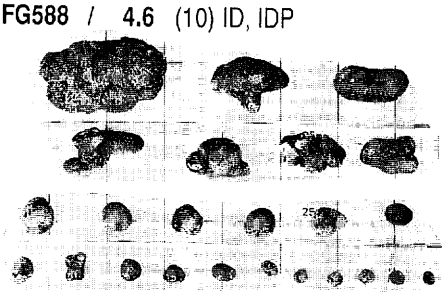

Appendix VIII-2 (continued)

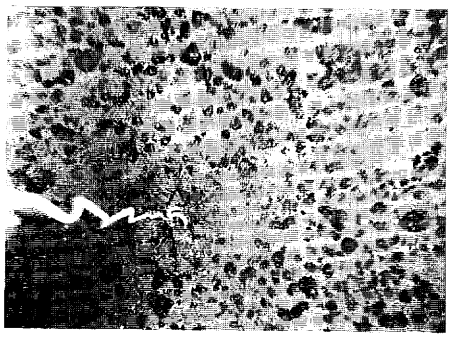

FG589 / 6.7 (15) IDP, ID

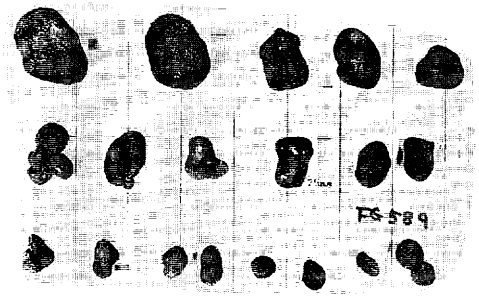

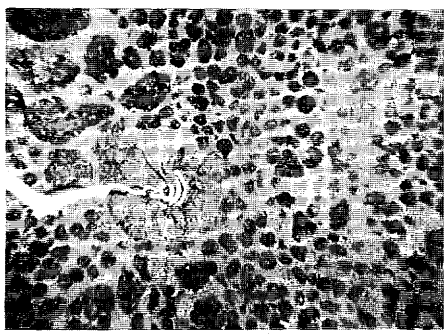

FG590 / 17.4 (25) ID, IDP

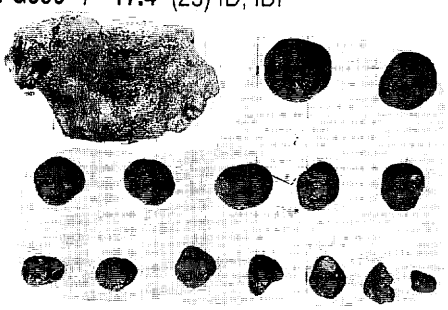

FG591 / 6.8 (-) ID, IDP

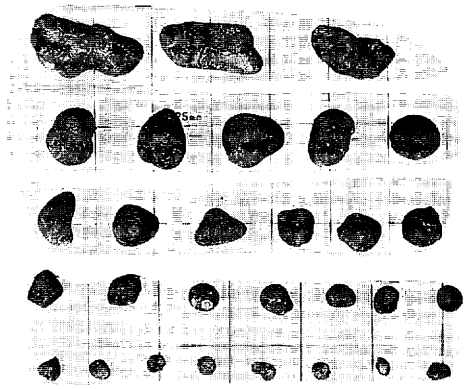

FG592 / 0.6 (-) ID, IDP

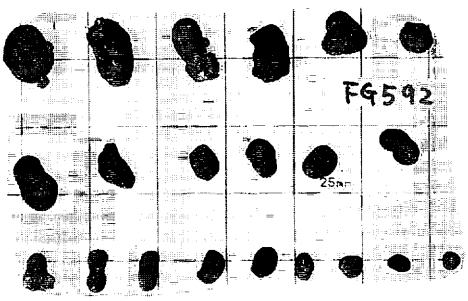

FG593 / 0.8 (-) ID, IDP

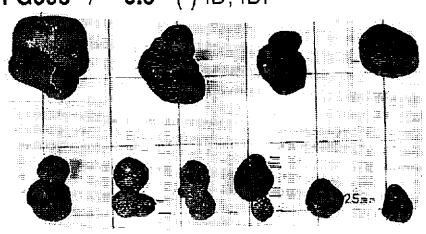

FG594 / 0.2 (-) ID, IDP

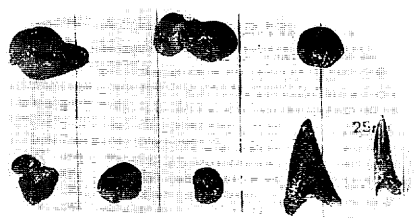

Appendix VIII-2 (continued)

FG595 / 36.4 (-) S, IS

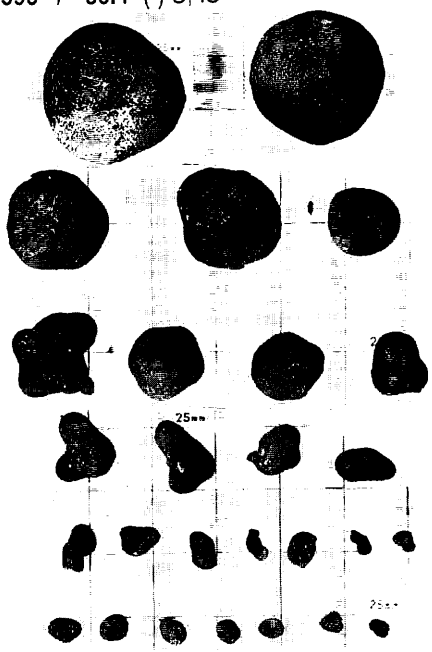

FG596 / 24.4 (-) S, IS

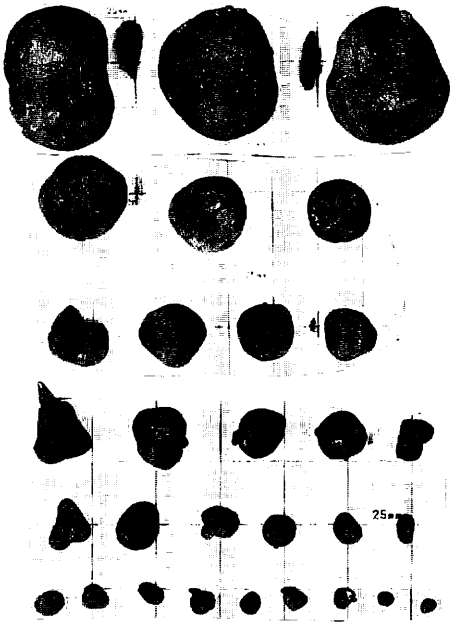

B92 / 37.9 (70) S, IS

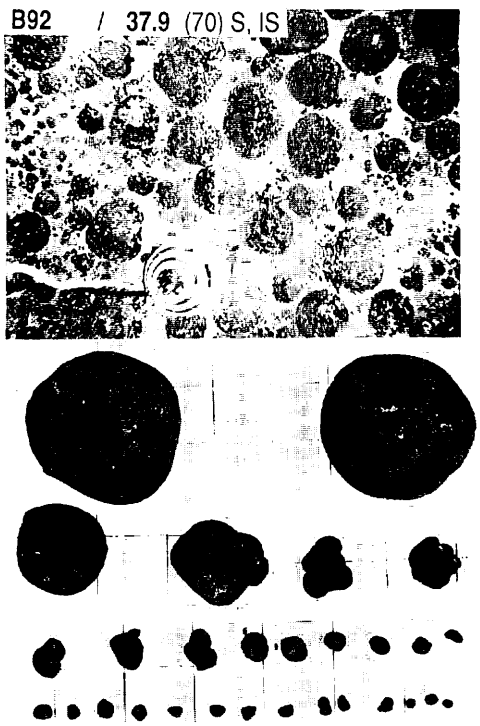

FG597 / 30.9 (-) S, T

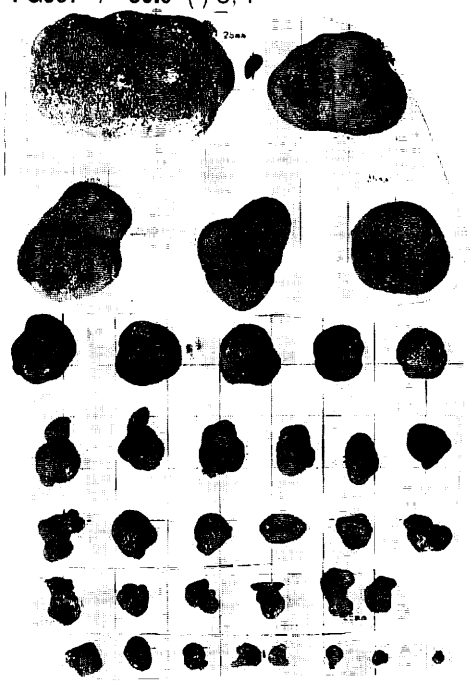

Appendix VIII-2 (continued)

FG598 / 27.2 (-) S, IS

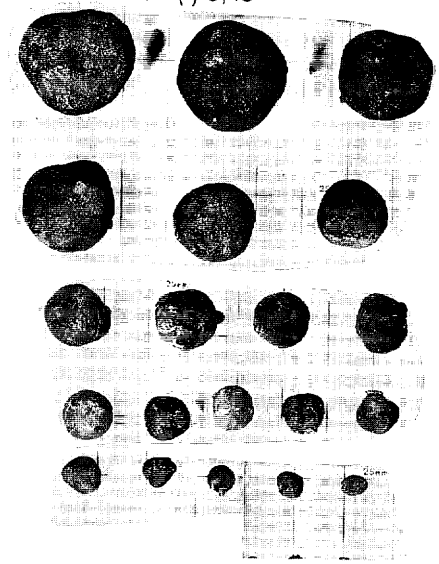

FG599 / 20.2 (-) T, IDP

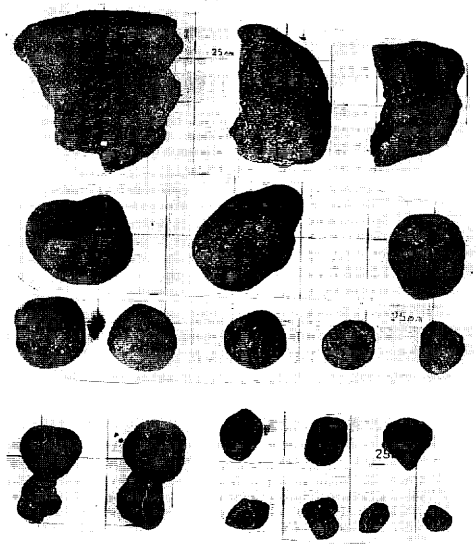

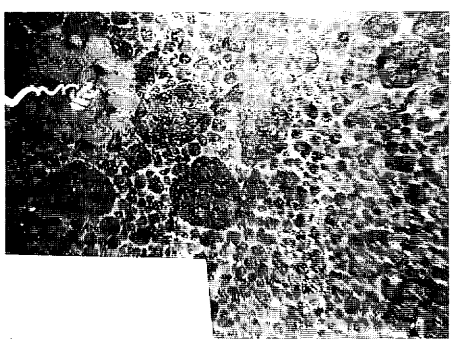

FG600 / 18.6 (80) T, ID

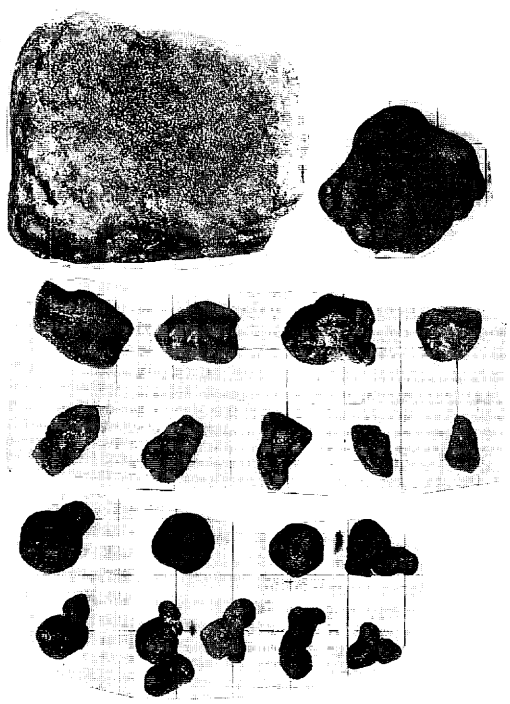

B93 / - (-) S

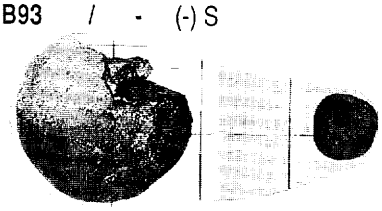

Appendix VIII-2 (continued)

FG602 / 1.1 (5) D, DP

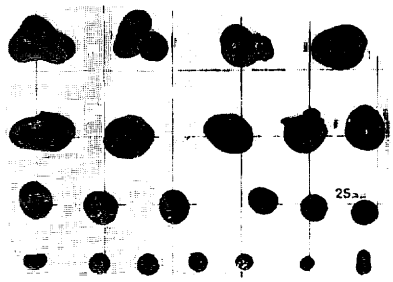

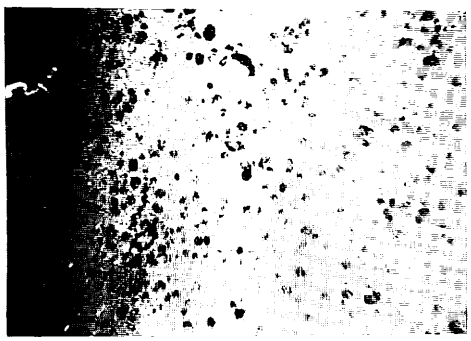

FG603 / 0.4 (5) IDP, ID

FG604 / 2.7 (5) D, ID

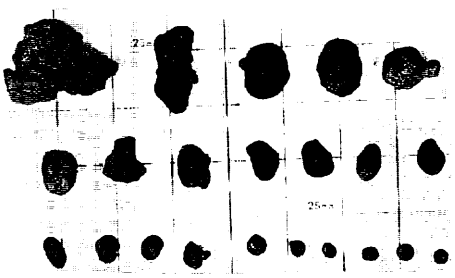

B94 / 0.5 (-) IDP

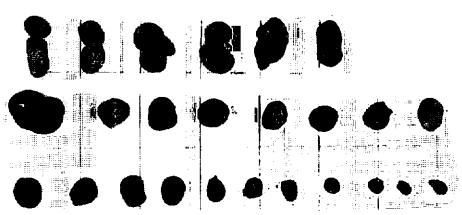

Appendix VIII-2 (continued)

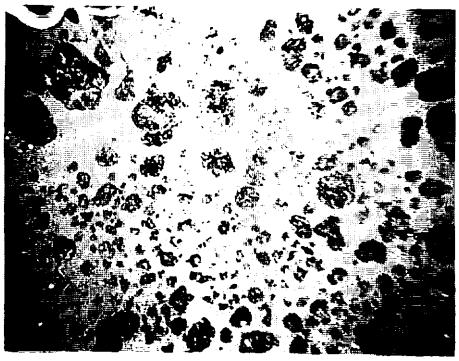

FG605 / 17.2 (40) T, IDP

FG606 / 17.3 (40) T, IDP

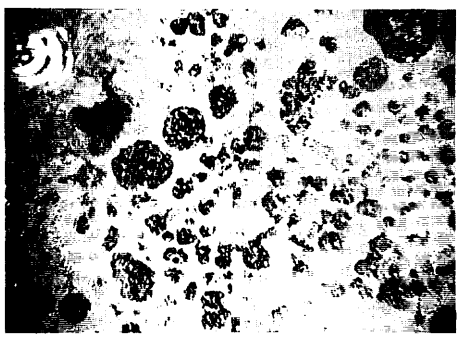

FG607 / 9.4 (40) T, IDP

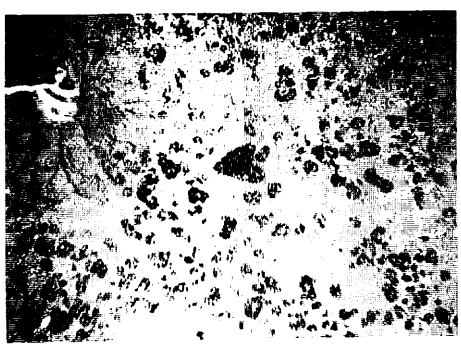

FG608 / 5.8 (20) D, ID

Appendix VIII-2 (continued)

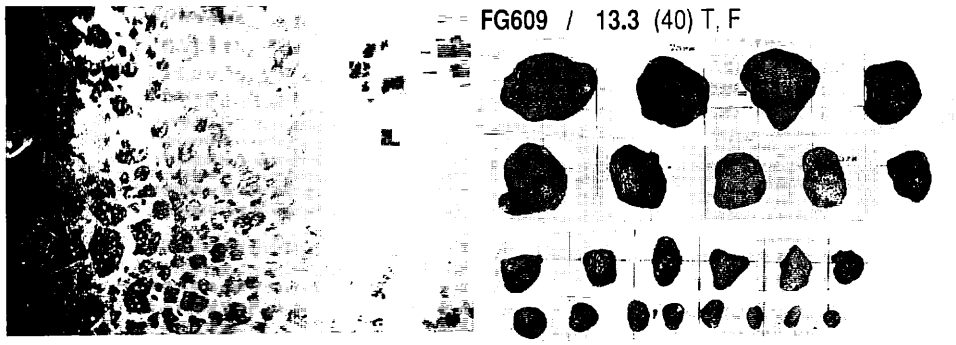

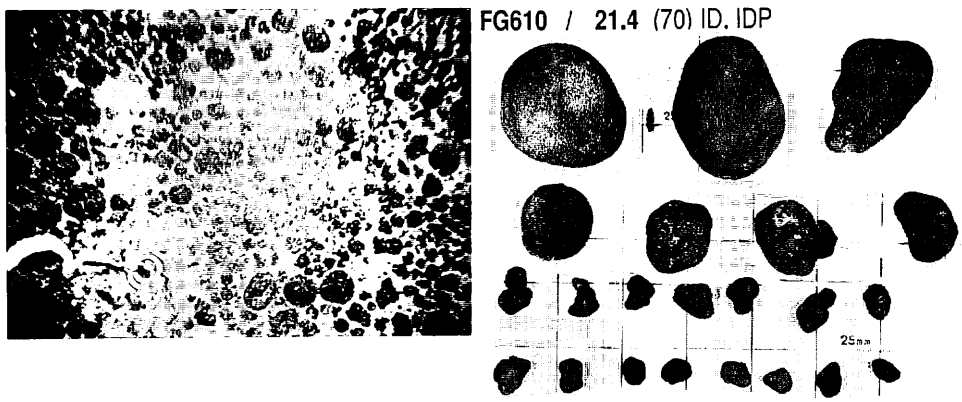

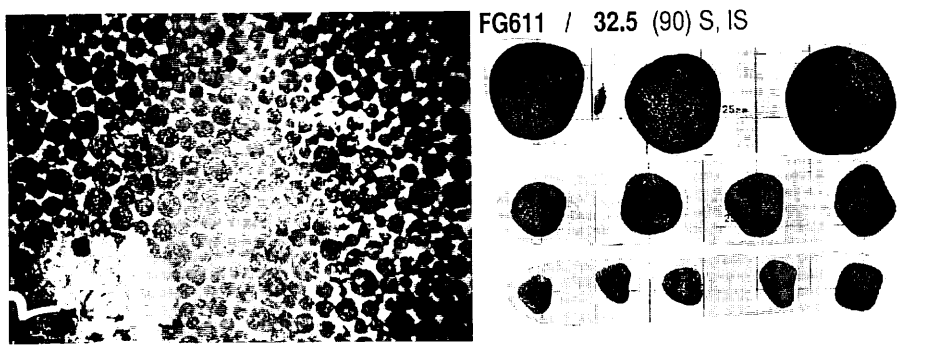

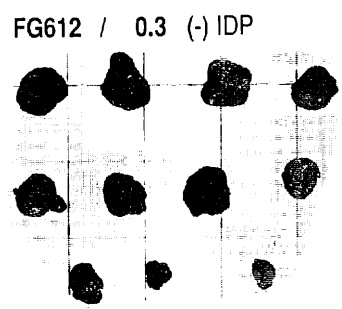

Appendix VIII-2 (continued)

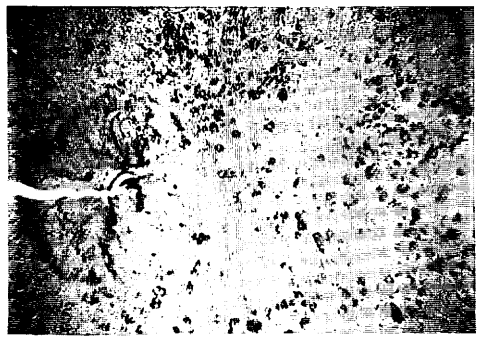

FG613 / 0.1 (10) ID, IDP

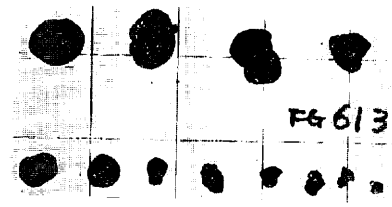

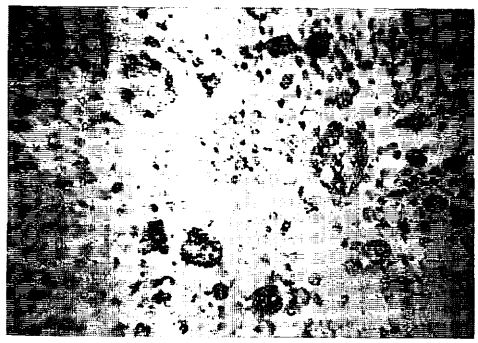

FG614 / 11.5 (20) T, ID

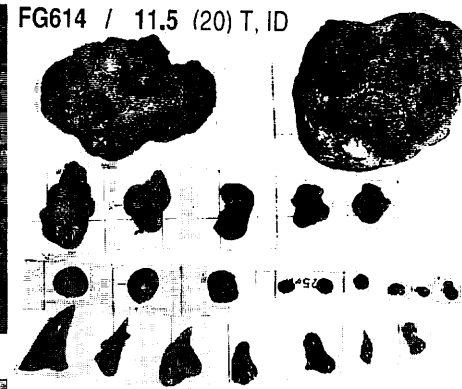

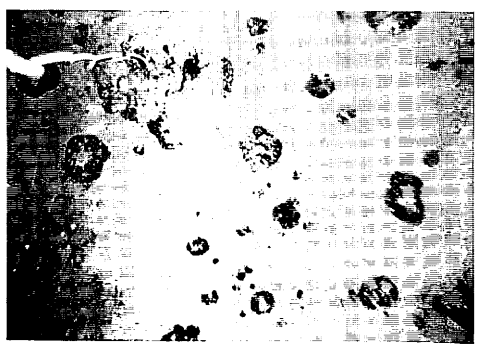

FG615 / 9.7 (10) ID, T

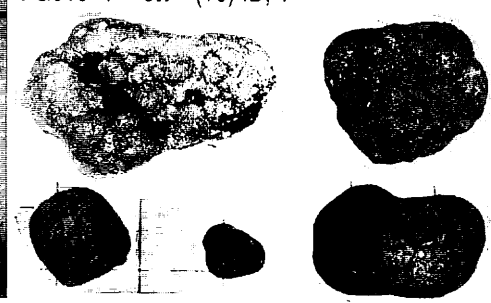

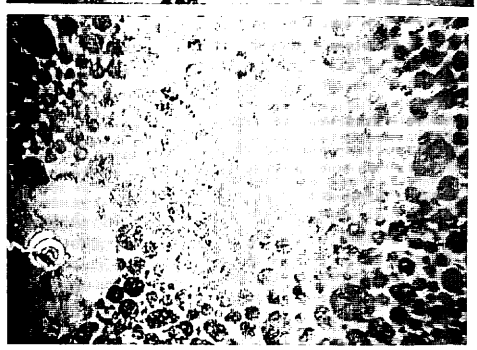

FG616 / 28.9 (80) IS, ID

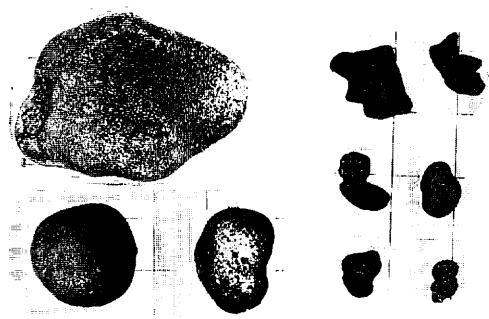

Appendix VIII-2 (continued)

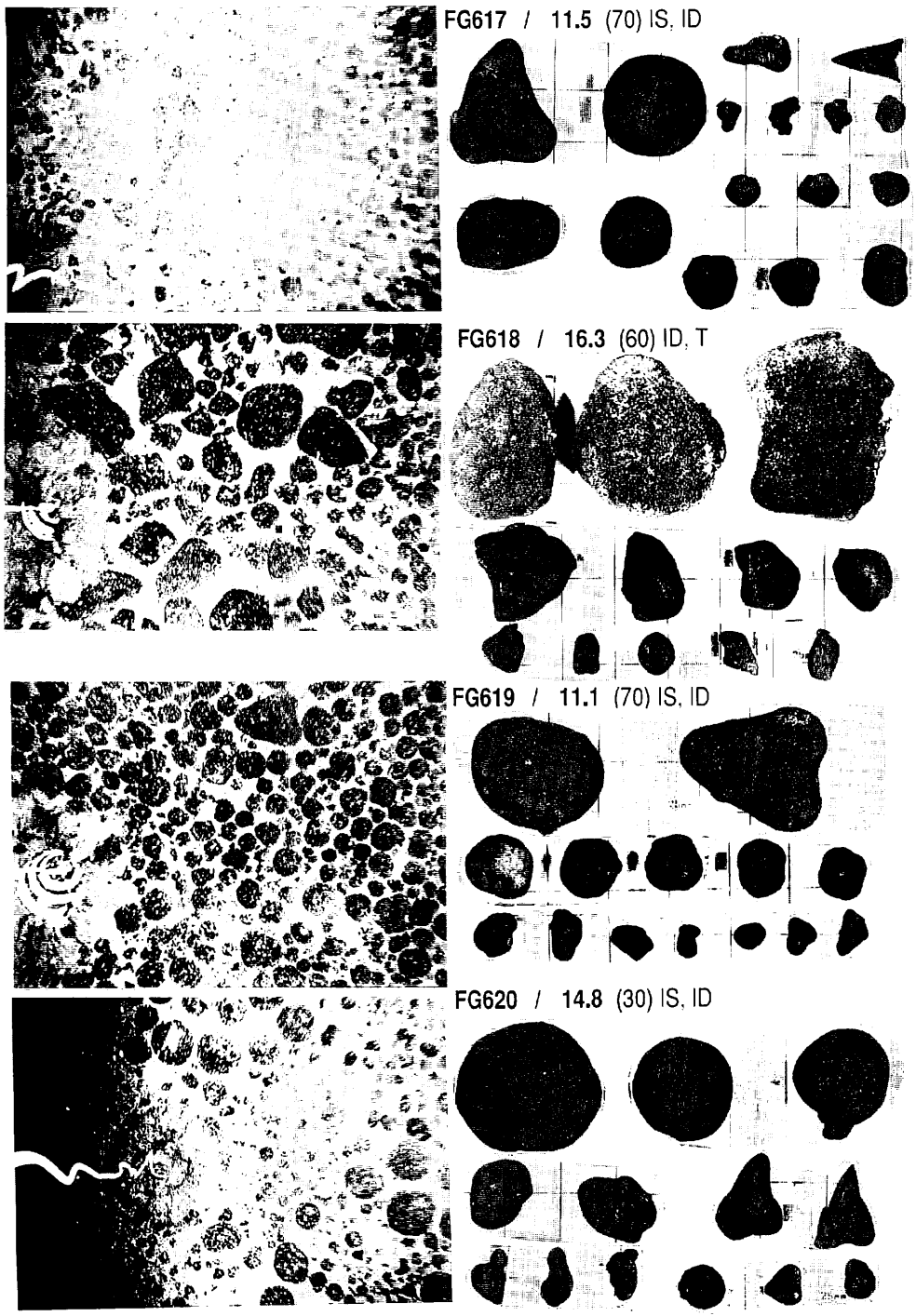

Appendix VIII-2 (continued)

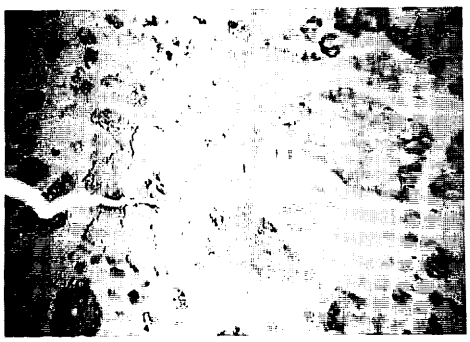

FG621 / 12.3 (20) T, ID

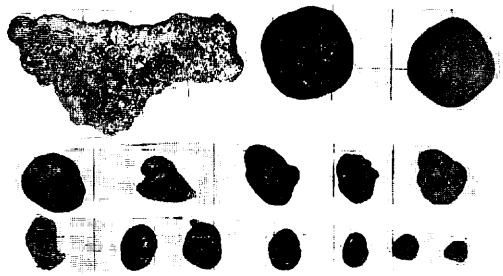

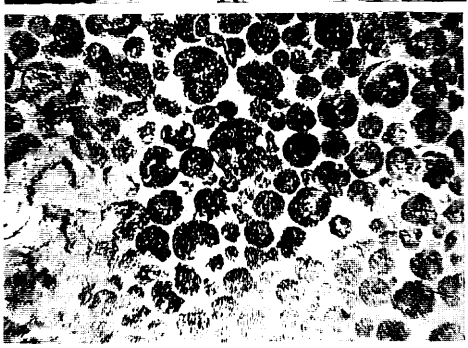

FG622 / 26.5 (80) IS, F

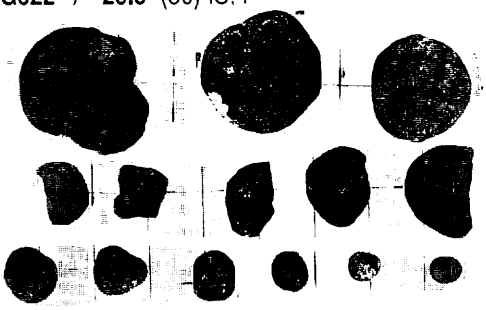

FG623 / 25.3 (50) T, ID

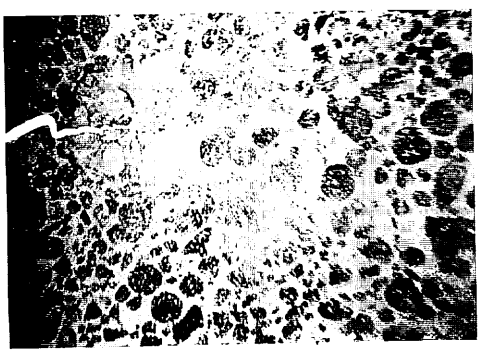

FG624 / 5.2 (50) IDP, IS

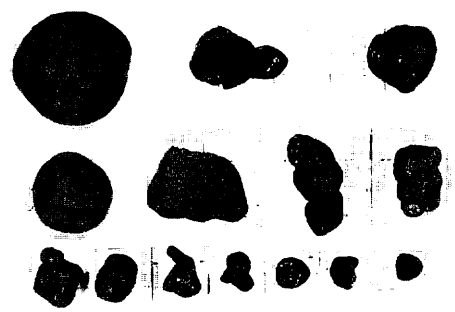

Appendix VIII-2 (continued)

FG625 / 13 (70) T, IDP

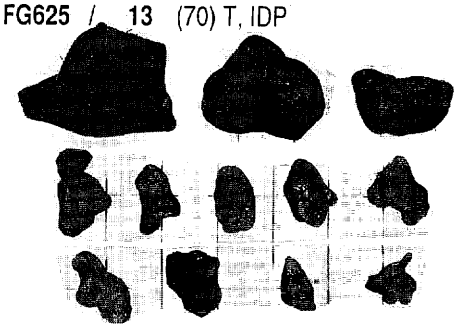

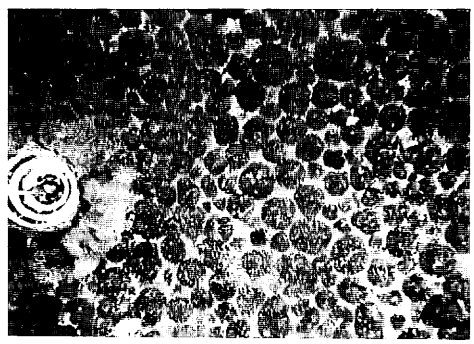

FG626 / 19.4 (80) S, D

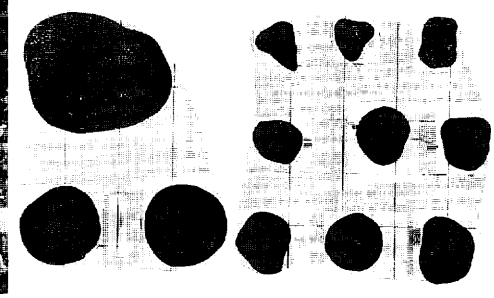

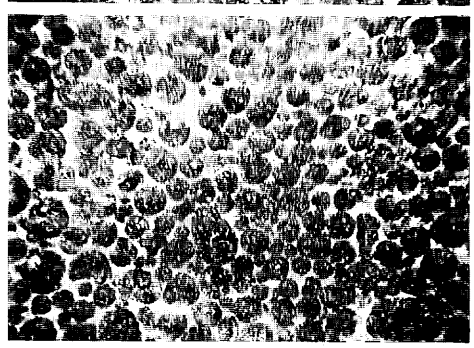

FG627 / 29.6 (80) S, IS

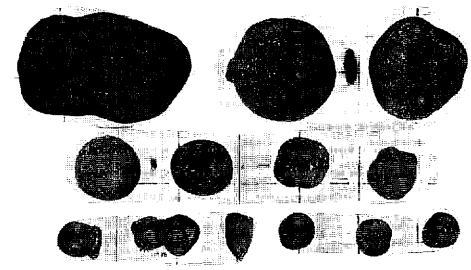

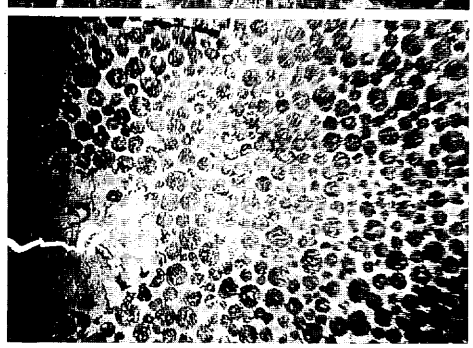

FG628 / 24.5 (70) S, IS

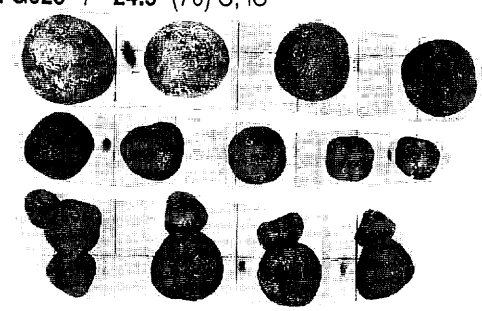

Appendix VIII-2 (continued)

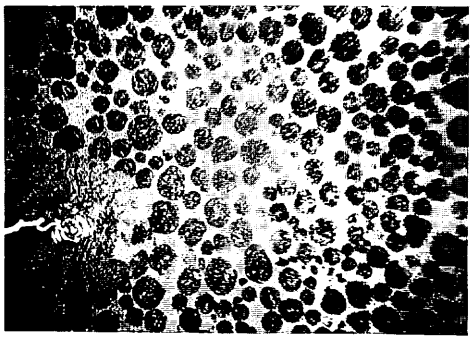

FG629 / 6.7 (50) S, IS

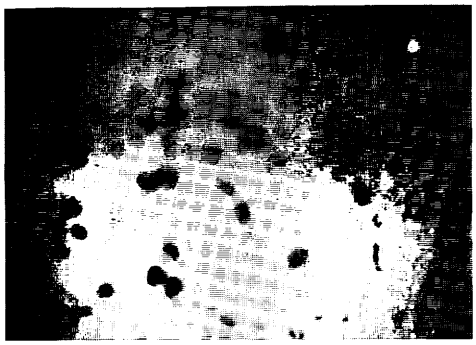

FG630 / 4.9 (5) ID, IDP

FG631 / 4.4 (10) T, F

FG632 / 16 (30) T, F

Appendix VIII-2 (continued)

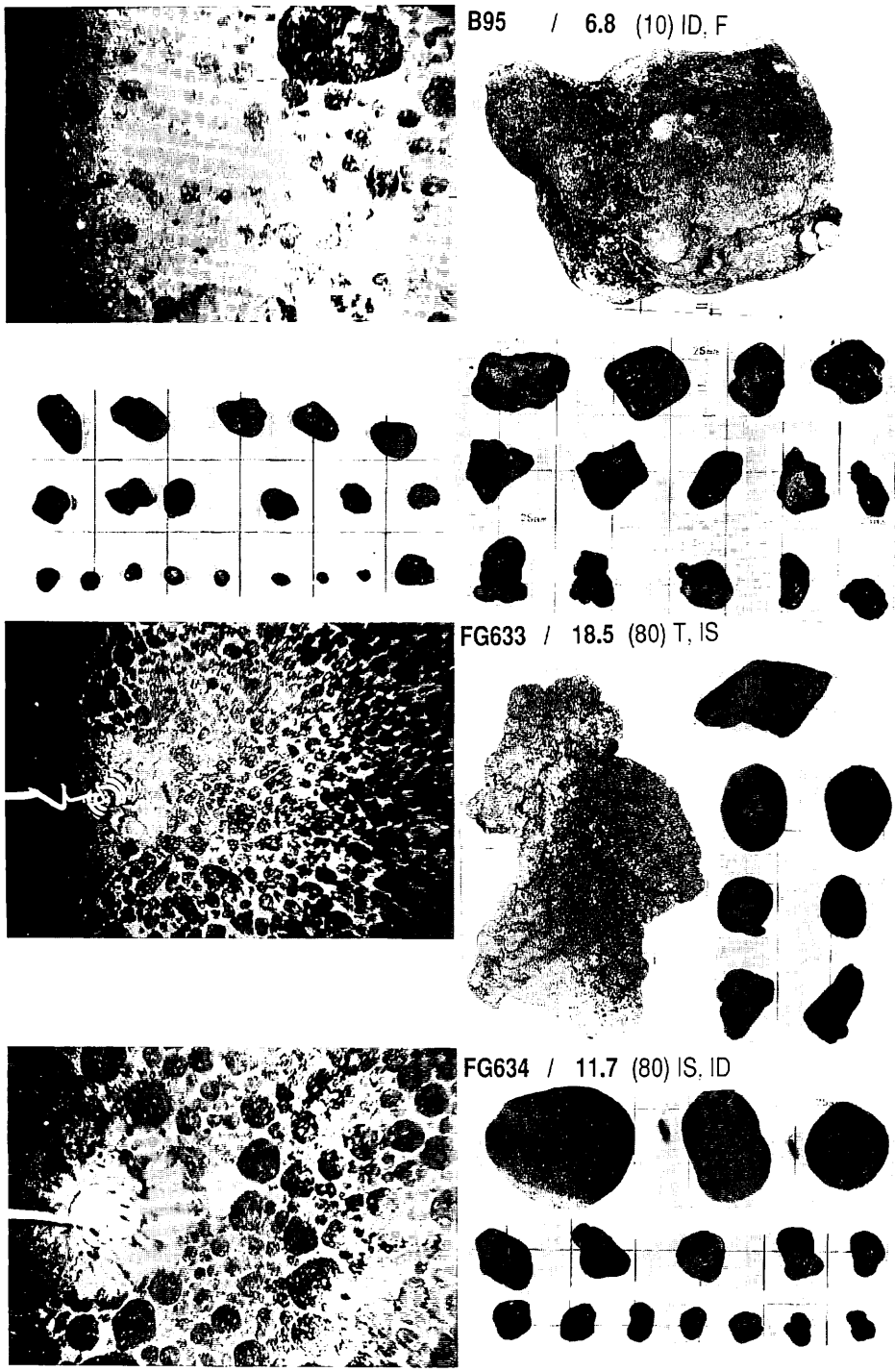

Appendix VIII-2 (continued)

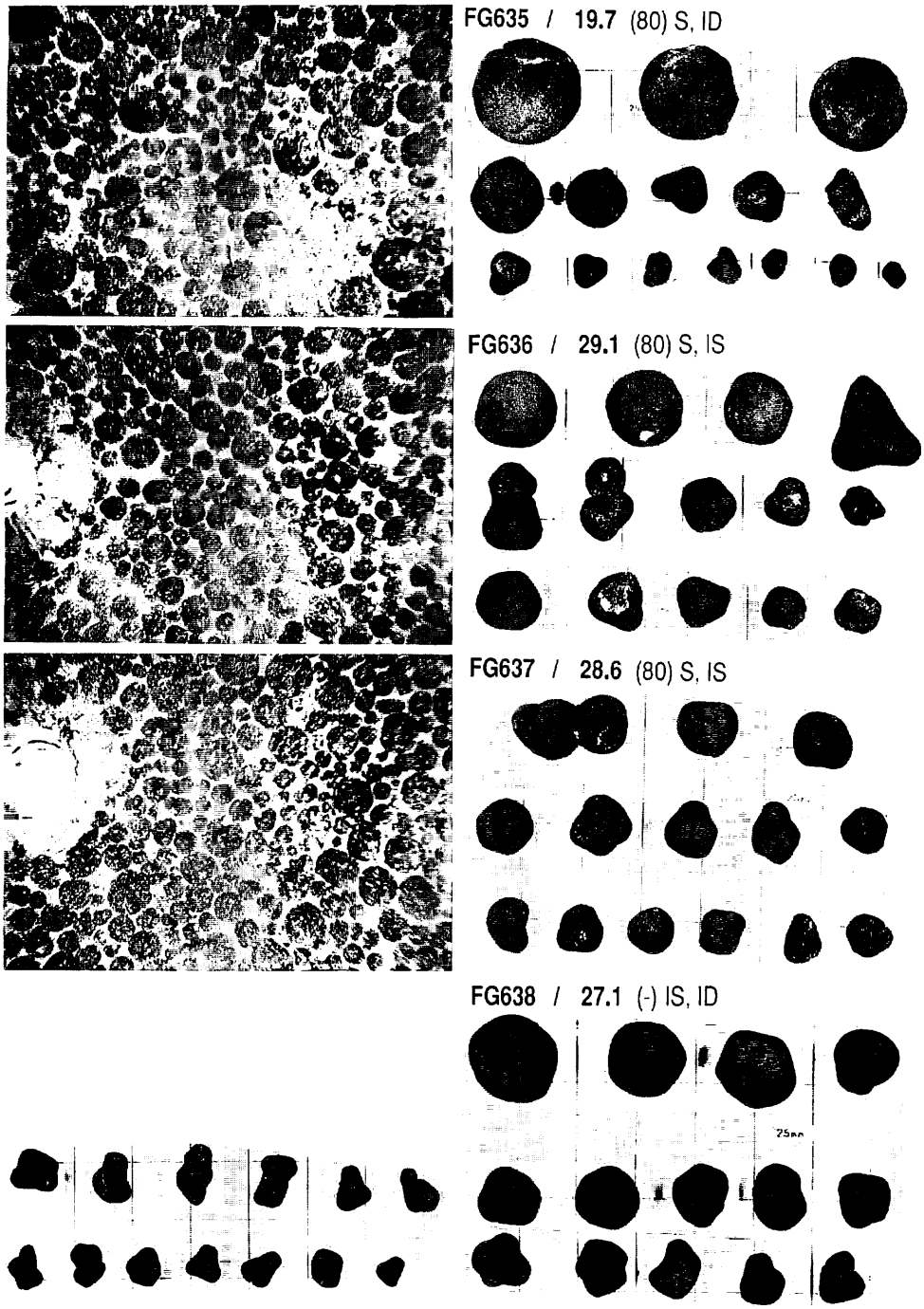

Appendix VIII-2 (continued)

FG639 / 19.2 (-) S, IS

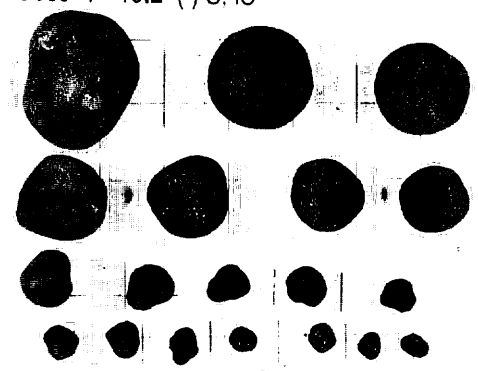

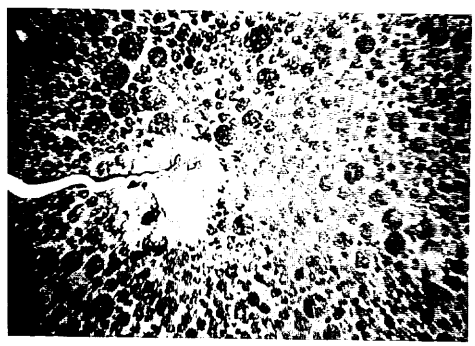

FG640 / 20.9 (80) S, IS

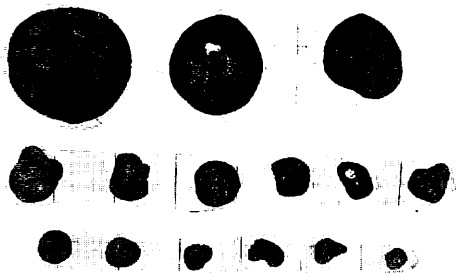

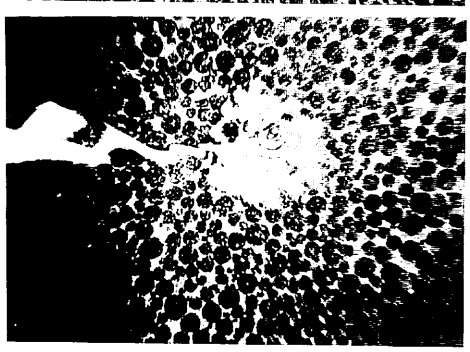

FG641 / 30.3 (85) ISP, ID

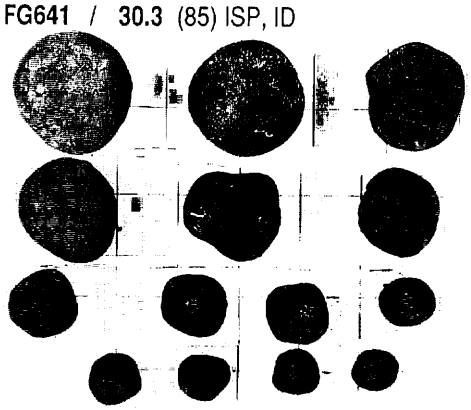

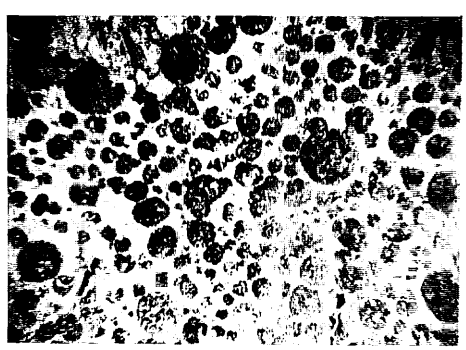

FG642 / - (50) ISP, ID

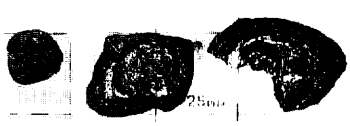

Appendix VIII-2 (continued)

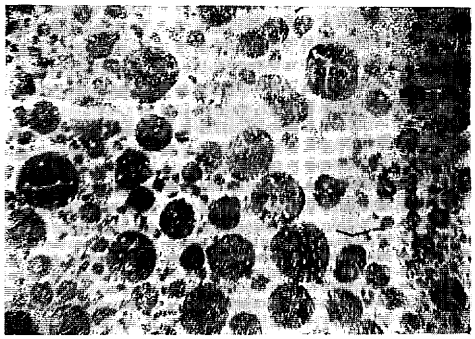

FG643 / 14.2 (40) IS, ID

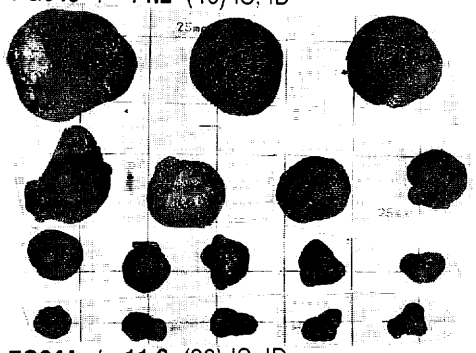

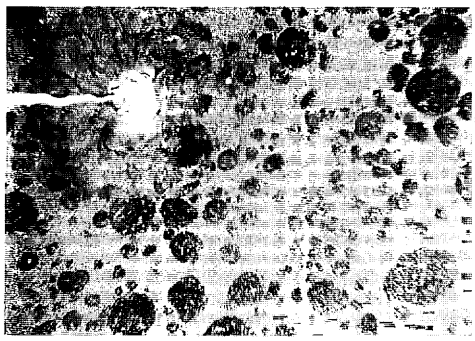

FG644 / 11.3 (30) IS, ID

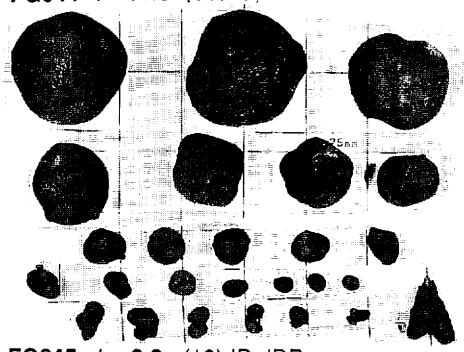

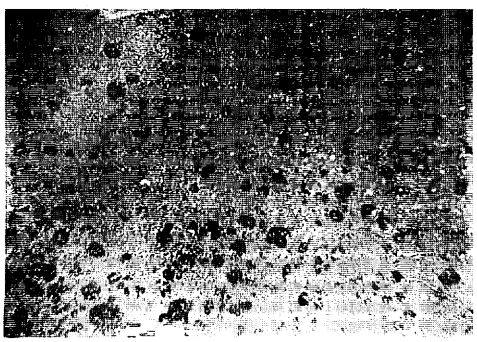

FG645 / 2.2 (10) ID, IDP

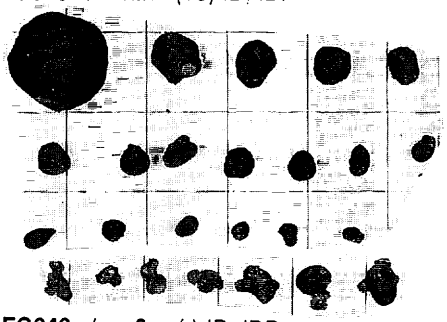

FG646 / 3 (-) ID, IDP

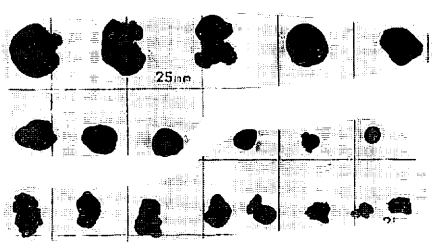

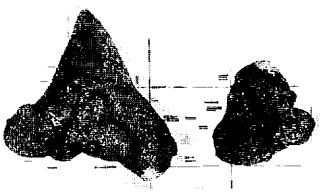

Appendix VIII-2 (continued)

FG647 / 0.6 (5) ID, IS

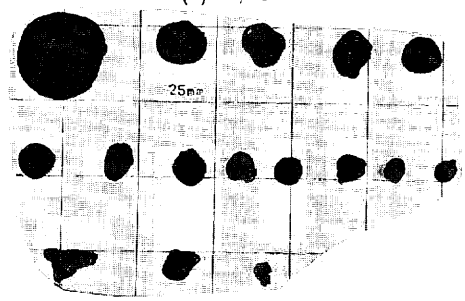

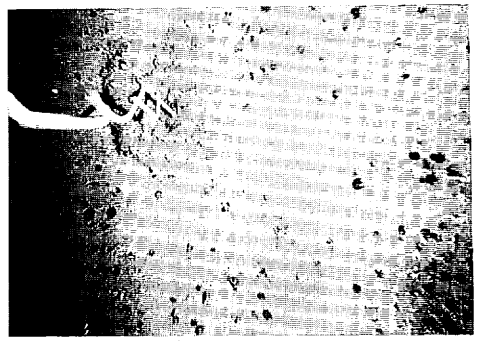

FG648 / 0.5 (5) ID, D

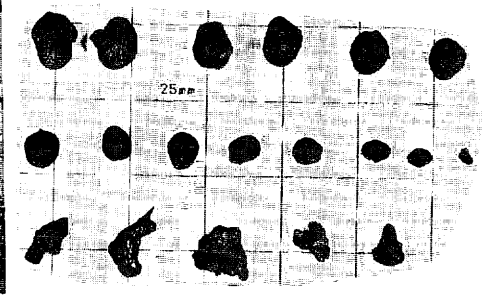

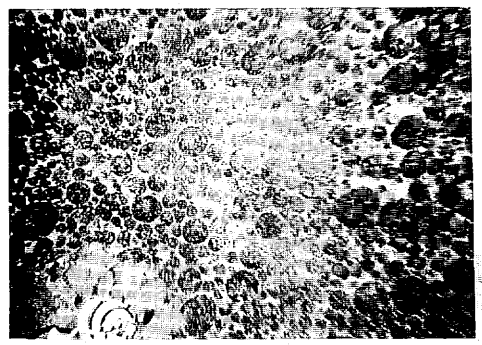

FG649 / 2.5 (85) IS, S

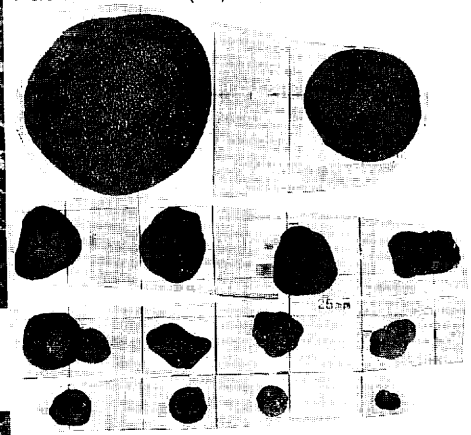

FG650 / 0 (100) C

Appendix VIII-2 (continued)

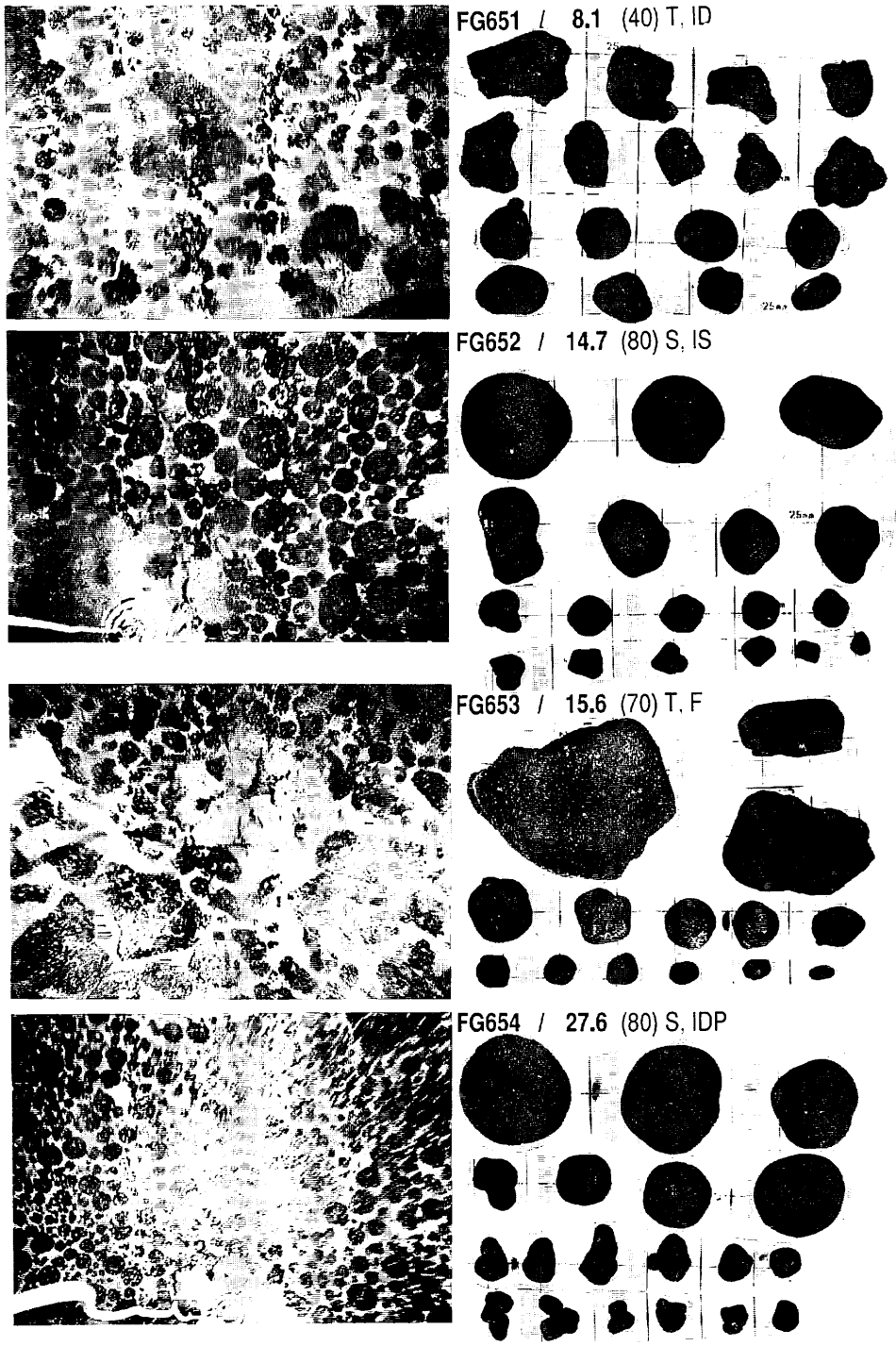

Appendix VIII-2 (continued)

B96 / - (-) ID, IDP

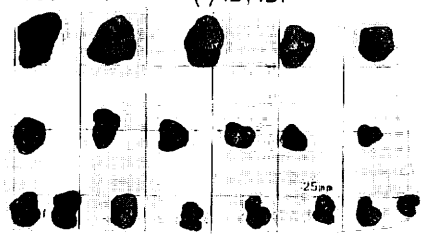

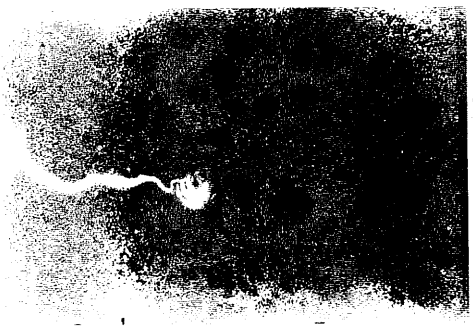

FG655 / 14.9 (30) S, ID

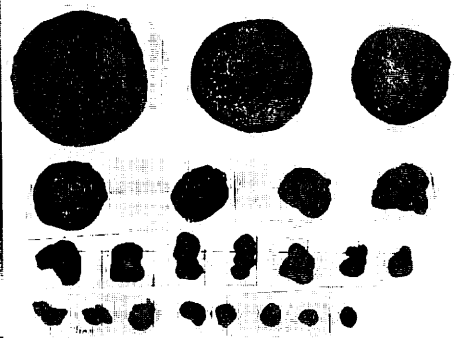

FG656 / 3.6 (15) ID

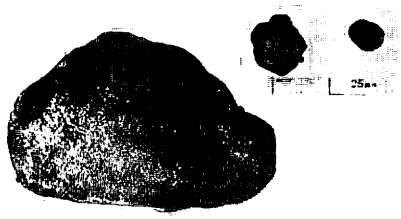

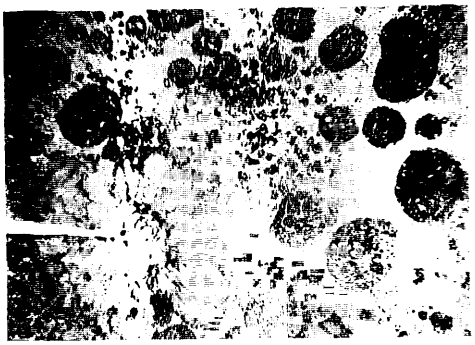

FG657 / 5 (20) IS, ID

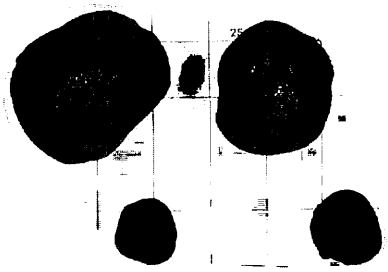

Appendix VIII-2 (continued)

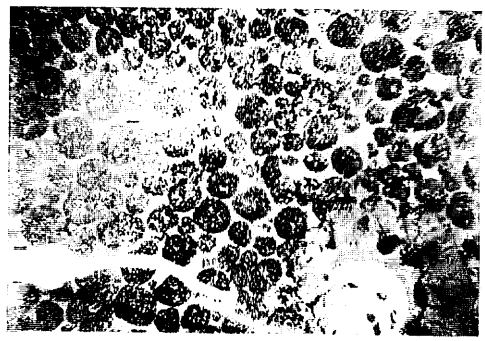

FG658 / 26 (80) IS, ISP

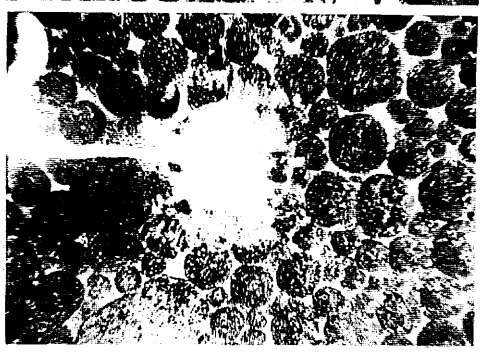

FG659 / 50.3 (85) S, D

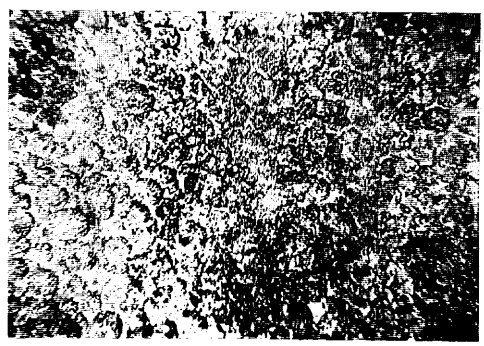

FG660 / 33.2 (90) IS, ISP

FG661 / 0 (100) C

Appendix VIII-2 (continued)

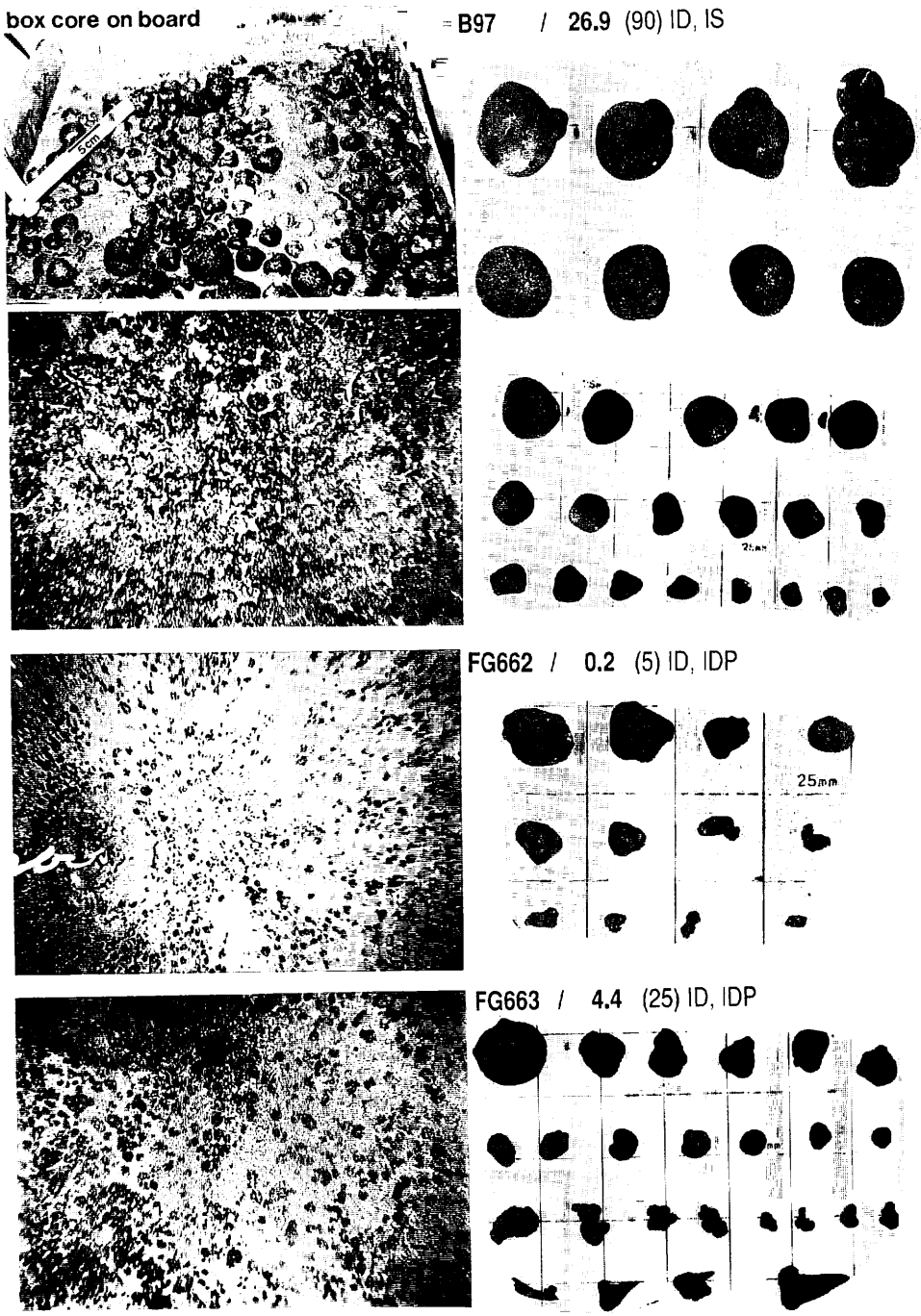

Appendix VIII-2 (continued)

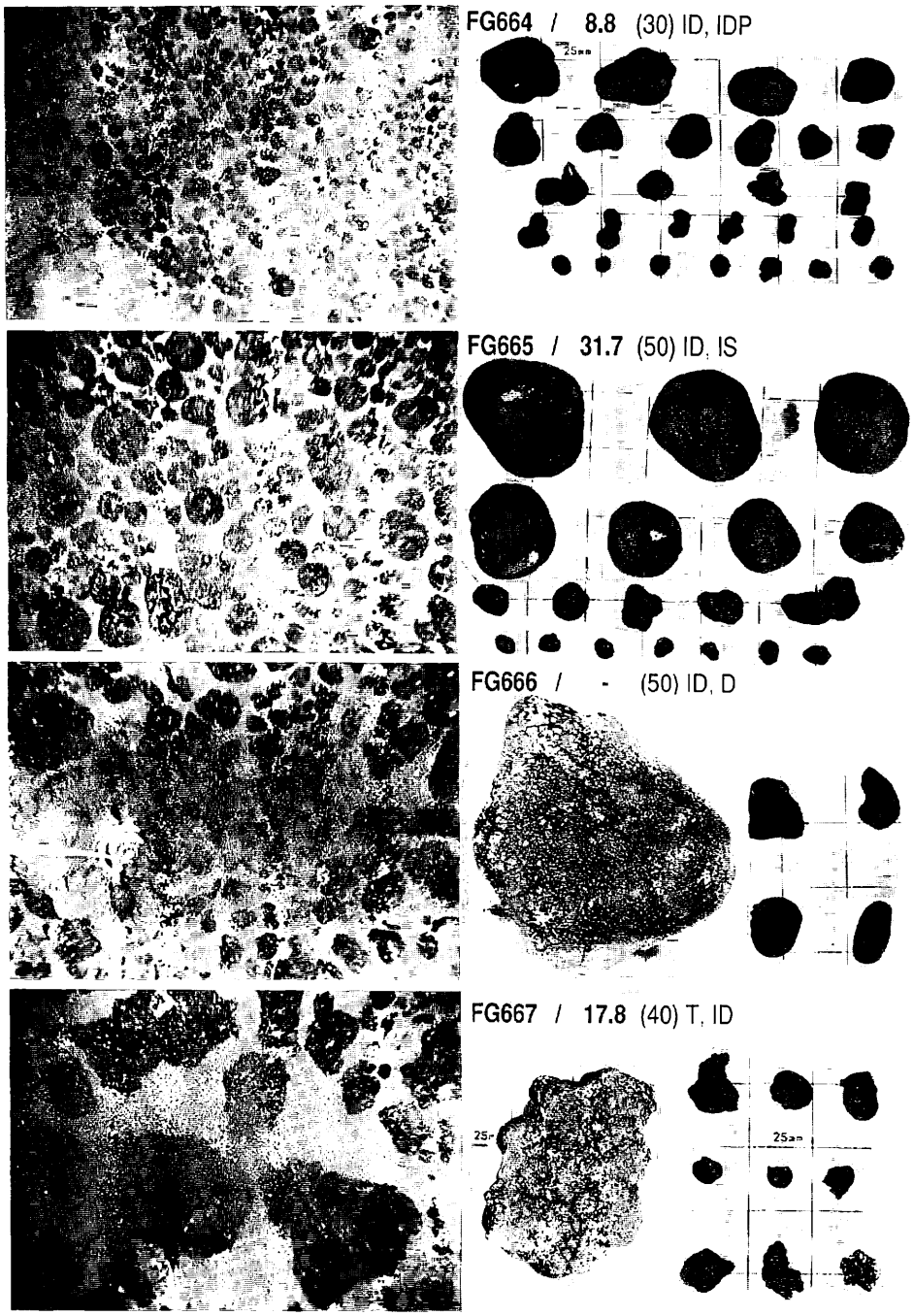

Appendix VIII-2 (continued)

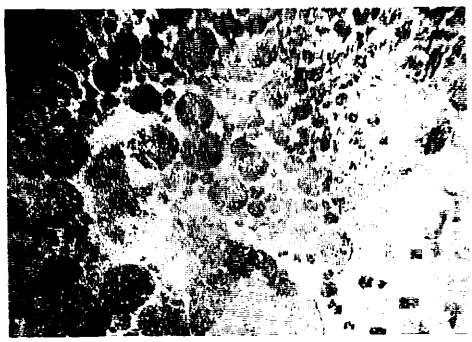

FG668 / 12.3 (70) T, S

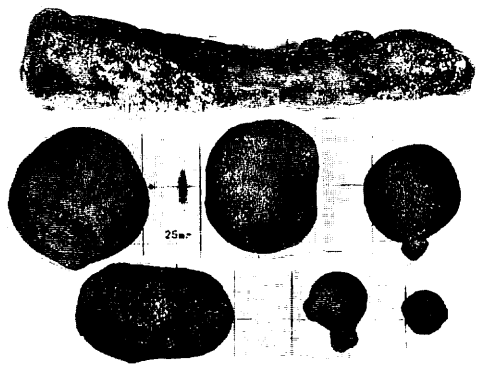

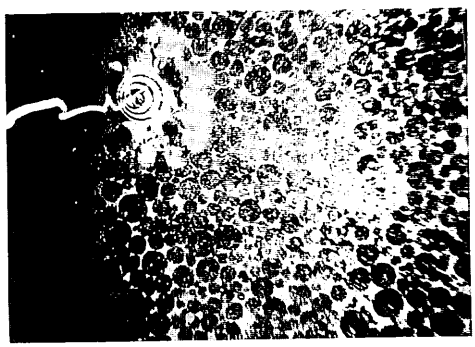

FG669 / 26.6 (85) S, IS

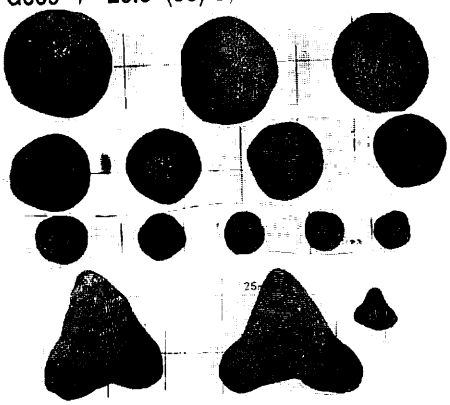

FG670 / 0 (100) C

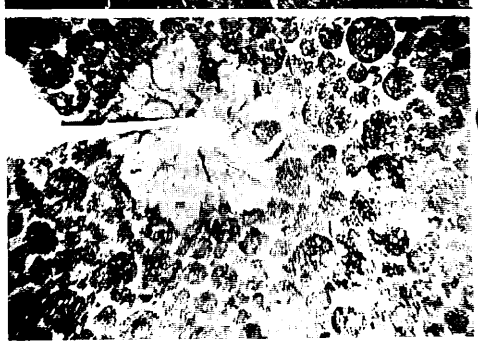

FG671 / 18.7 (80) F, IS

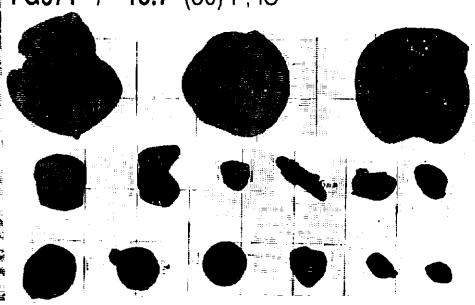

Appendix VIII-2 (continued)

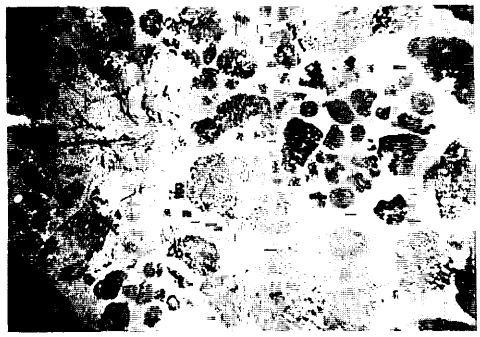

FG672 / 3 (30)IS, ID

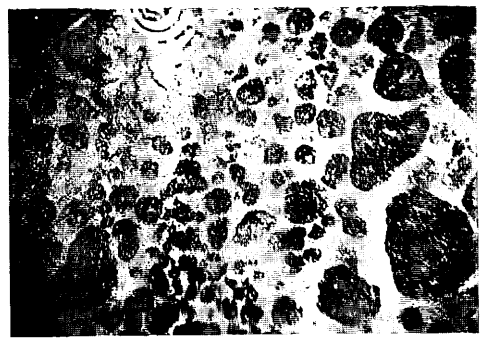

FG673 / 17.5 (40) T, ID

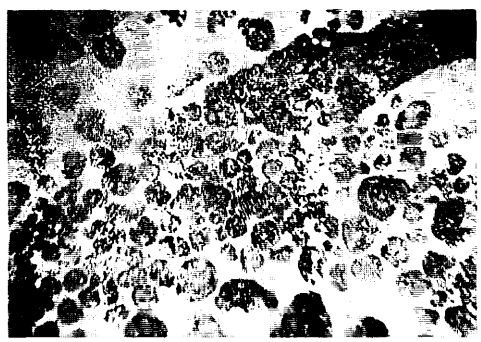

FG674 / 0 (100) C

FG675 / 29.8 (70) S, IS

Appendix VIII-2 (continued)

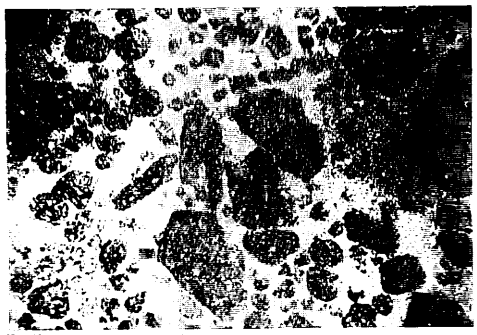

FG676 / 10.5 (50) ID, IDP

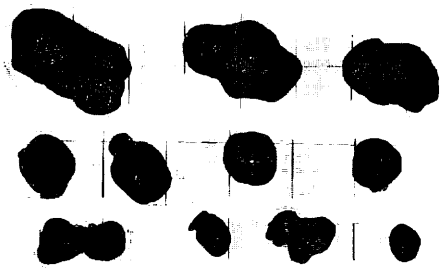

FG677 / 5.7 (70) ID, IDP

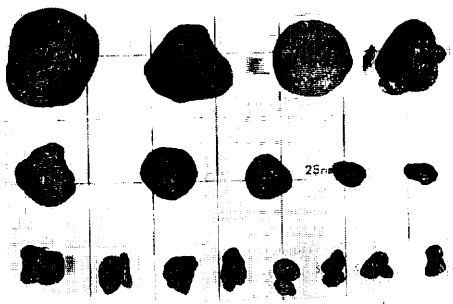

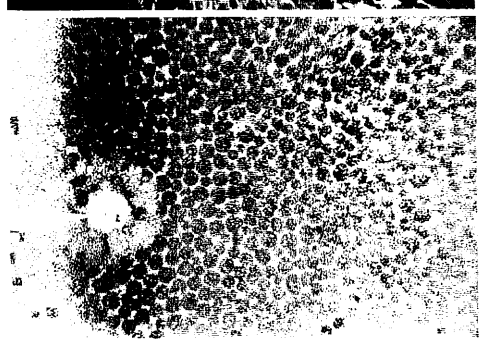

FG678 / 35.2 (90) IS, S

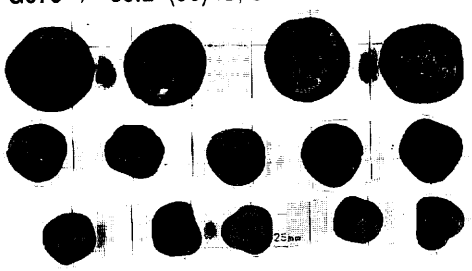

FG679 / 39.5 (-) IS, S

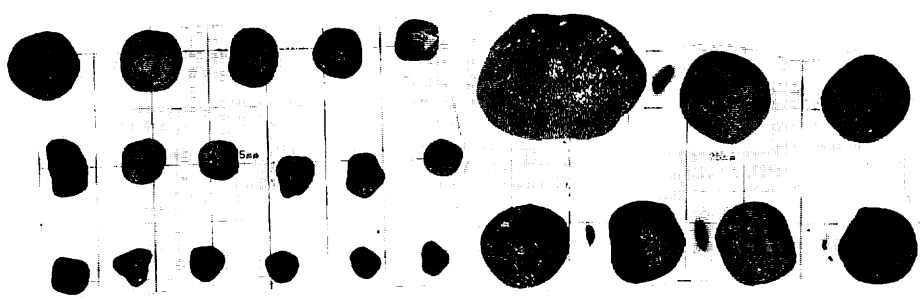

Appendix VIII-2 (continued)

FG680 / 36.7 (-) IS, IDP

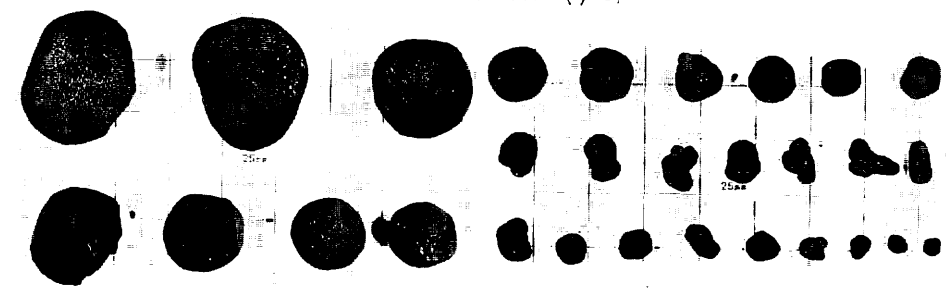

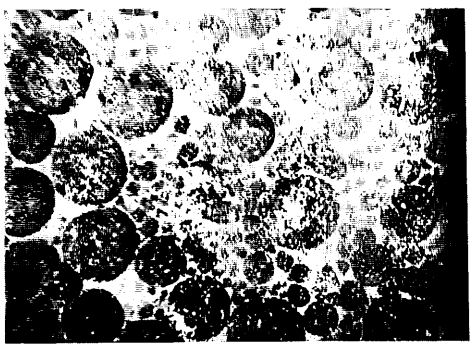

FG681 / 3 (80) S, D

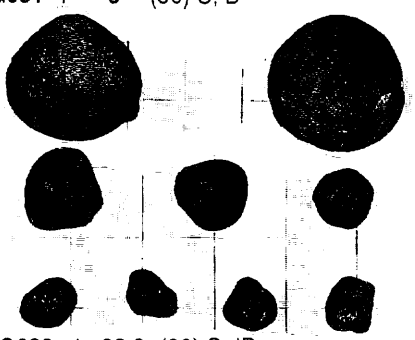

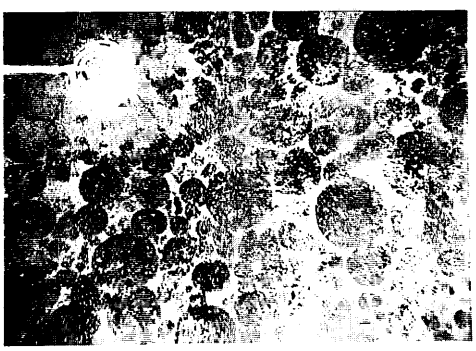

FG682 / 22.9 (80) S, ID

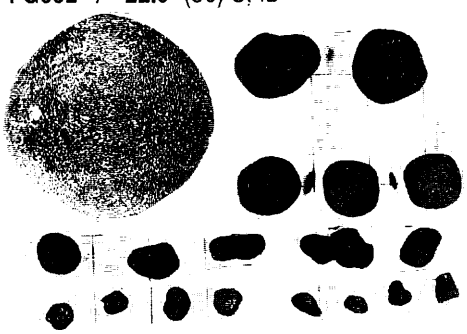

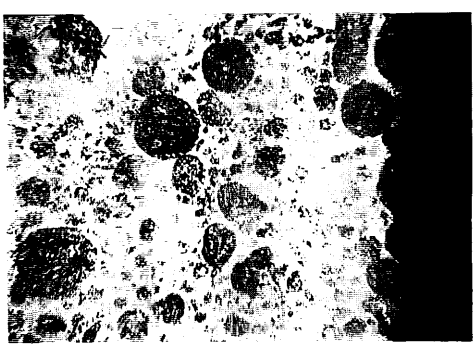

FG683 / 8.9 (40) T, ID

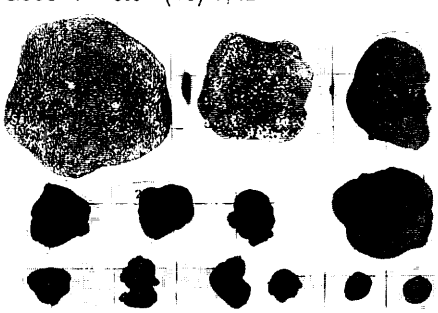

Appendix VIII-2 (continued)

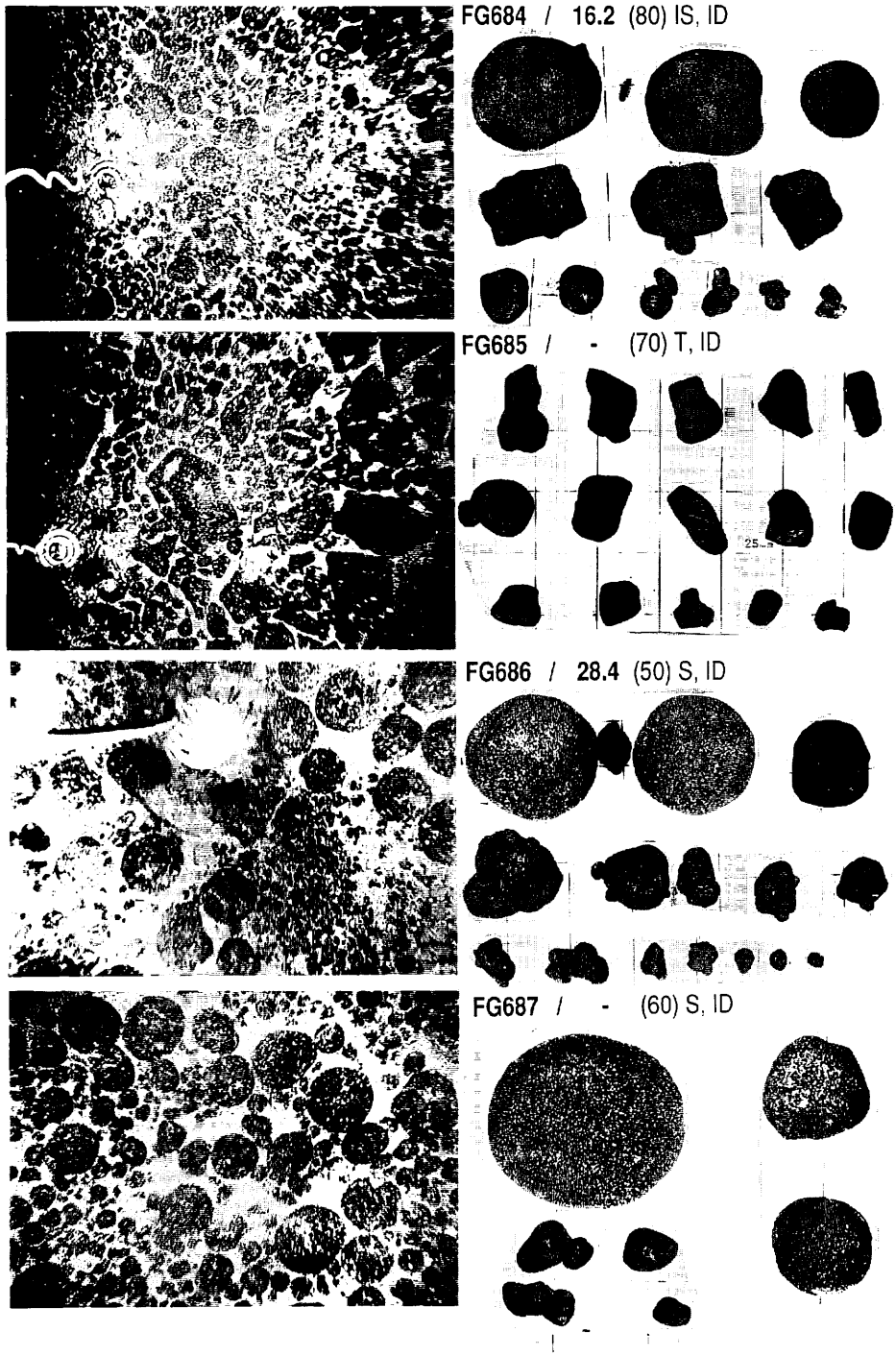

Appendix VIII-2 (continued)

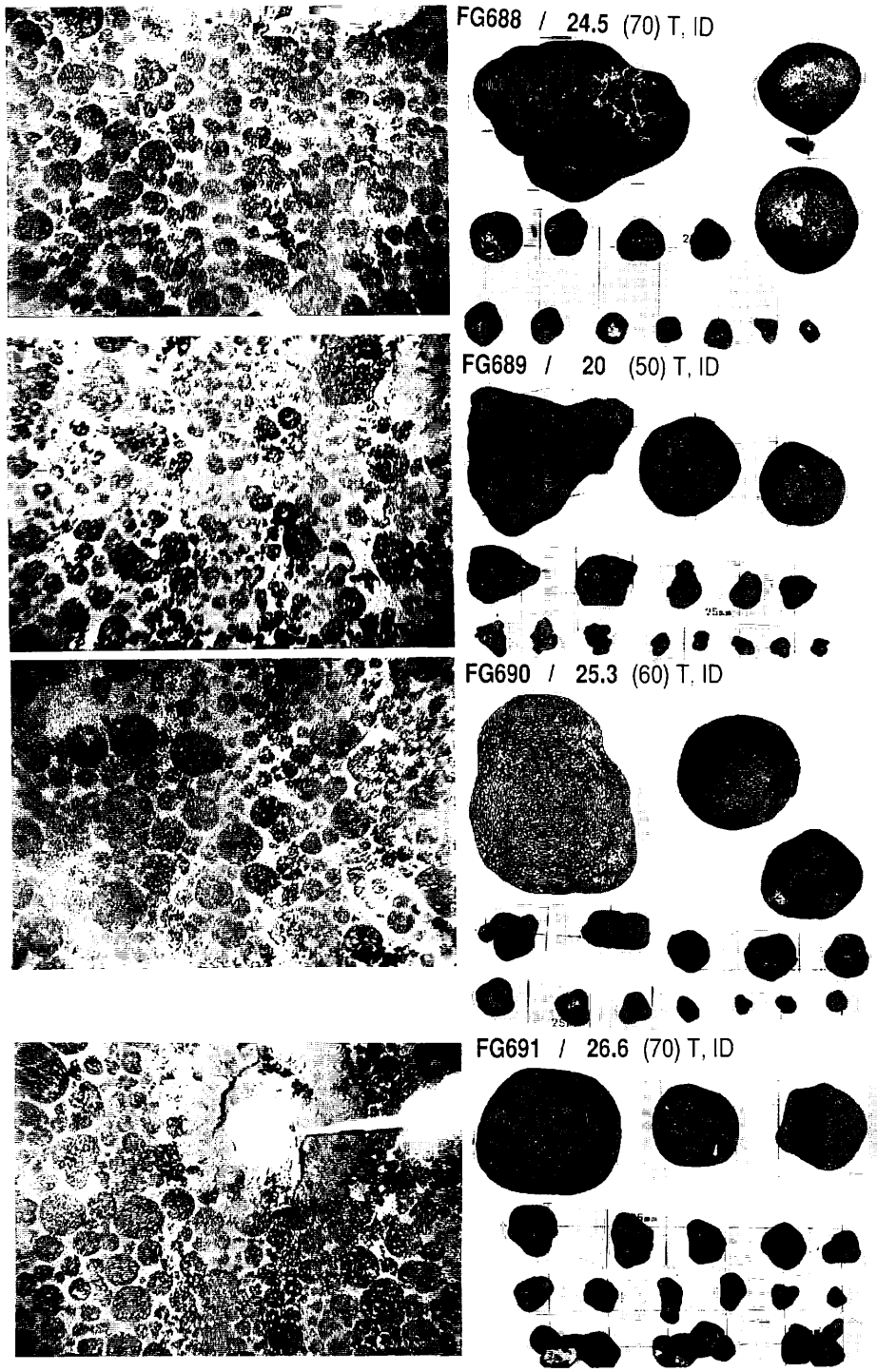

Appendix VIII-2 (continued)

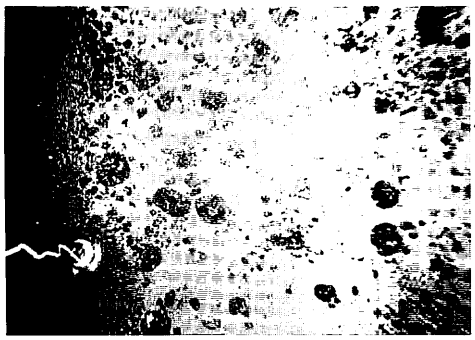

FG692 / 8 (20) IS, IDP

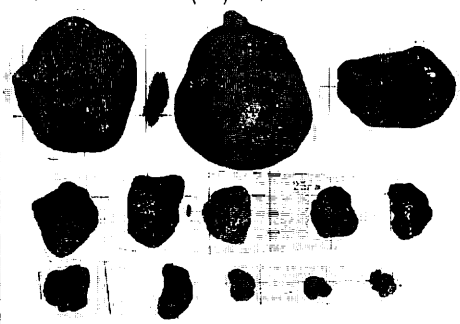

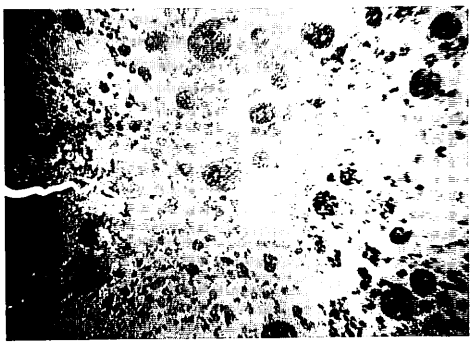

FG693 / 4.3 (20) ID, IS

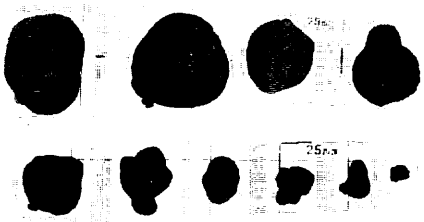

FG694 / 1 (100) C

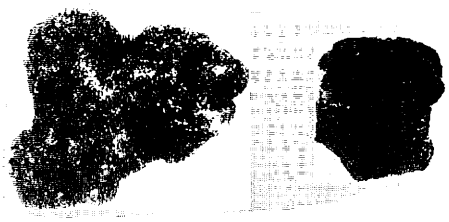

FG695 / 0.1 (100) C

Appendix VIII-2 (continued)

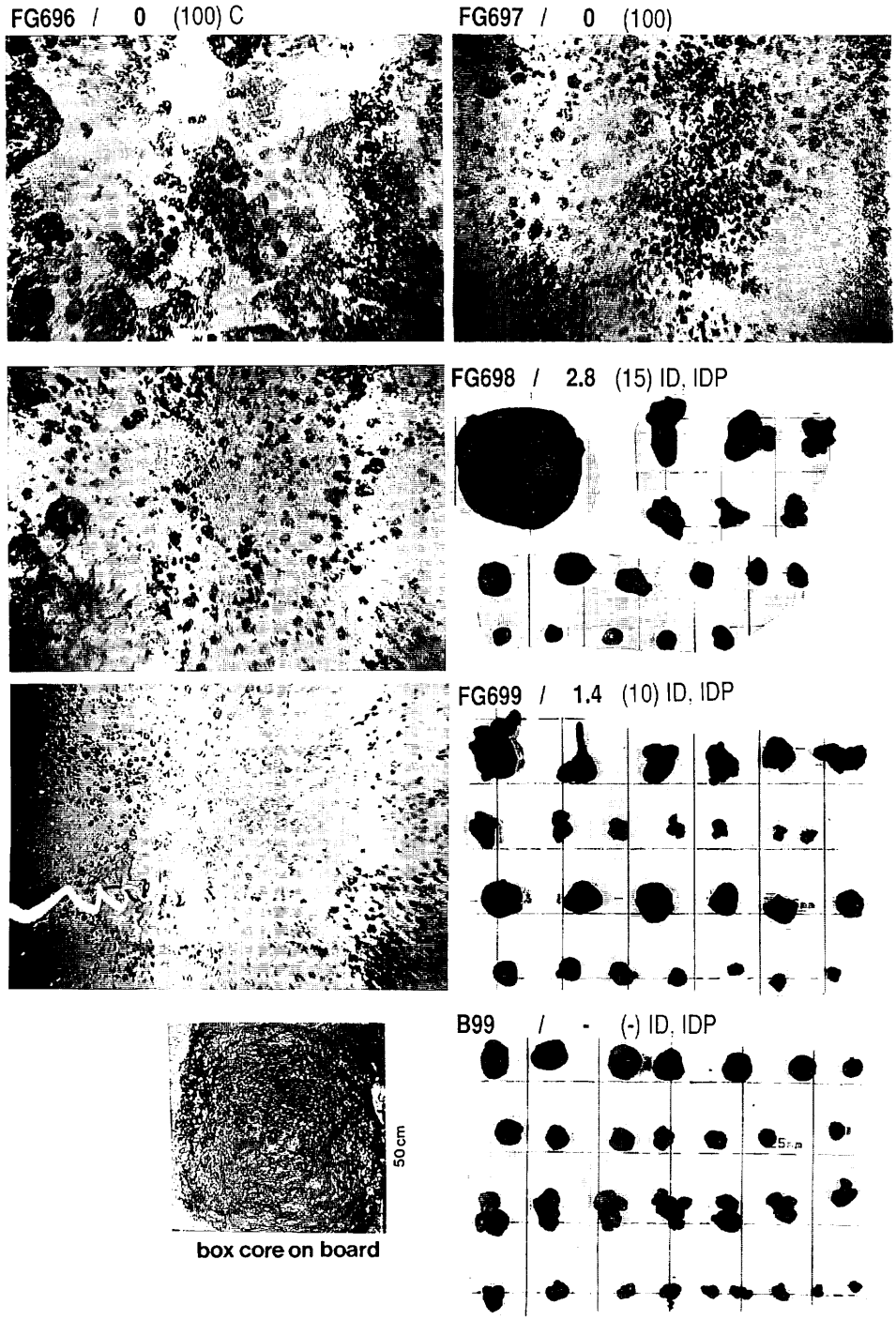

Appendix VIII-2 (continued)

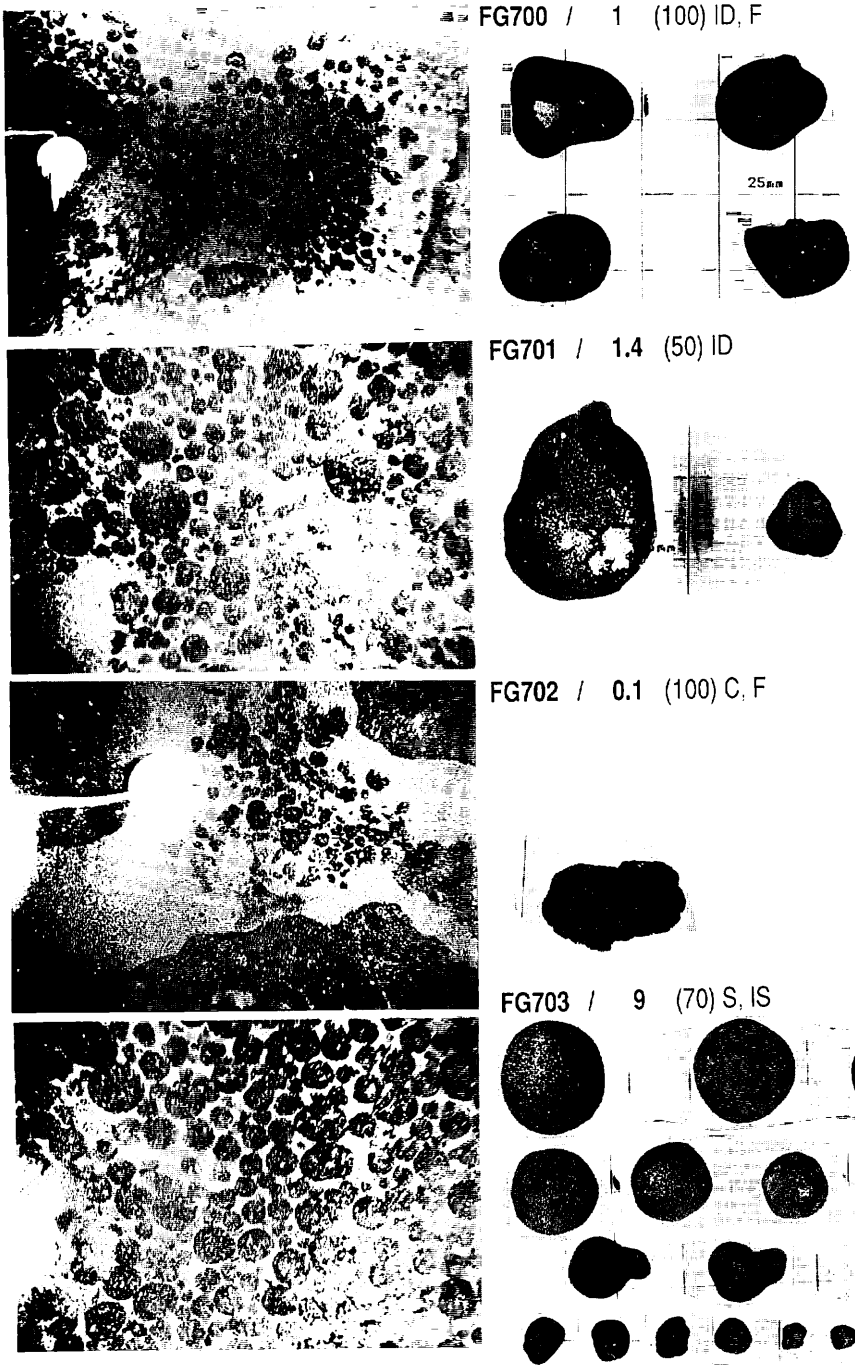

Appendix VIII-2 (continued)

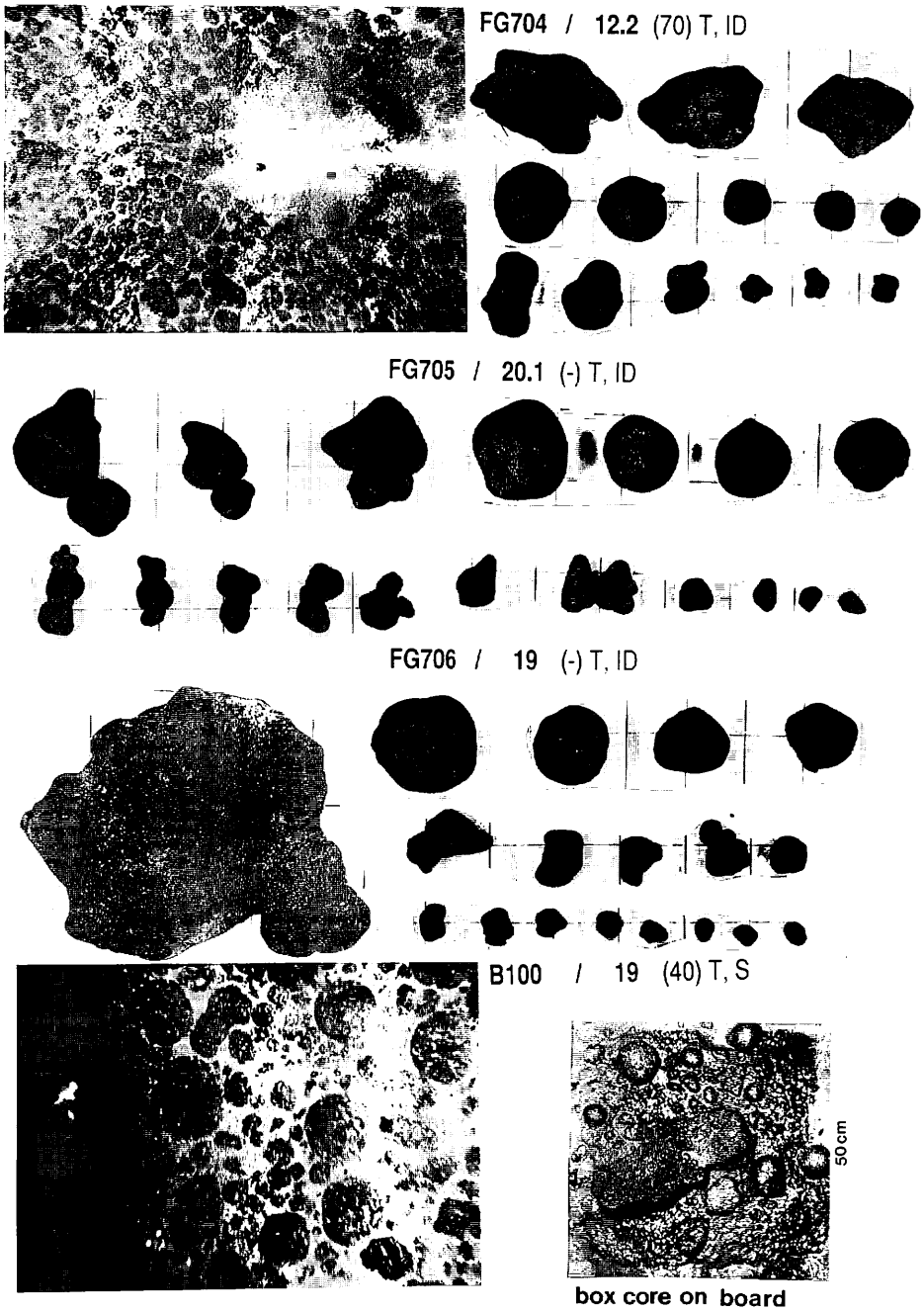

Appendix VIII-2 (continued)

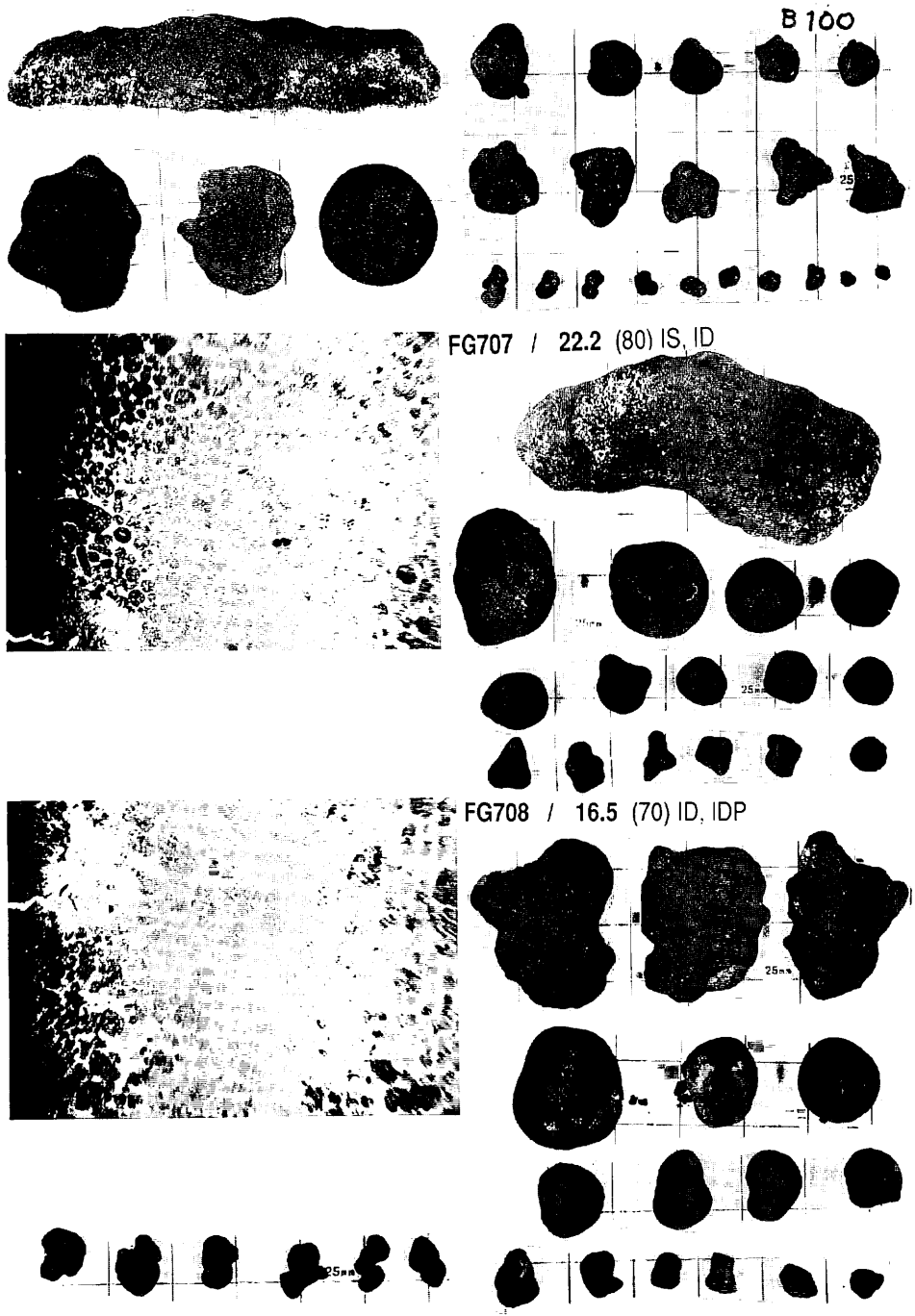

Appendix VIII-2 (continued)